DATA ACQUISITION AND FEATURE EXTRACTION FOR CLASSIFICATION OF PREHENSILE SEMG SIGNALS FOR CONTROL OF A MULTIFUNCTIONAL PROSTHETIC HAND

By

ELİF HOCAOĞLU

Submitted to the Graduate School of Engineering and Natural Sciences
in partial fulfillment of
the requirements for the degree of
Master of Science

SABANCI UNIVERSITY

Fall 2007

DATA ACQUISITION AND FEATURE EXTRACTION FOR CLASSIFICATION OF PREHENSILE SEMG SIGNALS FOR CONTROL OF A MULTIFUNCTIONAL PROSTHETIC HAND

APPROVED BY:

Assistant Prof. Dr. KEMALETTİN ERBATUR .....

(Dissertation Advisor)

Prof. Dr. ASIF ŞABANOVİÇ .....

Associate Prof. Dr. MUSTAFA ÜNEL .....

Assistant Prof. Dr. AYHAN BOZKURT .....

Assistant Prof. Dr. VOLKAN PATOĞLU .....

Assistant Prof. Dr. MÜJDAT ÇETİN ……

(Substitute Member)

DATE OF APPROVAL: .....

DATA ACQUISITION AND FEATURE EXTRACTION FOR CLASSIFICATION OF PREHENSILE SEMG SIGNALS FOR CONTROL OF A MULTIFUNCTIONAL PROSTHETIC HAND

Elif HOCAOĞLU

EECS, M.Sc. Thesis, 2008

Thesis Supervisor: Assistant Prof. Dr. Kemalettin ERBATUR

Keywords: EMG, Prosthesis, Feature Extraction, Pattern Recognition, Wavelets, Time-Frequency Resolution, Neuroscience, Biomedical Signal Processing, Transient Signal

ABSTRACT

This study focuses on the SEMG (surface electromyography) signals that carry the valuable information of the neuromuscular activity of a muscle and are utilized in the man-machine interfaces such as multi-functional prostheses. The SEMG signals measured from four different muscle groups of the forearm are weak, sophisticated and very sensitive to ambient noise. The first stage of this study is hardware design and implementation for the SEMG measurement. The fundamentals of the design are mainly based on the specifications of the SEMG signal and the factors that affect the signal quality. The second purpose of the thesis is applying various methodologies to the recorded SEMG signal to give meaning to its nature to be used in the further processes. The raw EMG signals have nonlinear characteristics and present useful information if they are quantified. For this purpose, various signal processing methods are applied to the SEMG signal to acquire useful information, features. Features of the signal are extracted to be used for classification of prehensile motions of multi-functional prosthetics. In this part, many algorithms that have been employed as feature extraction methods are compared with respect to their classification performance.

ÖZET

Bu çalışma, bir kasın sinir-kas aktivite bilgisinin yer aldığı ve çok fonksiyonlu protezler gibi insan-makine arayüzlerinde kullanılan yüzeyel elektromyografi sinyali üzerine odaklanmıştır. Önkol üzerindeki dört farklı kas grubundan ölçülen yüzeyel elektromyografi sinyali zayıf, karmaşık ve çevresel gürültülere karşı oldukça hassas bir sinyaldir. Bu çalışmanın ilk aşaması, yüzeyel elektromyografi sinyalinin ölçülmesi amacıyla kullanılan donanımın tasarımını ve uygulamasını içermektedir. Temel olarak cihaz tasarımı, yüzeyel elektromyografi sinyalinin özellikleri ve sinyal kalitesini etkileyen faktörler baz alınarak yapılmıştır. Tezin ikinci amacı ise daha sonraki işlemlerde kullanılmak amacıyla, kaydedilen elektromyografi sinyaline anlam kazandırmaktır. Doğrusal olmayan karakteristik özelliğe sahip olan elektromyografi sinyalinin kullanışlı bir bilgi sunabilmesi için sayısallaştırılması gereklidir. Bu amaçla çeşitli sinyal işleme yöntemleri uygulanmış ve sinyalin karakteristik özellikleri elde edilmiştir. Bu özellikler, çok fonksiyonlu protezlerin kavrayabilme ve tutabilme hareketlerinin sınıflandırılması için seçilmiştir. Tezin bu kısmında, sinyal karakteristiğini belirleyen birçok algoritma uygulanmış ve herbir algoritmanın sınıflandırma methodu altında performansları, başarı yüzdelerine bakılarak karşılaştırılmıştır.

To all disabled people in the world

ACKNOWLEDGEMENTS

First of all, I would like to gratefully thank to my family to their helpful attitude and endless patience.

Especially, I would like to give my special thanks to Ertuğrul Çetinsoy, Ph.D. Candidate and Emre Hocaoğlu, M.D. to their enthusiastic helps, valuable guidance and infinite supports throughout the development of my thesis.

I wish to thank my thesis defense jury for their valuable suggestions and comments regarding my thesis.

I would also sincerely thank to my close friends, Yasser El-Kahlout, Latif Koyuncu and Ferhat Öztaşkın for their support during my thesis.

TABLE OF CONTENTS

LIST OF FIGURES

TABLE OF ABBREVIATIONS

EMG	Electromyography
SEMG	Surface Electromyography
EEG	Electroencephalography
ECG	Electrocardiography
MUAP	Motor Unit Action Potential
CMRR	Common Mode Rejection Ratio
SVM	Support Vector Machine
FFT	Fast Fourier Transform
STFT	Short Time Fourier Transform
DWT	Discrete Wavelet Transform
WPT	Wavelet Packet Transform

1 INTRODUCTION AND PROBLEM STATEMENT

1.1 Introduction

The main motivation of this research is to supply mind-controllable and multi-functional prostheses to disabled people. Mind controllable prosthetics can only be achievable by using an interface between mind and prosthetics. Mind creates the biological signals in the human body. The conversion of the biological signals to the electrical signals makes the prosthetics controllable by mind. However, biological signals are very sophisticated signals to find comprehensible meanings in its structure. That is why it is an open research area for years. The first objective of this research is to collect the biomedical signals from the human body for exploration. The second objective of the thesis is to discover the biomedical signals to make them eligible for diverse targets. Biomedical signals have been used for various applications, such as clinical diagnosis, assistive devices. In this research electromyography (EMG) signals measured from the muscle are main concern as regards biomedical signals and used for multi-functional prosthesis.

Commercially available prostheses in the world have one or two degree of freedom, two to four hand functions, e.g. grasping and hand opening with a gripper and wrist rotations, and no production based on the multifunctional prosthetic hands close to the original one is produced. In this research, four different gestures, opening and closing of four digits and flexion and extension of thumb, constitute the functional specifications of the prosthetic hand. In order to make the prosthetics capable of performing all these gestures, EMG signals, firstly, are to be measured and secondly, measured signals have to be analyzed in detail to commend the prosthetics various properties of different gestures.

The EMG signals are measured with a biomedical data acquisition device. The hardware design of the device is one of the main parts of this thesis. The further issue after the measurement is exploring the measured and recorded data under the application of different methods. Therefore, the other important part of the thesis is analyses and making the identification of the EMG signals. Identified EMG signals are useful for increasing the

functionality of the prosthetics. Identified EMG signals shows different characteristics. These characteristics, also called features, are revealed after the application of the many diverse feature extraction methods. Hereafter, determined features are the name of the EMG signals. Features of the EMG signals enable us to classify them. Successfully classified patterns will be used in the multi-functional prosthetic hand. Achievement of each section directly depends on each other. More accurate data acquisition provides more quality features to be extracted from the EMG signal. More quality features provide more successful pattern classification. In other words, the best performance of data acquisition is the first step of multi-functional prosthetic hand.

1.2 Outline

In Chapter 2, a literature survey about the formation of the biopotential signals and their specifications and measurement techniques are discussed. In Chapter 3, the hardware design of data acquisition device both in theory and practice are revealed. SEMG signals are measured and recorded by data acquisition device for some implementations. In Chapter 4, various feature extraction methods that are applied to the measured SEMG signal by data acquisition device are explained and the determination of an appropriate method for the non-stationary signals is explained. In Chapter 5, the experimental results of each method discussed in Chapter 4 are shown in detail and the EMG signal classification is explained. In Chapter 6, all the experiments are reviewed and compared.

2 LITERATURE SURVEY

2.1 History of Surface Electromyography Processing for Multi-functional Prostheses

The prosthetics used for people who have had their arm amputated or people who were born without any arm facilitate their life making capable of daily activities own their own. EMG is an interface between human and prosthetics. EMG controlled prosthetics are multidisciplinary research area. EMG signal measuring and recording, EMG feature extraction and pattern recognition, mechanical construction of prosthetics. Control of prosthetics has been realized by classifying selected gestures accurately. The accuracy of classification depends on the quality of selected features. Graupe and Cline (1975) the first group to classify the EMG signals used the autoregressive coefficients as features from single channel and obtain 85% accuracy in classification performance [1]. Basmajian and De Luca (1985) stated that the median and the mean frequency are reliable to represent the signal characterization [2]. Zardoshti et al. (1995) extracted features by using the integral of absolute value, variance, number of zero crossings and auto-regressive model parameters from upper limb EMG signals and classified them with K-nearest neighbor classifier [3]. Englehart et al. (1998,2001) applied dimensionality reduction by principal component analysis on feature set that are obtained after the processes of short time Fourier transform, wavelet transform, wavelet package transform. Wavelet package transform is observed as the more successful method [4, 5]. Englehart et al. (1999) tried wavelets and gets 93.75% accuracy from four channels of biceps and triceps [6]. Crawford et al. used the amplitude of the steady state EMG data as features and get over 90% accuracy by using linear SVM based classifier[7]. Englehart (2001) proposed an altered version of the local discriminant basis (LDB) algorithm to increase the classification performance of the wavelet packet transform (WPT) by using a class separability cost function [8]. Zhang et al. (2002) used wavelet based neuro fuzzy methods to classify the EMG data and found successful [9]. Nishikawa et al. (2002) employed Fourier transform and the mean absolute value as features of the signal and proposed an online supervising mechanism that controls learning data [10]. Boostani et al. (2003) determined the energy of wavelet coefficients in nine scales and the cepstrum coefficients as successful

features [11]. Kilby and Hosseini (2004) compared the different wavelet families of DWT and WPT and classified them with neural network method [12]. Du and Vuskovic compared temporal and spectral methods with ART-based classifier. Though multiple trapezoidal windowing is a temporal method, it represents better efficiency than spectral method, short time Thompson transform [13] .Carreño and Vuskovic (2005) proposed an approach which extends the Engelhart's discrete wavelet package transform by subjecting two-scale, three-scale wavelet coefficients to temporal moment computation. This provides dimensionality reduction of feature vectors without losing significant data [14]. Liu et al. (2005) used Coiflet mother wavelet for real time EMG motion discrimination experiments. In that study, they used a normed wavelet coefficient to erase the phase lag and spectra summation was chosen as feature extraction method [15]. Zheng et al. proposed that optimization techniques are necessary to determine the optimal feature subsets [16]. Arieta et al. (2006) obtained the feature vector containing eight samples for each channel by using FFT of the EMG signal and proposed online learning method to be used in the adaptive joint mechanism [17]. Zhao et al. (2007) used absolute mean value, absolute mean value ratio, and fourth order autoregressive model as feature extraction methods and weighted Euclidean distance method as classifier to obtain faster pattern recognition [18]. Shenoy et al. (2007) proposed that SVM method presented the high accuracy classification performance in real time applications [19].

2.2 Biomedical Aspects and Signal Specifications

Making an imitation of an original system (Figure 2-1), first of all, requires exploration of the real mechanism. This issue exactly overlaps with a multi-functional prosthesis (Figure 2-2) and an original limb. In this chapter, a summary of voluntary muscle contraction processes in the human body will be given and measurement techniques of electrical signals generated in the body and specifications of the biological signals will be discussed. This chapter reveals the sophistication of a biological signal measurement and complication of the imitation of an original limb.

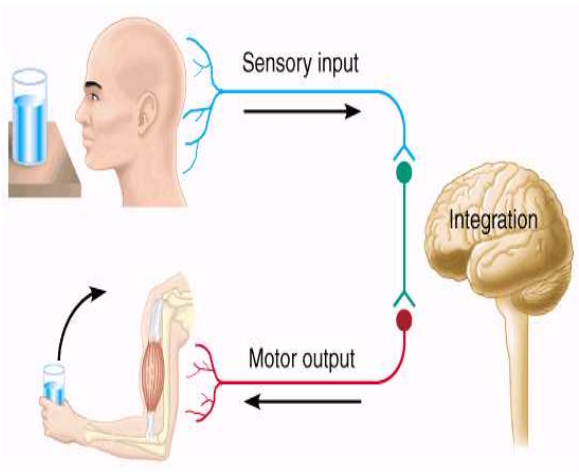

Figure 2-1 Original system [20]

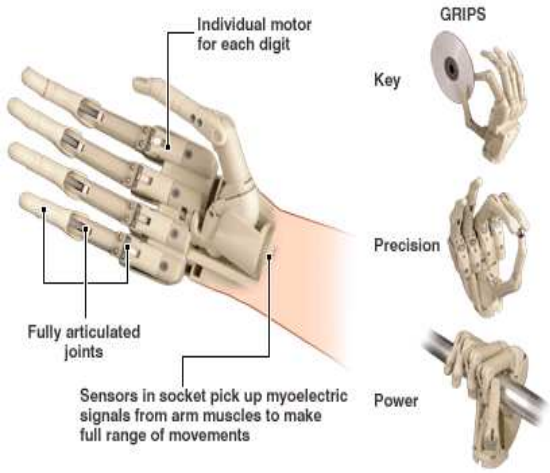

Figure 2-2 Multi-functional prosthesis [21]

2.2.1 Muscle Anatomy & Measurement of Muscular Activity

We are able to interact with and control the world around us through a complex and excellent system, the motor system. Our interactions with the environment could be automatic or may require conscious control in Figure 2-3. Sensory information from the environment is received by our nervous system, and we either ignore this information or produce a movement as a reaction that is involuntary or voluntary.

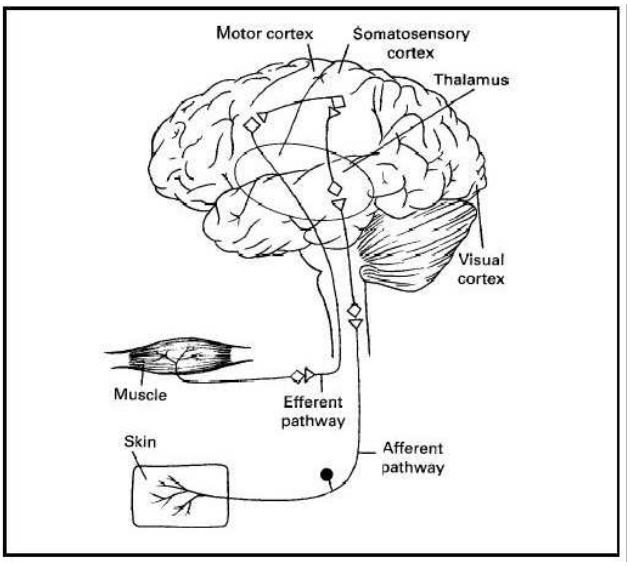

Figure 2-3 A nerve pathway [22]

Voluntary movements are mostly controlled by the motor cortex of our brain. The motor cortex is mainly formed by two well defined cortical areas; area 4 or primary motor cortex and area 6 in Figure 2-44. These cortical areas receive tasks from the various lobes of the brain. Most of the movement tasks are planned in the frontal lobe and sent to the motor cortex in the form of electrical activities via the axons of the neurons of the frontal cortex. The motor cortex, with the aid of information from the other areas of the brain, decides the best way of desired motion as revealed in Figure 2-55 [23, 24].

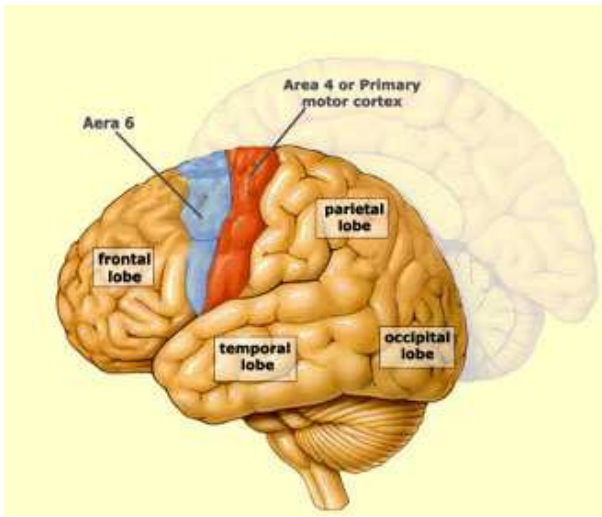

Figure 2-4 Area 4 and Area 6 of the motor cortex [25]

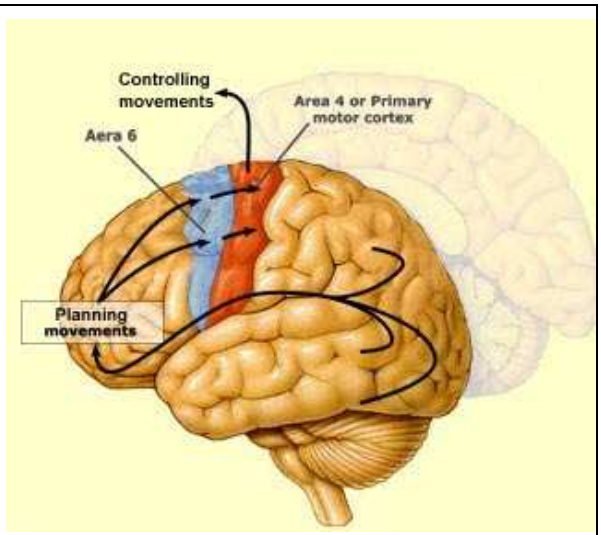

Figure 2-5 Controlling and Planning Movements [25]

The primary motor cortex, also called the precentral gyrus or Brodmann's area 4 is composed of well defined regions which are responsible for the movement of different body parts as in Figure 2-66.

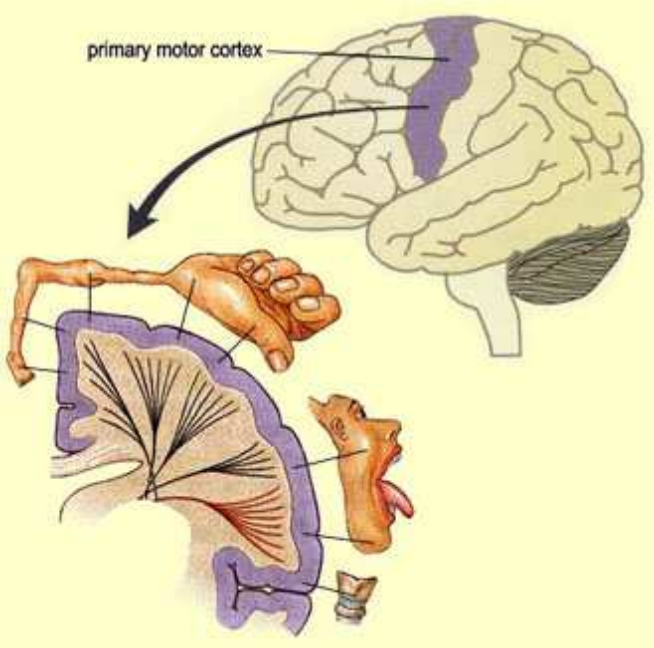

Figure 2-6 Motor cortex tasks [25]

Electrical signal transmission of voluntary movement from brain to the muscle is executed by the aid of motor pathways. The motor pathways originate in the brain or brainstem and descend down the spinal cord to control the α-motor neurons (motor neurons or second motor neurons). The cell bodies of motor neurons are located in the ventral horns of the spinal cord and send their axons out via the spinal roots and directly control the muscles. The most famous pathway is the so called "pyramidal system" or the "corticospinal pathway", which begins with the large pyramidal neurons of the motor cortex, travels through the midbrain, pons, medulla, spinal cord and finally ends on or near the α-motor neurons. The axons of α-motor neurons leave the spinal cord and become motor nerves (peripheric nervous system) which stimulate the target muscles that provide the desired motion shown in Figure 2-7.

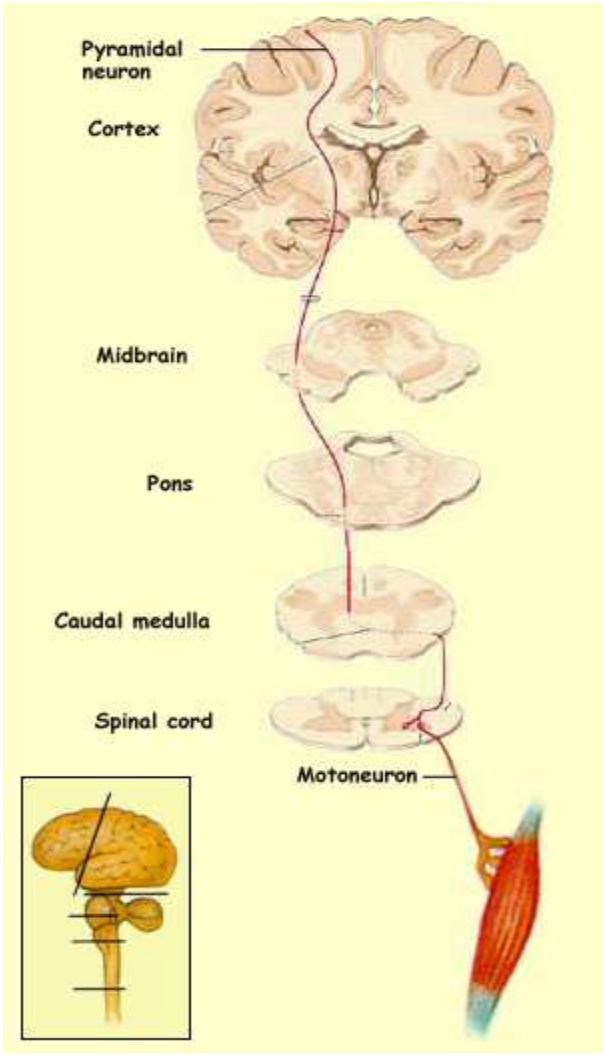

Figure 2-7 α motor neuron [25]

Our skeleton is composed of bones that provide support and act as pivot points. Skeletal muscles which are classified as “striated muscles” produce the movement by contraction. The nervous system administrates the related skeletal muscles for an optimum movement. Some muscles work together, some work antagonistically and this arrangement results in a great amount of combinations in terms of direction and strength of the movements.

Striated muscle cells are multinucleated cells which are filled with myofibrils composed of series of repeated units called sarcomeres (Figure 2-88 and Figure 2-99). A sarcomere is bounded by Z lines on each end. On both sides of each Z line, there are I bands which are

composed of thin filaments that project from Z lines. In the center of each sarcomere there is the A band that is composed of thick filaments and overlapping thin filaments [24, 30].

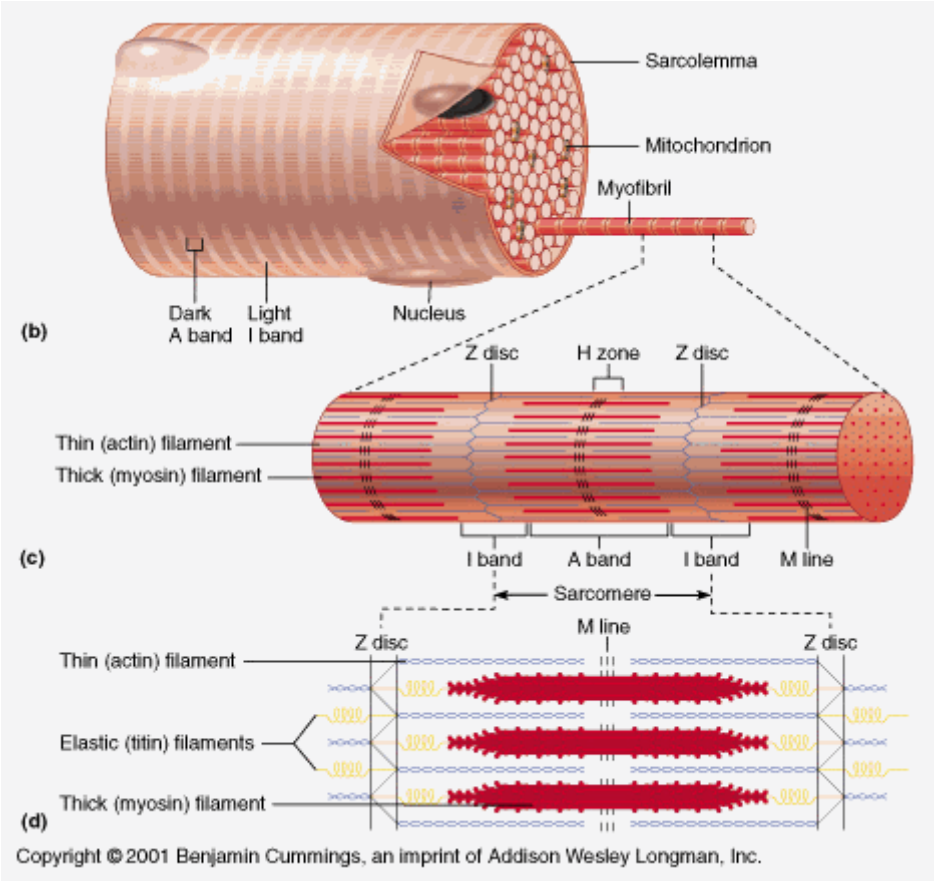

Figure 2-8 Sarcomere structure [26]

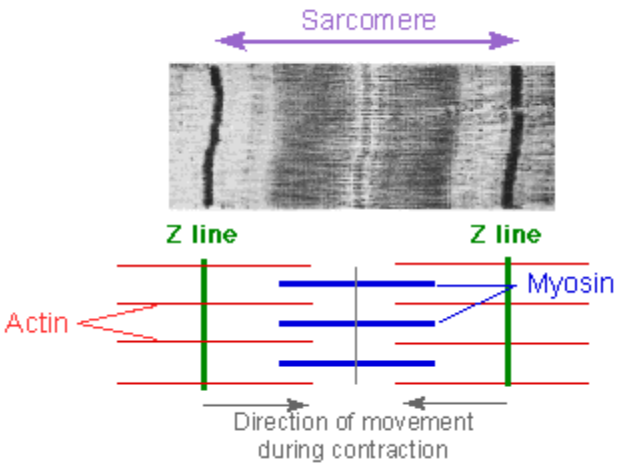

Figure 2-9 Photomicrograph and schematic demonstration of sarcomere [26]

Myosin molecule - the thick filaments- is a protein composed of two polypeptide chains. Each myosin has a globular head and a long tail. Myosin tails lay together to form the body of the thick filament and myosin heads hang off the body. Thin filaments are composed of actin, troponin and tropomyosin. Actin is the main component and forms a double helix that has binding sites for myosin (Figure 2-1010).

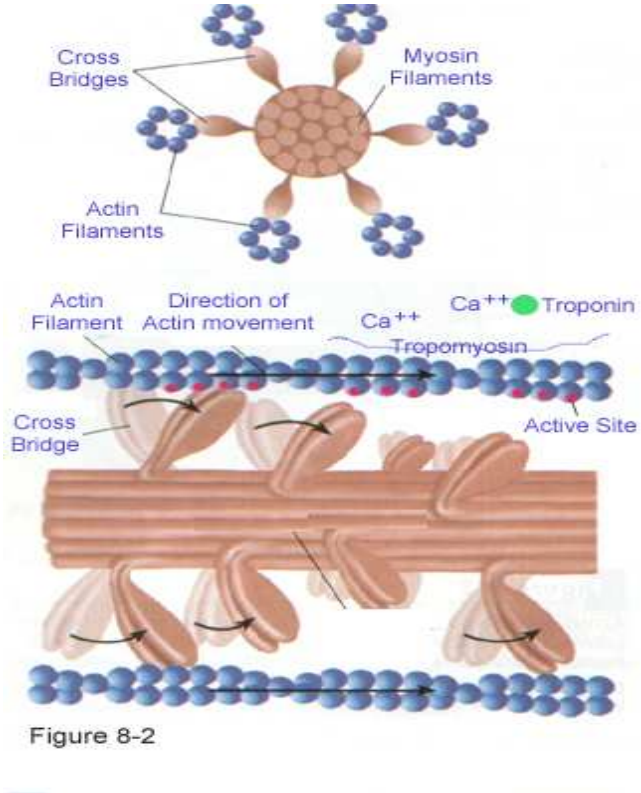

Figure 2-10 Demonstration of Filaments [26]

The change in the length of the muscle cell, resulting in muscle contraction, is explained by the "sliding filament theory". A reaction between the myosin heads and the actin molecules result in cross bridge formation and following conformational changes in the myosin heads. These events end up with sliding of the thick and thin filaments across one another, shortening the sarcomere (Figure 2-1111).

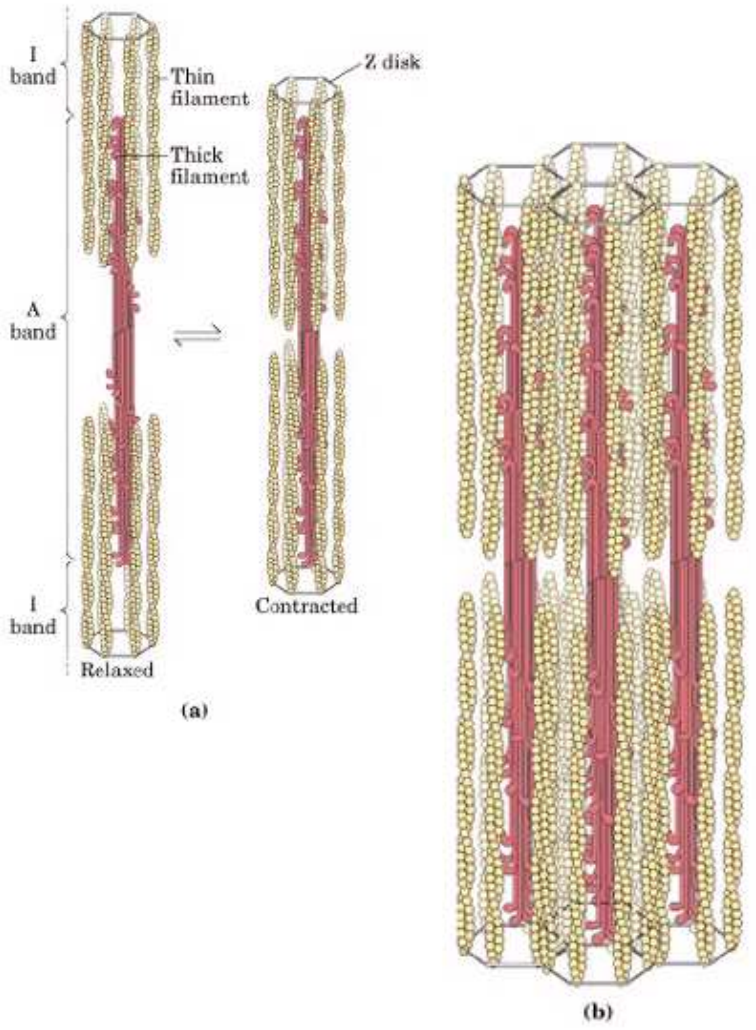

Figure 2-11 Sliding Filament Theory [27]

When an action potential is produced in a muscle fiber, the intracellular level of calcium is increased. Intracellular calcium binds to troponin which in turn, effects the location of tropomyosin resulting in exposition of "myosin binding sites" on the actin molecule. Repeating cross bridging between myosin and actin during the transient period of increased intracellular calcium level, cause muscle contraction (Figure 2-122).

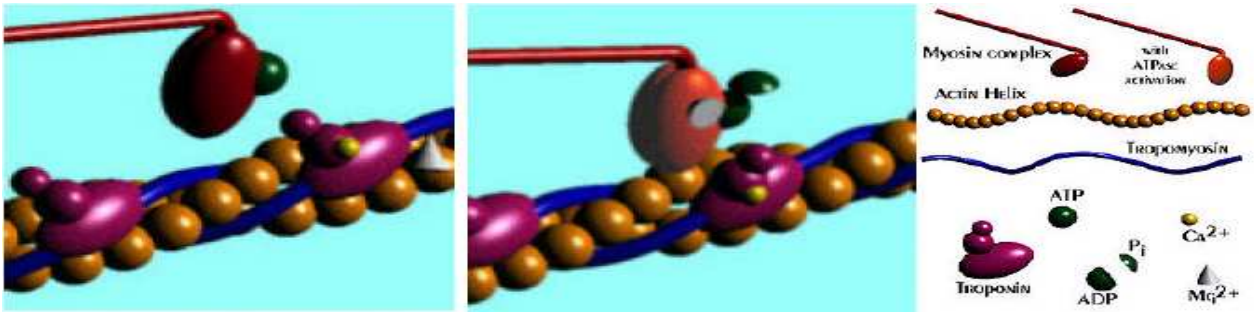

Figure 2-12 Actin myosin binding [28]

2.2.2 Hodgkin-Huxley Membrane Model

The structure of the nerve fiber consists of proteins and double layer of lipids and the neuron membrane can be modeled as an electrical capacitor. The thickness of the membrane is on the order of 10nm and according to some experimental results; the capacitance of the cell membrane is approximately 1-2μF/cm^2. This provides relative dielectric permitivity (ε_r) in between 11 and 22 [29].

Since the lipid bilayer membrane is semi permeable to ions, ions are dispersed across the membrane. The potential differences exist across the cell membrane due to the separated ions. The charged ions, K^+, Na^+, Cl^-, Ca^+ generates currents through the membrane and the currents continue along the neuron[28]. The potential differences caused from the dispersed charged ions are described by using the Nernst Equation;

$$E_i = \frac{RT}{zF} \log \frac{[i]out}{[i]in} \quad , \tag{2.1}$$

where R is the thermodynamic gas constant, T is the absolute temperature, z is the ionic valency, F is the Faraday constant and [i] is the concentration of the ion of interest. In an extracellular side of a typical neuron contains ~460mM Na^+ and ~10mM K^+, whereas the concentration constituents of an intracellular side of the membrane are ~50mM Na^+ and ~400mM K^+. Since the concentration differences across the membrane and semi-permeable specification of the membrane cause resting potential as ~70-80 mV. [29]

Figure 2-13 schematically depicts the cell membrane and its resistor-capacitor model. A typical cell membrane is formed by intrinsic and extrinsic proteins, double layer lipids, intracellular and extracellular receptors. Some scattered proteins on the membrane make pores that provides with ions transfer across the membrane. These proteins are modeled by electrical resistors and double layer lipids are represented as capacitors.

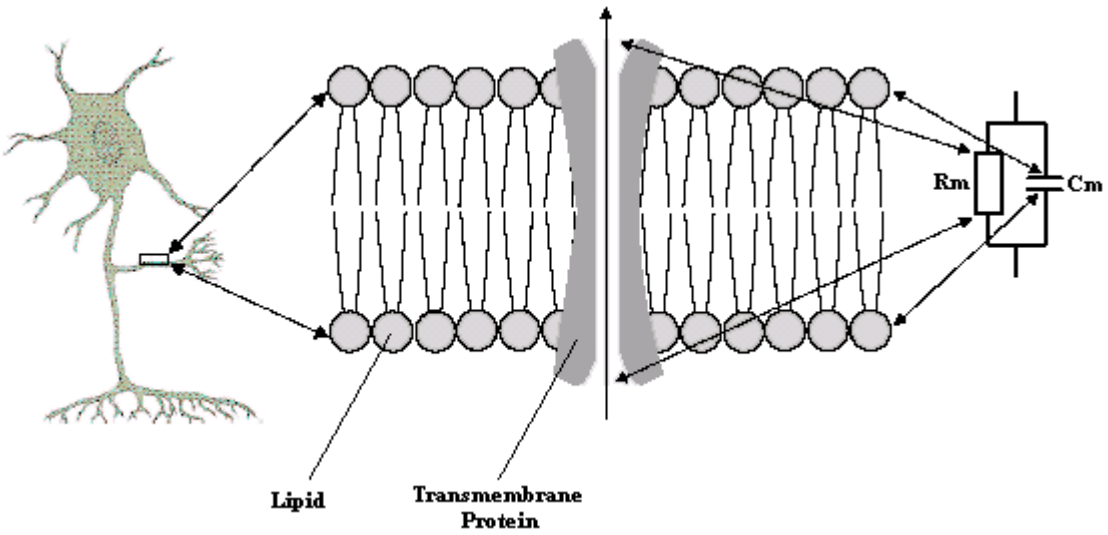

Figure 2-13 Cell membrane and its resistor-capacitor model [32]

The Hodgkin – Huxley model of a nerve membrane was generated by making experiments on giant axon of a squid. In the giant squid nerve experiment, some ions, K^+, Na^+ and the various other ions (mainly formed by Cl^- ions) became the interested chemicals. These other ions which are the less significant effect on the membrane model are called leakage ions. As to Hodgkin Huxley, electric current flows into the cell through the channels during the activation and represented by the parallel conductance model. The currents are demonstrated on this model, that are generated by Na^+ ions, K^+ ions, the leakage ions and capacitive current[33]. The net current flowing to the cell through the channels charges the membrane capacitance and gives rise to potential difference (V_m).

Here is the equivalent circuit model (Figure 2-14) for a patch of cell membrane and the mathematical model of a membrane that is based on the Kirchhoff's circuit law.

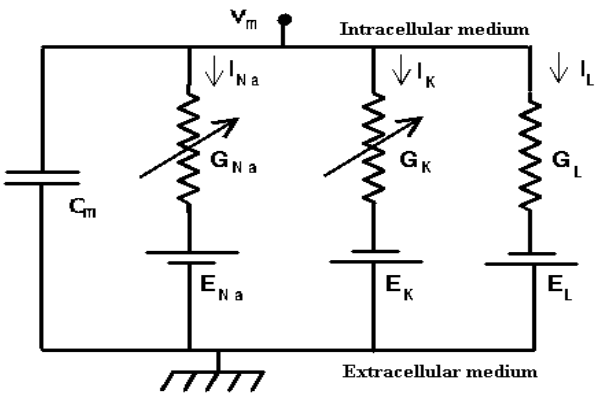

Figure 2-14 The equivalent circuit model of the cell membrane

$$I_m = C_m \frac{dV_m}{dt} + (V_m - E_{Na})G_{Na} + (V_m - E_K)G_K + (V_m - E_L)G_L \quad , \qquad (2.2)$$

where I_m is the membrane current per unit area [mA/cm²], C_m is the membrane capacitance per unit area [F/cm²], V_m is the membrane voltage[mV], E_{Na}, E_K, E_L are the Nernst voltages for Na^+, K^+ and leakage ions[mV], G_{Na}, G_K, G_L are the Na^+, K^+ and leakage conductances per unit area[S/cm²].

2.2.3 Action Potential

Action potential provides communication between neurons and the target muscle. It occurs owing to electrostatic potential difference between the intracellular and extracellular area of the neuron. Since the cell membrane has semi-permeable property that some ions are allowed to enter to or exit from the cell, whereas some are not allowed. The reason of potential difference is caused by the distribution of ions inside and outside of the cell and its permeability property. The action potential can be divided into five phases: resting potential, threshold, rising phase, falling phase, recovery. When the cell is inactive, its voltage equals to resting potential, that is -70mV. If the membrane of an excitable cell becomes depolarized beyond a threshold, action potential starts (Figure 2-15). Action potential occurs when opposite charges exist on two sides of the cell membrane.

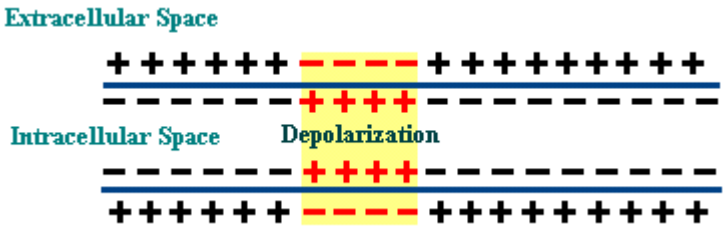

Figure 2-15 Initial Phase of the Action Potential: Depolarization

The duration of an action potential takes the order of few milliseconds (Figure 2-16).

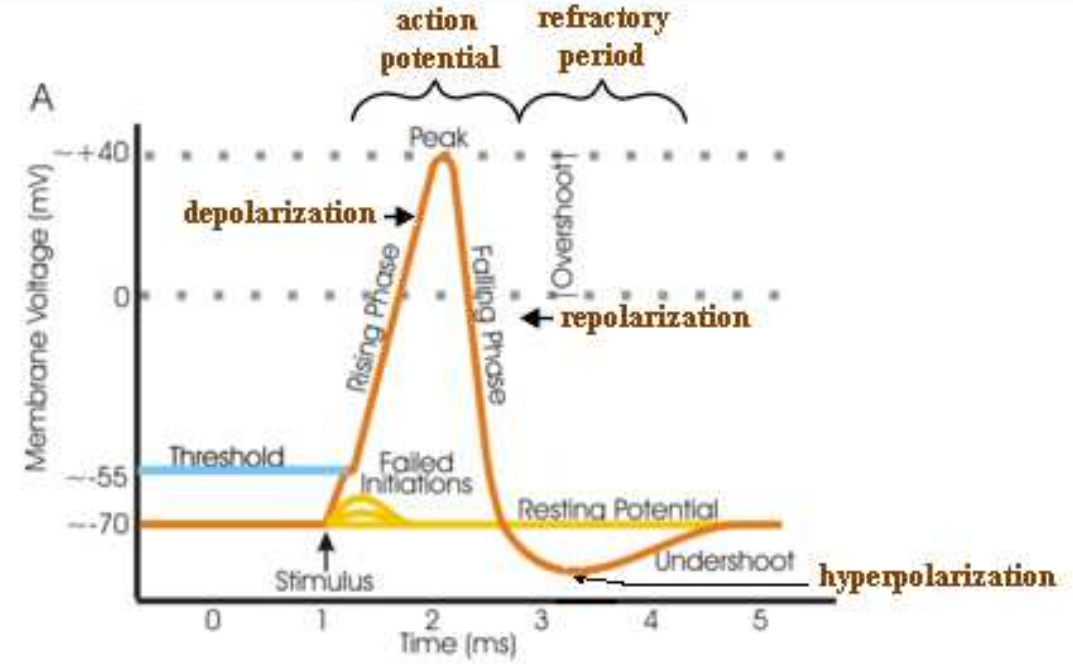

Figure 2-16 Action Potential in Time [34]

An action potential continues at the end of the axon. To illustrate, in this research, we are interested in the action potential that propagates from the brain to the spinal cord and also throughout the motor neuron. At the end of the axon, action potential stimulates the neurotransmitters in the synapse (in Figure 2-17) to starts a new action potential travel for continuation of the signal, e.g. from spinal cord to alpha motor neuron ended in the forearm (in Figure 2-18).

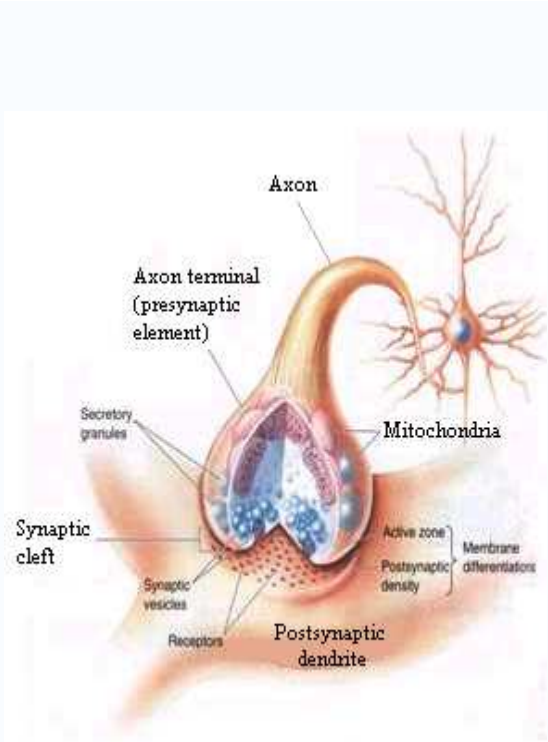

Figure 2-17 Synapse at an axon terminal [24]

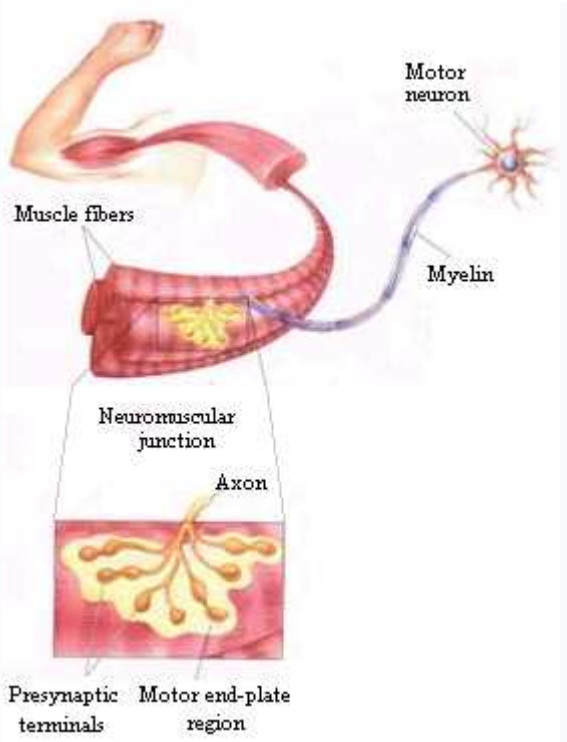

Figure 2-18 Action potential pathway [24]

As observed from the Figure 2-19, action potential is separated into several phases and each of them reflects the potential changes of the cell. The resting potential occurs when there is no action potential. In this phase inside of the cell is polarized by -70mV relative to the outside. The action potential takes place owing to the two main reasons, the changes of ion concentrations of the both sides of the cell membrane and existence of semi-permeable membrane to the ions. The fluids in the intracellular and extracellular area have Na^+ and K^+ ions and their transportation is supplied by Na^+–K^+ pumps placed across the cell membrane. Their transportation is based on a rule that when two K^+ ions pumped into the cell for every three Na^+ ions pumped out. Na^+ and K^+ pumps play a significant role in the resting membrane potential.

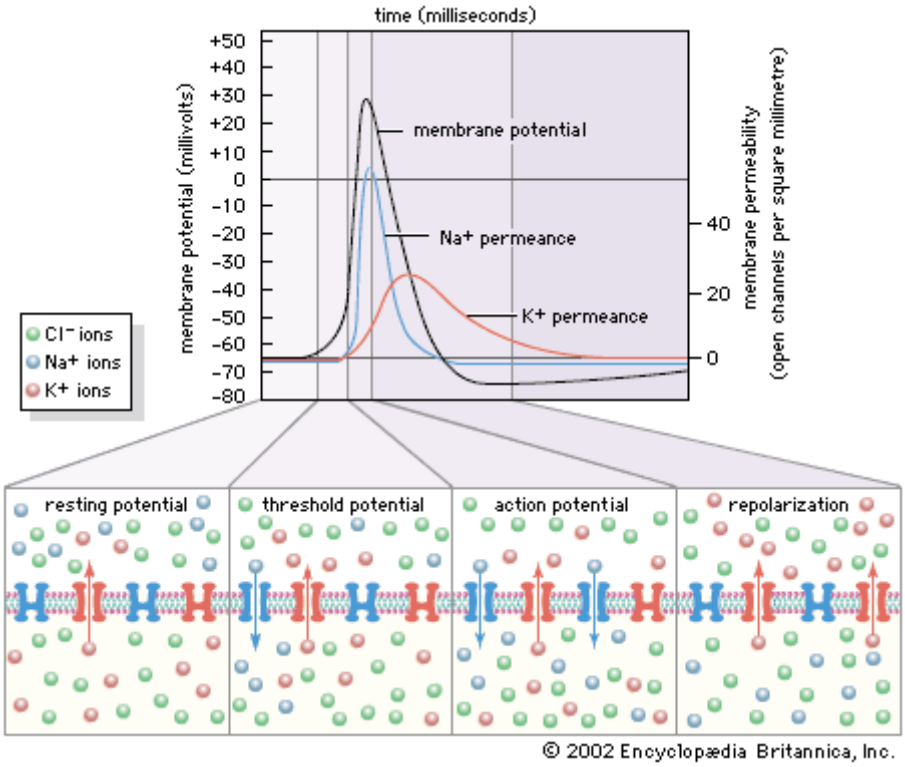

Figure 2-19 Na^+, K^+ ion changes During Action Potential [35]

Apart from the Na^+ and K^+ pumps, there are also potassium leak channels that affect the resting potential value of the cell membrane. Depending on the Na^+ and K^+ ions concentration, diffusion of the ions across the open ion channels of the membrane occurs under the influence of their electrochemical gradients. If equilibrium exists only based on diffusion and electrochemical gradients, the number of Na^+ ions which transferred will equal to the number of K^+ ions. As mentioned before, the cell membrane is 1.5 times more permeable to the K^+ ions. The potassium leak channels are always open to K^+ ions. Therefore, the cell's resting potential is closer to the equilibrium potential of K^+ (E_K=-80mV) than equilibrium potential of Na^+ (E_{Na}=60mV).

Depolarization is started by opening of the Na^+ channels and the entrance of the Na^+ ions into the cell. Since more Na^+ channels open, the Na^+ current is over the K^+ leak current and the potential of inside of the cell membrane becomes positive. When membrane potential becomes +50mV (peak value), gates of Na^+ ions start to close and the amount of influx of the Na^+ ions to cell reduces. At this time the voltage sensitive activation gates on the voltage-gated potassium channels start to open. Since the voltage-gated K^+ channels are open, K^+ ions diffuse out. The transfer of the K^+ ions makes membrane potential negative and causes

repolarization phase of action potential occurs, so inside of the cell reaches its resting potential value, -70mV.

2.3 Measuring Biopotential

As illustrated in Figure 2-20, action potential is transmitted via α motor neuron to a motor unit that composed of many muscle fibers. Under the electrodes which are placed on the surface of the skin, there are many muscle fibers to be sensed. Therefore, the measured signal is the superposed of the all the action potentials. The triphasic sum is called Motor Unit Action Potential (MUAP). Since it is bipolar signal which has symmetric distribution of negative and positive amplitude, its mean value becomes zero [36].

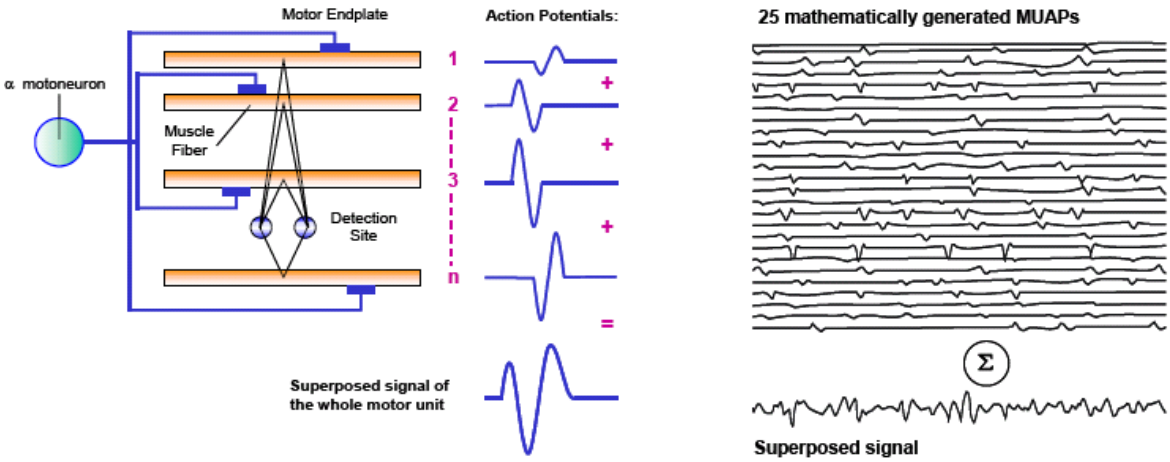

Figure 2-20 Superposition of the Action Potentials [36]

2.3.1 Electromyography (EMG)

Biomedical signal is an electrical signal acquired from the any organ is a function of time and defined in terms of amplitude, frequency and phase. EMG abbreviated as electromyography is a biomedical signal and the measuring and recording technique for electrical potential during the contraction of muscle fibers. EMG indicates level of muscle tension while under the load carriage or stationary position condition.

EMG signal is an invaluable information source for biomedical engineering. EMG signals are open to use of clinically neurological diagnosis and biomedical applications, e.g. biomechanics, motor control, neuromuscular physiology, movement disorders, postural control, physical therapy. EMG can be classified into two fields as to intended use, neurological EMG and kinesiological EMG. Neurological EMG observes the artificial muscle response stimulated by external electrical impulses under the static condition. Kinesiological EMG observes the neuromuscular activity of muscles under various conditions, e.g. different static and dynamic motions, trainings and treatments (rehabilitation).

A simple model for the EMG signal is represented as $x(n) = \sum_{r=0}^{N-1} h(r)e(n-r) + w(n)$ where x(n) is the modeled EMG signal, e(n) is the firing impulse, h(r) is the MUAP and w(n) is zero mean additive white Gaussian noise and N is the number of motor unit firings. EMG signal is a random signal whose value at each instance is a random variable [37].

The raw SEMG signal is directly recorded from the skin via electrodes, that is, this signal does not go into any processes or filtering application, is just superposed of all MUAPs under the surface electrodes. The raw EMG signal composed of spikes shows random characteristics, namely, can not be exactly reproduced again during the recording. The random characteristics of the raw signal occur due to the changeable recruited motor units. The frequency range of raw EMG signal is in between 2 to 500Hz (skeletal muscles), the dominant energy of the EMG signal exists in the 50 and 150Hz range and amplitude range of the EMG is between +/- (50uV-5mV) [38].

The EMG recordings present various results according to genre, age and also each individual. For instance, EMG amplitude is recorded as higher value for females with respect to the males under the same conditions due to the requirement of more motor unit contribution to that action for women.

2.3.2 Biopotential Electrodes

Muscle action potential, hence, currents are measured and recorded by an interface between the body and the electronic devices. These interfaces are called electrochemical

sensors, namely electrodes. During the measurement, currents flow to the data acquisition devices. This current is very small; but has never zero value and therefore, biopotential electrodes need to have good conducting specification to transmit the body currents to the circuit. Biopotential electrodes change the ionic current into the electronic current. Since charges in the body are carried by the ions, currents in the circuit are caused by flow of ions.

Electrodes are classified as to their various specifications, e.g. their polarity, geometry and their internal (invasive) or external (non-invasive) usage [39, 29, 2]. There are two types of electrodes with respect to their polarity specifications, polarizable and non-polarizable electrodes. In non-polarizable electrodes, current passes freely through the electrode-electrolyte interface, and requires no energy for transmission. In the experiments of this research, silver/silver chloride (Ag-AgCl) electrodes are used; since their characteristics are very close to perfectly non-polarizable electrodes. As observed from the Figure 2-21, Ag metal is coated with the soluble ionic compound containing Ag^+ and Cl^-. AgCl can be soluble in water very low speed, so Ag/AgCl electrode is immersed into the electrolyte pool which contains Cl^- ions. In order to prevent the dissolution problem of surface layer of electrode, electrolyte should be saturated with AgCl. Two chemical reactions occur under these conditions. The first one is oxidation of Ag atoms from the surface layer of the electrode and the second one is the precipitation caused by the reaction of Cl^- ions in the electrolyte and free Ag^+ ions leaved from the structure of layer. In human body, Cl^- has very high concentration, so its concentration remains constant [39].

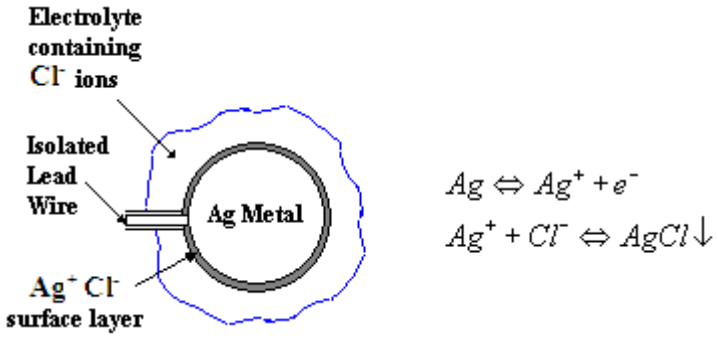

Figure 2-21 AgCl EMG Electrode

Two types of electrodes can be used for sensing the EMG signal, which are classified fundamentally as invasive and non invasive electrodes. The needle electrode, the invasive one, directly contacts with to the muscle tissue and can measure just one MUAP of the target

fiber without any interference. The surface electrode, the non-invasive one, is placed onto the surface of the skin and measure the superposed MUAP of the target muscle under the skin.

In surface electrode applications, recorded EMG signal is more sensitive to the several parameters than needle electrode applications; it, however, is preferred to invasive method [40]. Electrode placement, noise and artifact problems and selection of surface electrode types have direct impacts on measuring and recording of EMG signal.

There are many types of EMG electrodes as far as their geometry is concern, e.g. monopolar, bipolar, tripolar, multipolar, barrier or patch and belly tendon electrodes [39, 2].

Bipolar electrodes which have two conductance parts (active parts) are used with one reference electrode (inactive part) situated at distal placement of bipolar electrodes. It has advantageous side in the case of noise elimination and is sensitive to gradually changes in the muscle activity between two electrodes, whereas is very sensitive as regards the electrode placement constraints.

Monopolar electrodes record the signal by using one electrode and also need an electrode to be used like reference electrode and placed over the low muscle activity area for comparison. Monopolar electrodes outperform as to sensing variations in absolute levels of electrical activity [41].

2.3.3 Factors Influencing the Quality and Fidelity of the SEMG Signal

EMG signal very sophisticated and non-stationary signal carries additive noises during its traveling time from its origin to the target muscle. Recording high quality and fidelity raw EMG signal requires awareness of internal and external factors [42] negatively affecting the signal structure and their solutions. These factors disturbing the EMG signal during the recordation can be accumulated into several groups;

I. Causative Factors: They directly affect the signal and can be divided into two classes.

   i. Extrinsic Factors:

Extrinsic Factors discussed in detail below are caused by electrode structure and placement.

Since the EMG signal characteristic can be defined as low amplitude and easily affected by the ambient noise, some methods to be able to measure the signal are developed. The reasonable technique is measuring EMG signal from two points of the muscle by subtracting them from each other and exposing the result to the amplification process. The detection points on the skin play an important role in the signal quality. In other words, electrode placement is a big issue on its own. The shorter or longer than required displacement between center of two electrodes causes changing on the signal characteristics, e.g. frequency spectrum, bandwidth. In practice, the selection between the electrodes is determined with respect to the size of muscle. In this research, the first muscle group, the second muscle group, the third muscle group and the last muscle group are responsible for flexion of the two, three, four and five numbered digits; extension of the two, three, four and five numbered digits; flexion of the thumb; and the extension of the thumb, respectively. The first group contains flexor digitorum superficialis and flexor digitorum profundus, the second group consists of extensor digitorum, the third group is composed of flexor pollicis longus and the last group contains the extensor pollicis longus, extensor pollicis brevis and abductor pollicis longus [31]. The distances between metal parts of the electrodes for are selected as two, two, two, one cm respectively.

Apart from the distance between two electrodes, their locations and orientations on the muscle also play a significant role in the measured signal characteristic. Various measurements of EMG signal occur if the electrodes are not placed in a suitable way. For instance, for the EMG measurement with the bipolar electrode, placement of two electrodes plays an important role in the amplitude and frequency spectrum of the EMG signal. As observed from the Figure 2-22, when the top electrode is located to the innervations zone of the muscle, for second electrode various placement selections give rise to different results. When the electrodes are placed onto the near the tendon of the muscle, measured signal is weak. Since muscle fibers are getting thinner and their number diminishes near the tendon area. In addition, it is difficult to locate the electrodes in this narrower side of the muscle. Motor point is not also a reasonable selection for electrode placement area. Moreover, the edge of the muscle for as a placement location leads to cross talk problem caused by neighbor muscles. The best result is obtained when the electrodes is placed onto the middle point of the muscle (between motor point and the tendon insertion or between two motor points). Orientation of the electrodes has to be arranged in a line of the muscle length so both of the electrodes contact with the same muscle. [42].

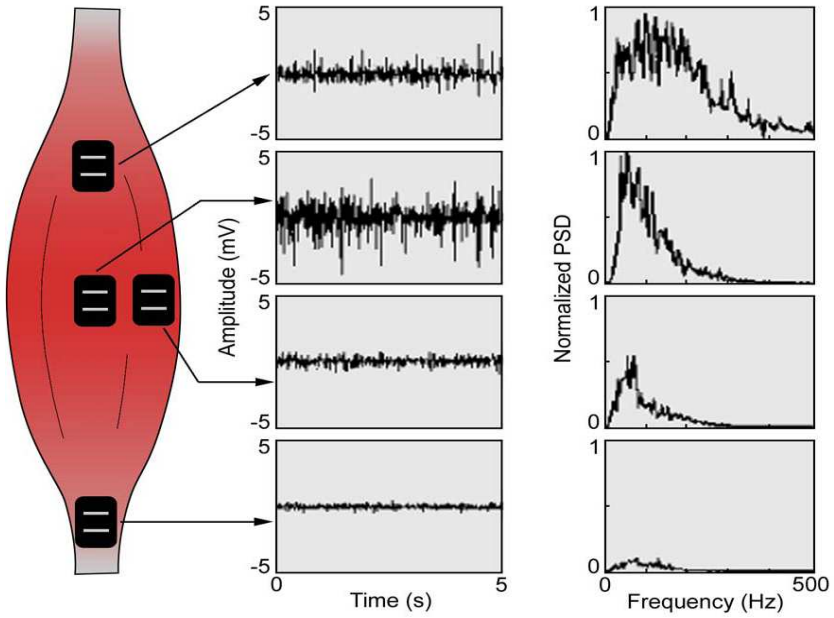

Figure 2-22 Importance of Electrode Placement Selection [42].

Another characteristic of electrode which will affect the signal fidelity is area of electrode. The amplitude margin of the signal is directly proportional to the size of the conductance area, since the conductance surface transmits the superposed amplitude signal which collected from the muscle fibers under the conductance part of the electrode. The 1cm length of electrodes is advised for good detection surface area. In this research, 1cm diameter, disposable surface electrodes are used. [42 ,44].

The resistance between two electrodes should be less than 10kΩ. However this value should also be accepted to some extent. Too much low resistance can be realized if both conductance of bipolar electrode are closer than necessary distance, that is, short circuiting can occur in these couple of conductance. In other words, resistance value between these two conductances is a kind of indication of placement accuracy of electrodes over the muscle of interest [36].

ii. Intrinsic Factors

- Characteristic of tissue and its cleaning conditions

Tissue structure shows difference for all individuals that emanate from the lipid thickness between the electrodes and muscles (Figure 2-23), skin conditions, e.g. level of cleanliness, hair density on the surface of skin and affect the signal structure directly.

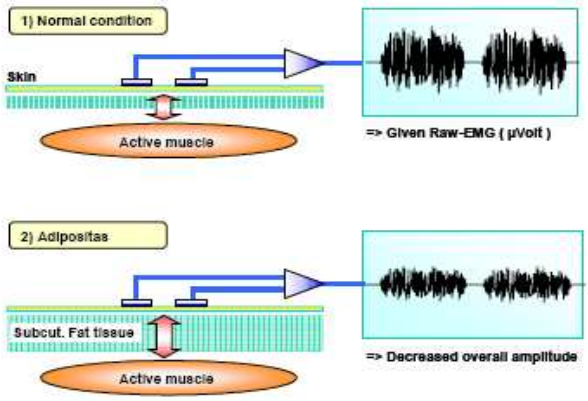

Figure 2-23 Effect of the characteristic of the tissue [36]

- Other intrinsic factors

Blood flow, fiber diameter, depth and location of active fibers and thickness of the tissue between the surface of the muscle and electrode are also other physiological, anatomical and biochemical factors. In this research, effect of the depth of active fiber is demonstrated on the Figure 2-24. The flexor pollicis longus muscle is placed deeper than the other muscle groups. It is the one of the main reasons that its amplitude is smaller than the others.

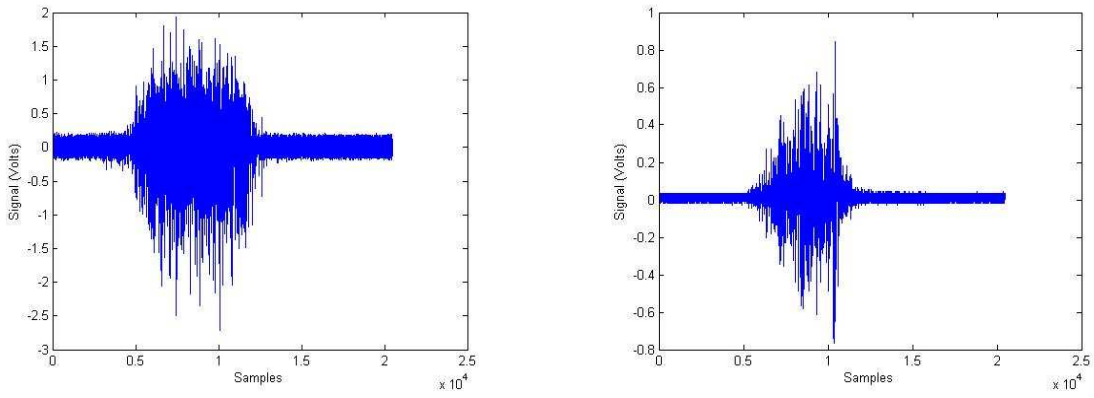

Figure 2-24 Extensor Digitorum and Flexor Pollicis Longus (from left to right)

II. Intermediate Factors

Neighboring muscles in the vicinity of measured muscle generates a significant amount of EMG signal and this cross talk contaminates to the measurement. Cross talk effect should not pass the limited which is 10%-15% of the main EMG signal. The other interference which highly affects the EMG signal by its electrical signal is ECG signal (Figure 2-25). The electrocardiogram (ECG) is the electromyogram (EMG) of the heart muscle [43]. ECG signal especially dominates on the upper trunk/shoulder muscles EMG recordings.

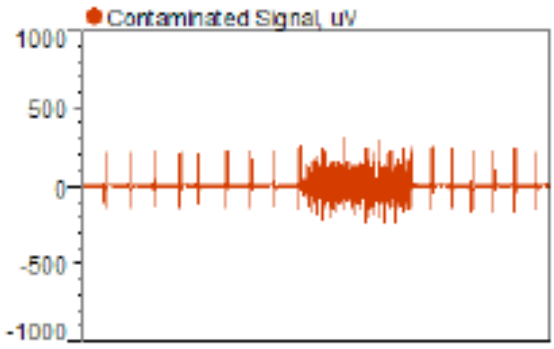

Figure 2-25 ECG cross talk on EMG signal [36]

III. Deterministic Factors

These factors are related to the anatomic specifications of the muscles. The active muscle numbers, motor firing rate, mechanical interaction among muscles affect the measured SEMG information. Changing in the time interval and amplitude of the MUAP also make some differences in the measurement.

2.3.4 Characteristics of the Electrical Noise

i. Inherent noise in electronics component

Electronics components produce the noise and the frequency range of this noise is in between 0 Hz (DC) to several thousand Hz. The effect of this noise can not be removed from the system; but reduced using high quality components and logical circuit design.

ii. Ambient Noise

The reason of this noise is caused by electromagnetic radiation, which affects the entire environment, e.g. human body and electronic circuits.

iii. Power line Noise

Power line noise is caused by the surrounding sources. The frequency of the noise is 50/ 60Hz and its amplitude is larger than the EMG electrodes [44]. Other devices and humans around the sources are exposed to the surface current. It seems as AC power source. The power line interference is very large signals with respect to the EMG signals. In addition, power line noise is usually constant, whereas EMG signal is random and changes continuously. Since the measured output signal is the subtraction of two sensed signal from two electrodes, then the result shows only difference of the signals acquired via two EMG channels. However, the noise can only be removed in ideal case of the electrodes and instrumentation amplifier (In-Amp). In reality, both electrodes and In-Amp do not present pure EMG signals.

iv. Motion Artifact

Instability of the electrode placement on the skin and cable movement between the electrodes and signal conditioning circuit lead to motion artifact problem. The solution of this noise is can be solved by making proper design. The frequency range of the motion artifact is between 0 Hz and 20 Hz.

v. Inherent Instability of Signal

Since the characteristic of the signal is non-stationary and random and unstable frequency region in between 0 Hz to 20 Hz is observed since the quasi-random nature of the motor unit's fire reveals at that range.

2.3.5 The Importance of Isometric and Anisometric Contraction on This Research

The small movement on the active muscle fiber directly affects the objective EMG signal. If area on which the electrodes are placed changes due to the non stationary condition, the target fibers which are responsible for the target motion also change; therefore measured signals digress from their object.

Anisometric contraction whose muscle is responsible for both force and motion causes non-robust measurements due to its varying motor unit position under the electrodes. The alternation in the length of muscle leads to displacement of the electrode and requires area of the surface of the muscle changes. That is since isometric contraction in which a muscle exerts force but does not change in length is selected for studying. Under the requirement of quantitative relations between the EMG signal and force, isometric contraction has to be preferred. Even in this circumstance, their graphs can not show the idealistic linear result.

This issue directly shows its importance on this research. To illustrate, disabled people can not make anisometric movement with their muscles responsible for their amputated organ. For hand amputees, they do not have a chance to move their digits due to the lack of their hand. That is since, in reality, all the measured SEMG signals have to be collected by making isometric contraction from them. In this research all the experiments are progressed on the isometric contractions and extensions by fixed the hand under static load. All the experiments are done under approximately 100 % MVC (maximum voluntary contraction).

3 DATA ACQUISITION

Giving a meaning to raw EMG signal exposes to some formations, i.e. detection, decomposition, processing, classification. Before digital signal processing of SEMG signal, high and low frequency noise and artifacts have to be eliminated to get the best performance for further processing. In this chapter, the configuration and the material to be used in the EMG data acquisition device will be discussed with their reasons. Satisfactory prehensile EMG classification directly depends on high quality feature selection. Successful feature selection can only be acquired with a data acquisition device which has high accuracy and fidelity. Acquired and processed SEMG signals will be used for multifunctional prosthesis. The prosthesis can make four motions, flexion and extension of thumb, and flexion and extension of the other four digits. However, there should be an interface between the device and prosthesis to perform the classification of these four different motions. To transfer the analog signal obtained by the data acquisition device to digital environment for the processing MCC Data Acquisition Hardware (DAQ) is used.

As discussed in the previous chapter, SEMG signals are sensed with bipolar electrodes and sent to the data acquisition device. Figure 3-1 shows all the main processes SEMG signals have to be exposed to. In this chapter, the first part of this chain will be discussed in detail. As seen from the Figure 3-1, to collect the data from surface of the skin, various conditioning methods will be applied. The data acquisition system is divided into two main parts to obtain the result accurately. The first part called circuit on electrodes which is directly placed onto the electrodes as close as possible for high SNR measurements contains the amplifier and prefilters. The second part called the base circuit which is the base for the filtering purposes and power supply includes active band pass filter, common mode signal reduction part and an active rectifier.

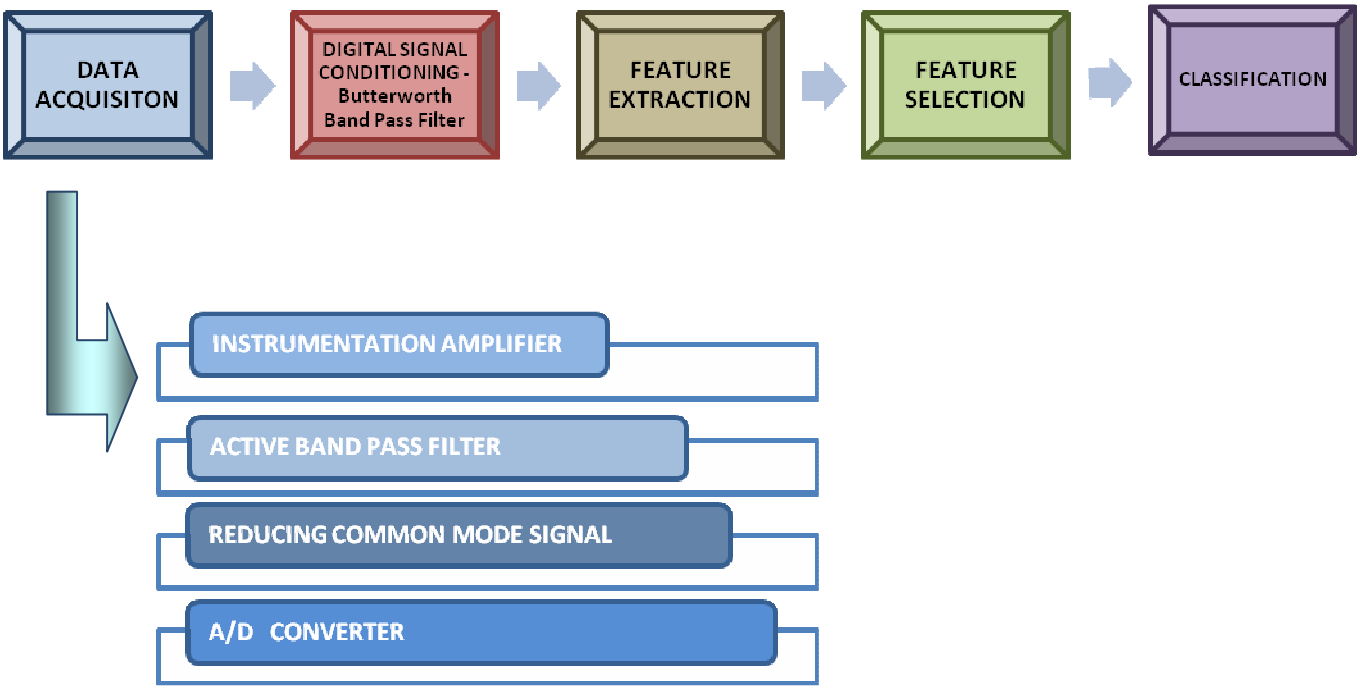

Figure 3-1 Schematic Description of SEMG Signal Processing

USB-connected analog and digital I/O module (DAQ) contains 8 single ended inputs. It has 11 bits resolution. Since only 4 channels are in use in this research, data can be acquired from four channels at 12,5kS/s.

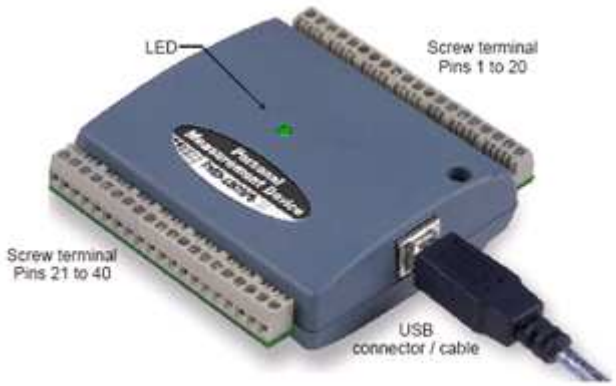

Figure 3-2 DAQ Hardware (Measurement Computing)

A/D conversion is executed by sampling and quantization of the analog signal. However, A/D conversion causes the loss of data due to using the only sampled part of the

signal. In order to minimize data lost from original signal Nyquist theorem has to be considered.

According to Nyquist theory, sampling frequency has to be bigger than or equal to maximum frequency signal contains. Since the SEMG signal is in the range of 6-500Hz, then maximum frequency used in Nyquist theory becomes 500Hz.

$$f_s \geq 2f_{\max} \Rightarrow f_{s_{\min}} = 2*(500) = 1000Hz \qquad (3.1)$$

Selection of sampling frequency less than 1000Hz causes undersampling and it leads to aliasing. In other words, reconstruction of the signal is lack of accuracy from the original one. To prevent aliasing and increase the similarity between analog and digital signal, sampling frequency is selected as 2048 Hz [45]. Selection of more than sufficient sampling frequency is called oversampling. Avoiding data loss can be compensated by oversampling the original signal. Interpolation of samples with more data reveals the more realistic digital signal to the original one.

Due to the A/D conversion and 11 bit resolution of the DAQ, quantization error exists. This error is the main drawback of analog to digital conversion and the digital signal processing.

$$\Delta = \frac{V_{ref}}{2^N} = \frac{10V}{2^{11}} = 0.00488\,V = 4.88mV \quad , \qquad (3.2)$$

where N: number of bits and Δ: quantization error

In this case, the digitization process is able to resolve input voltage fluctuations that are more than or equal to 4.88 mV. There are some important criteria that determine the analog to digital converter (here it is DAQ) specifications. The first one is that the ADC has to include the full span of input voltage to prevent the loss of useful data. In this study, the method is to keep the output signal between pick to pick amplitude of ±5V. It has to be stated that it is better to select the resolution higher than 4.88mV. However, in such a case A/D range has to be smaller. In other words, there is a trade off between resolution and range. If there are various A/D options for this study an A/D that has higher number of quantization bits is selected. The second essential issue for A/D selection is input noise of the system. One advantage of 4.88mV resolution is the elimination of the contribution of the low amplitude noisy signals that are in the microvolt range to the output.

3.1 Configuration of the Circuit on Electrodes

Placing the first stage of the circuits onto the electrode site provides the elimination of the ambient electrical noise during the amplification process of the SEMG signal. Hence, the SEMG signal emitted directly from the muscles is amplified without amplified 50/60Hz (50 Hz in EU) power line noises. Formerly, to eliminate the 50Hz ambient noises, notch filters were in use; however it brought together with some problems. Most of the energy in the signal is in the frequency range between 50-150Hz and notch filters can not behave ideally. Therefore, elimination of power line noise (50 or 60 Hz depending on country) and its neighbors cause loss of an important part of the useful data. Since longer wire between the electrode and the in-amp will cause more noise dominance on the weak electrode signal, the best solution is placing the instrumentation amplifier to electrodes as close as possible.

The entire circuit contains AD8221 as an Instrumentation amplifier and OP1177, 0P2177 and OP4177 precision low noise, low input bias current operational amplifiers. Since the signal is low amplitude, 1% tolerances resistors are used in the circuit.

In the following figures, the production processes of the circuits on electrodes are seen. Figure 3-3 is the open form and Figure 3-4 emphasizes the electrode placement on the circuit. Arrow-1 defines the 1 cm distance between bipolar electrodes for small size muscle, arrow-2 is employed for 2 cm distance for middle sized muscles and the arrow-3 provides good sensation for long muscles.

To reduce the electromagnetic noise from the signal, shielded cable is used as seen in Figure 3-5 and firstly nonconductive tape (Figure 3-6) and then ground connected aluminum foil is applied on the circuit (Figure 3-7). Against the environmental damage on the circuit components and sliding of the aluminum foil, silicon is liquefied and stiffened on it. Figure 3-8 shows the last condition of all the electrodes for signal measuring. To eliminate the motion artifact caused both by the motion of cable and electrode in its electrolyte, strips are used.

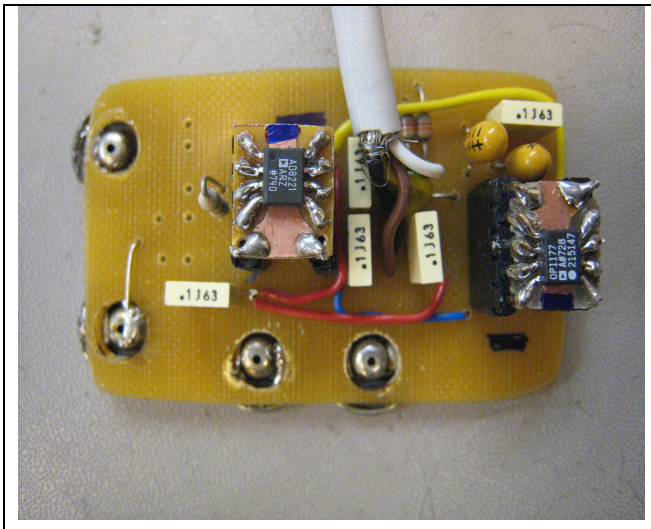

Figure 3-3 Top view of the circuit on electrode

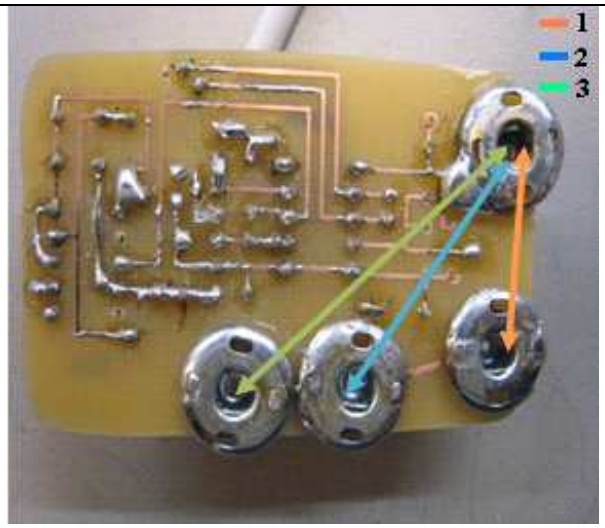

Figure 3-4 Electrode placement options

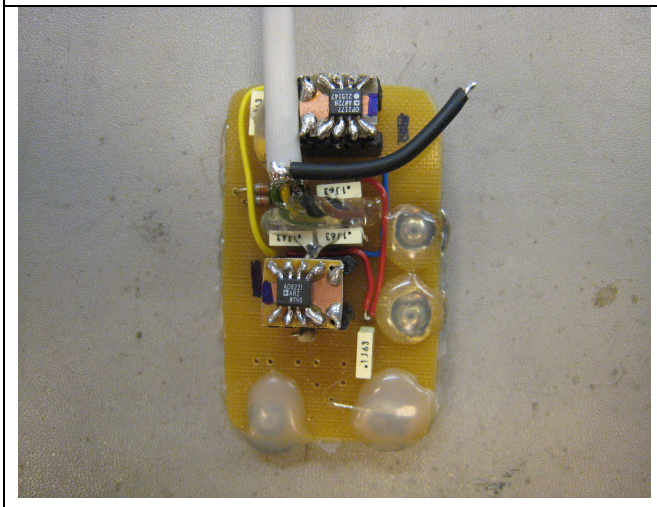

Figure 3-5 Shielded cable against electromagnetic noise

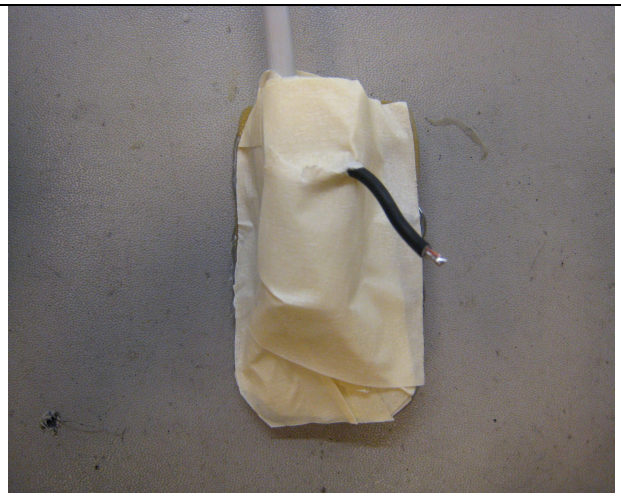

Figure 3-6 Fixation of cables

Figure 3-7 Shielding with Aluminum foil

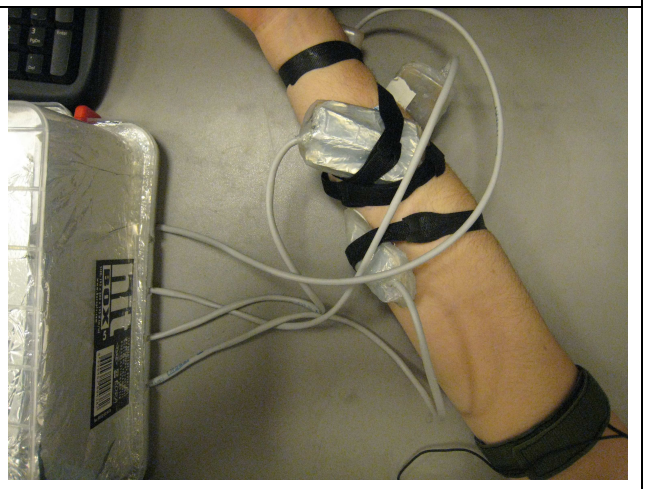

Figure 3-8 The last product in an implementation

3.1.1 Pre-Filters

The circuit is separated into two parts to reduce noise. The first one contains some pre-filters which are a passive low pass filter and an active high pass filter and amplifier. The reason of placement of pre-filters in this part emanates from the roughly elimination of the noises out of the 20-500 Hz frequency range. The amplifier is used for increasing the amplitude of the difference input signal which is about in the range of 0-10 mV.

There are many factors that limit the circuit performance. RFI (radio frequency interference) which is one of the degradation reasons appears as a DC offset on the signal within the range of about 3 Hz and 300 GHz. To diminish this effect on the EMG signal, high frequency parts of the input signals have to be subtracted from the total signal. In other words, the bandwidth of the input signal is narrowed. Passive low pass filter for each input signal is composed of simple R and C components reducing the RFI effect. As seen from the figure, each of the capacitor, C_c and C_d has different mission on the circuit. C_c which is a part of the low pass filter employed as reducing common mode signal; whereas C_d used for minimizing the mismatch effect between the R and C_c and improving the CMRR performance of AD8221 selected bigger than Cc. Their values are computed as seen below;

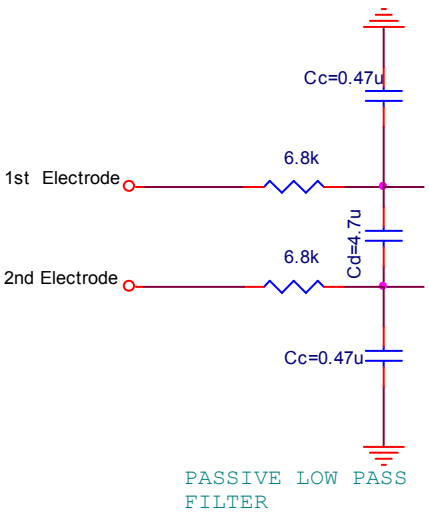

Figure 3-9 Passive low pass filter

Filter Frequency$_{cut\ off}$=500Hz

Filter Frequency$_{cut\ off}$ = $1/(2\Pi RC_c)$ (3.3)

Since R=6.8kΩ then, C_c=47nF

Cd >10C_c & selected as 0.47uF

Since the impedance of the capacitors becomes very low at high frequencies, high frequency component of the input signal is ceased. As it is mentioned the value of the C_d value plays an important role in the circuit stability. Very large selection of the C_d with respect to the others can cause small loop and cause instability problems as represented below.

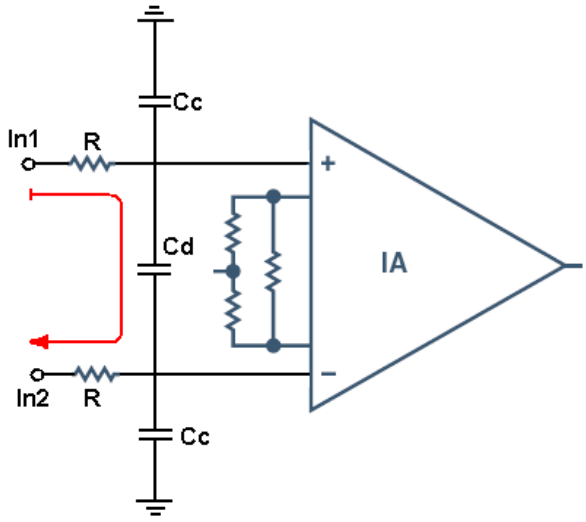

Figure 3-10 Importance of C_d selection

To decrease portion of low frequency signals, an active high pass filter is placed between reference and output pins of the in-amp. Hence, low frequency signals which are less than 20Hz at the output feed back to the system from reference input and the difference between input and reference is forced to zero. The value of components of active high pass filter shown below is computed as regard to cutoff frequency. Since cutoff frequency of active high pass filter is 20Hz, and R and C values are computed by using that equation below as 80k and 100nF respectively.

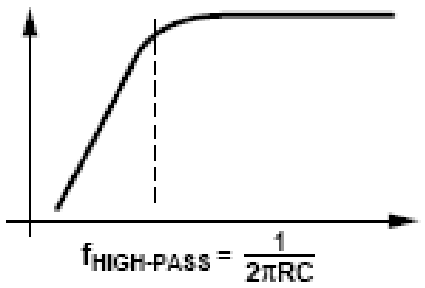

Figure 3-11 Expected frequency response of the filter

$$f_{Cutoff} = \frac{1}{2\pi RC} \Rightarrow 20Hz = \frac{1}{2\pi RC}$$

$$\Rightarrow RC = 0.007957$$

$$R = 80k \qquad (3.4)$$

$$C = 100nF$$

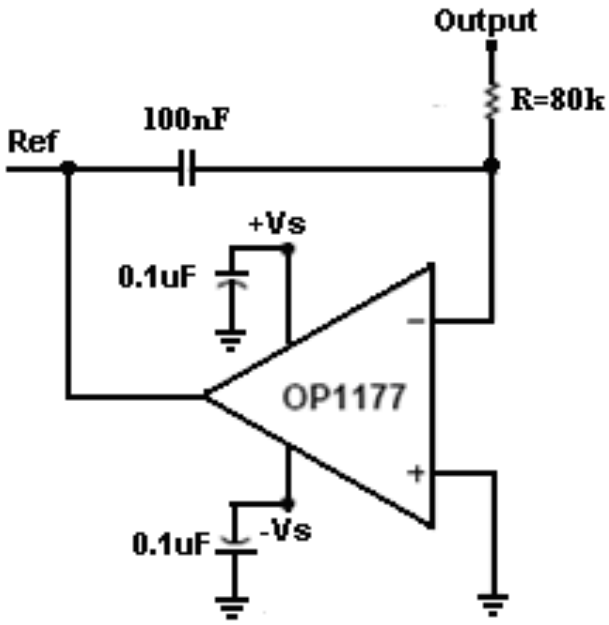

Figure 3-12 Low-frequency suppression

0.1uF non-polar and 10uF tantalum capacitors are employed in order to filter the ripples caused by the power supply in spite of the fluctuation of the voltage value. Noises caused by both environment and individual artifact have disturbance effect on voltage supply pins and are observed on the input signal. These two capacitors are employed as a by pass capacitor to send the noises to the ground.

3.1.2 Reducing Common Mode Voltage

The common mode rejection ratio (CMRR) of a differential amplifier is a measure of the tendency of device to eliminate the input signals that are common to both inputs. The effect of CMMR especially appears on small voltage signals that are easily affected by the voltage offset (common mode). Despite the fact that differential amplifier take the difference of two input, due to the non-ideal specification of op-amps the output of the signal shows the information with a voltage offset [49]. In this research, this issue is minimized by selecting the highest CMRR instrumentation amplifier. Much kind of biopotential applications require at least CMRR of 80dB. AD 8221 used as an instrumentation amplifier has 80dB CMRR until 10 kHz and 110dB at 110 kHz. Since there is a power line noise and our body has a capacitance of 100 to 400 pF, we store the common mode voltage in our body which

negatively affects the system [50]. This common mode signal is seen our measured signal as an offset voltage. The second solution after selecting In-Amp has high CMRR is using the inverting amplifier by sending the same signal to our body inversely.

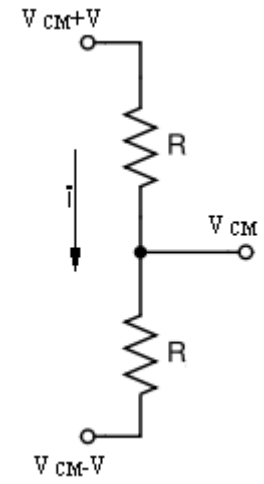

Figure 3-13 Detection of common-mode voltage

$V_{CM}+V-(V_{CM}-V) = 2V$ (3.5)

$2V/2R=i \rightarrow i.R= V$

Then midpoint voltage becomes as following;

$V_{CM}+V-iR = V_{CM}$

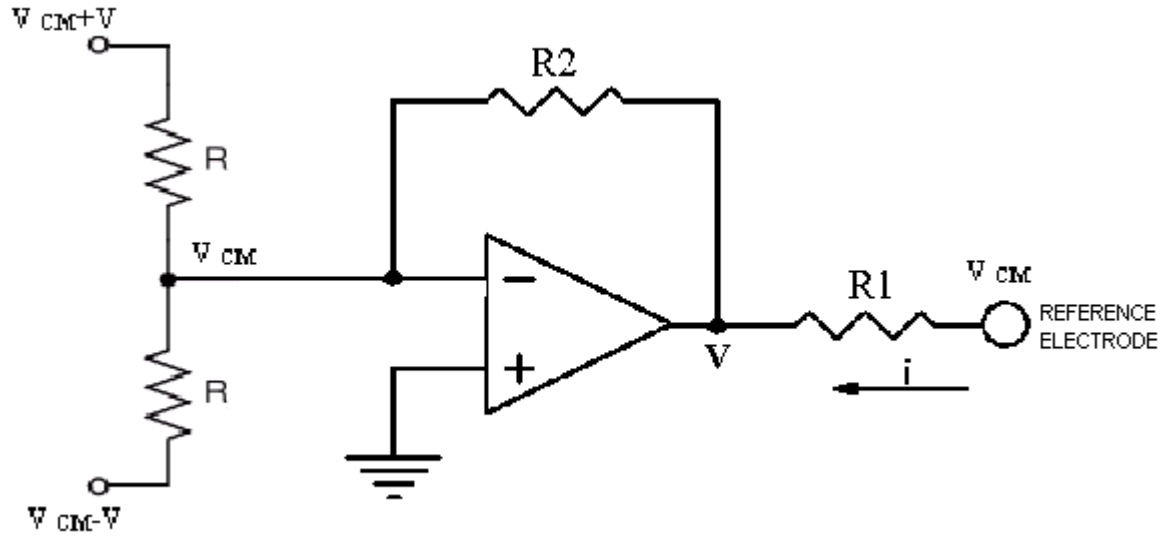

Figure 3-14 Reducing common-mode voltage

$$V = -\frac{R2}{R/2}.V_{CM} \rightarrow V_{CM} = i.R_1 - V_{CM}\frac{R_2}{R/2} \rightarrow V_{CM} = i.\frac{R_1}{1+\frac{2R_2}{R}} \quad (3.6)$$

The value of R is selected bigger with respect to the R_{Gain}. Since 2R and R_{Gain} are connected in parallel. Not to affect the value of $R_{Gain,}$ R is selected as 82k.

The gain range of In-Amp is obtained as 1 to 1000 with setting the external resistor, R_{Gain}. Since raw SEMG signals have 0 to 10 mV and R_{Gain} is set to 39 Ω and the gain is acquired as 1000. This is the maximum gain that can be obtained according to AD 8221 gain-bandwidth product. By selecting gain as 1000, the output voltage remains inside of the saturation voltage limit of the amplifiers. This selection is made so as to prevention of EMG data loss.

3.2 Configuration of the Base Circuit

3.2.1 Active Band Pass Filter

Despite the fact that low and high pass filtering are used at the beginning, some low and high frequency signals can pass into the amplifier due to the non ideality characteristic of electronic components. Therefore in the base circuit a fourth order active band pass filter is used [46, 47, 48]. The first part of the filter is the high pass filter and a second part of it is low pass filter. To increase the filter quality, it is doubled and fourth order filter is included to the system. In spite of the gain reduction, cutoff specification is increased. To compact the system, OP4177 that contains 4 low-noise Op-Amps is used.
The values of R and C are calculated according to cut frequency values (20 & 500Hz).

For high pass filters;

$$f_{Cut\,off} = \frac{1}{2\pi RC} \Rightarrow 20Hz = \frac{1}{2\pi\sqrt{R_1 R_2 C_1 C_2}} \tag{3.7}$$

For low pass filters;

$$f_{Cut\,off} = \frac{1}{2\pi RC} \Rightarrow 500Hz = \frac{1}{2\pi\sqrt{R_1 R_2 C_1 C_2}} \tag{3.8}$$

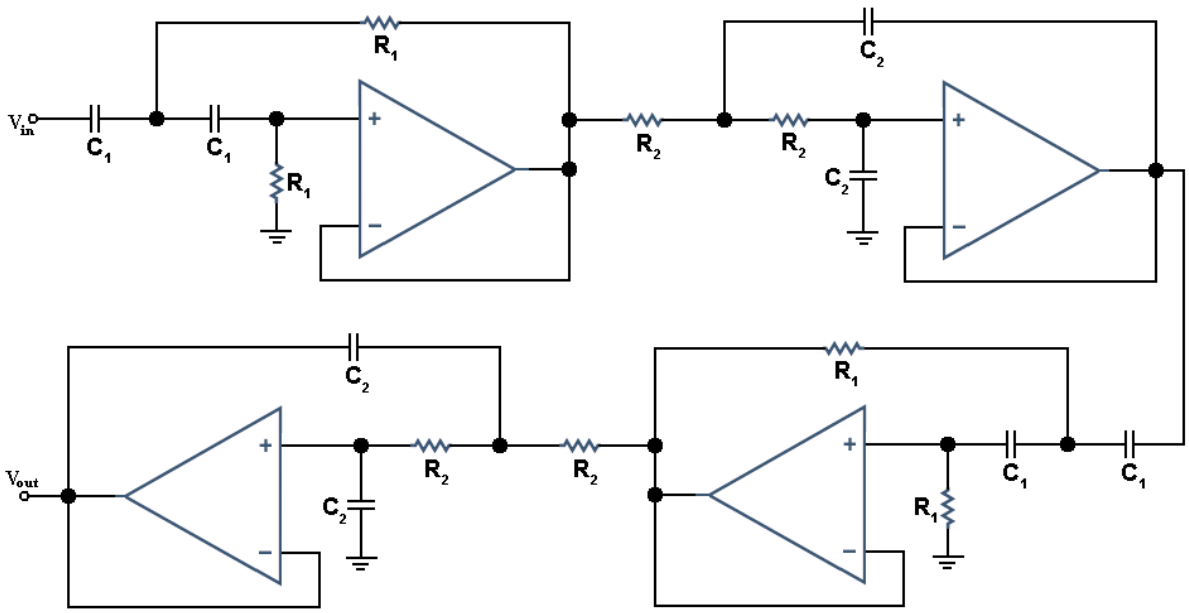

Figure 3-15 Active band-pass filter on the base circuit

3.2.2 Full-Wave Rectifier

EMG signals occur in both positive and negative voltage range; however only positive part of the signal is usable in some of the applications, e.g. window methods. Therefore, negative part of the signal has to be removed from the entire signal. Half-wave rectifiers can make negative part of the signal away and solely positive parts remain. Since the SEMG signal is hardly sensed, negative parts have to be taken into consideration and performed as positive voltage [37]. This is since full-wave rectifiers are preferred in SEMG signal processing circuit configuration [47, 48].

Various configurations on the full wave rectification are designed. The main point to be considered in the selection of the full wave rectifier is preventing ripple effect on the output signal.

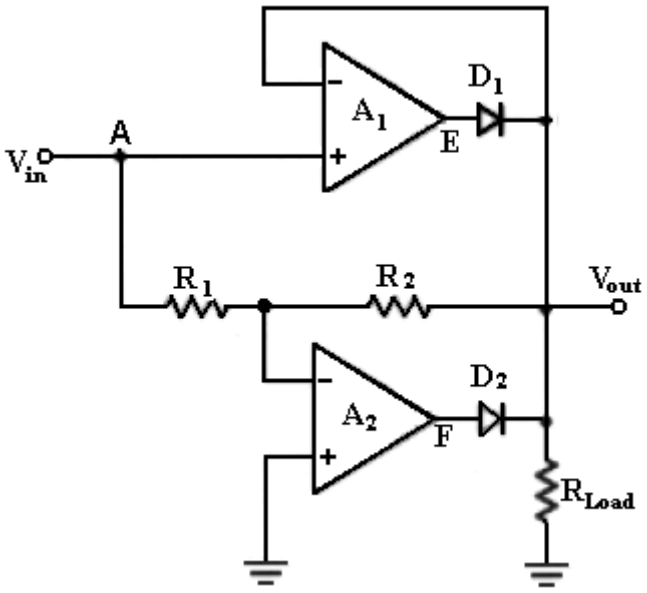

Figure 3-16 Rectifier on the base circuit

The continuation of the rectifier constitutes the R_{load} value. R_1 and R_2 are selected as 1kΩ to make gain of transfer function unity. As observed from the transfer characteristic of the circuit, while the positive voltage remains positive, negative voltage is converted to positive but amplitude of voltage does not alter.

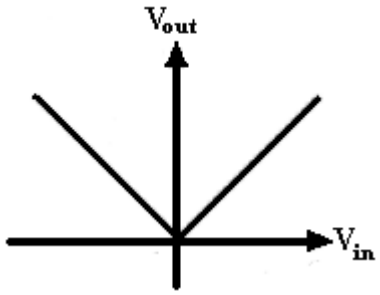

Figure 3-17 Input-output graph of the rectifier circuit

Full wave rectifier was added at the beginning of the research to be used for further signal processing applications in time domain and also to study the force-SEMG signal relationship. However, apart from the passive and active band pass filter, digital Butterworth band pass filter has to be employed. Since analog filters do not represent the ideal characteristic, Butterworth filter is used to reject almost all the rest of the undesirable frequency bands. In this case, if rectified signal is exposed to digital Butterworth filter,

rectification changes the frequency spectrum of the EMG signal and Butterworth filter rejects not undesirable frequency bands of the raw EMG signal but that of different signal whose frequency spectrum is altered due to the rectification. Since frequency information is a distinctive characteristic for EMG signal and time – frequency based processes are included in the further processes, the base circuit output is determined as active band pass filter. In other words, if a rectifier can be used only if there are ideal characteristic filters in the circuit or just time - domain based processes are applied to the signal.

3.2.3 Reference Circuit

Since there are four electrodes used simultaneously, each of them also needs four reference electrodes. To compact the system and reduce the need of number of reference electrode a buffer is used. Four reference outputs of the common mode reduction part of the circuit are connected to the buffer to send the V_{CM} to the reference electrode.

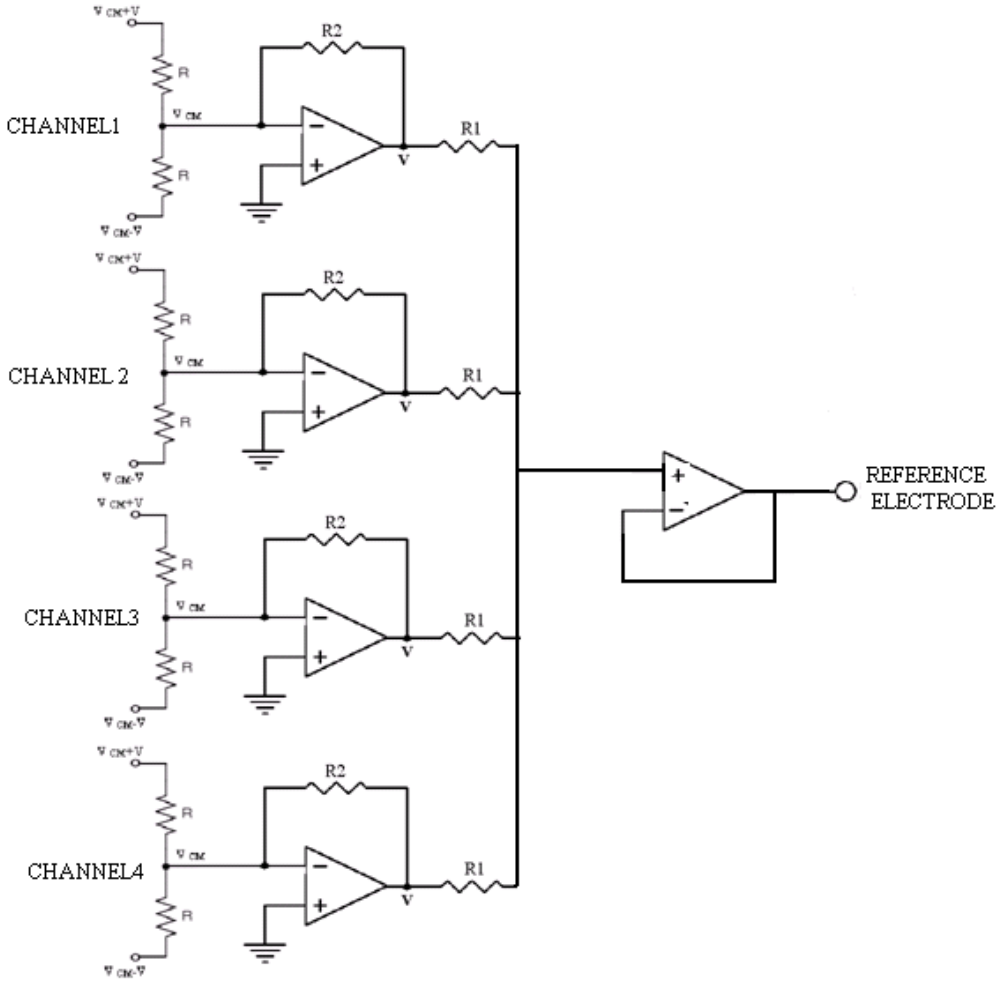

Figure 3-18 Active common-mode rejection using reference electrode

3.2.4 Negative Voltage Generator

To energize the system without adding line noise into the signal, a Li-Po (lithium-polymer) battery is used on the system. However, to supply the negative voltage for components, negative voltage generator is also needed. The voltage of the battery is 11.1 V and the negative voltage generator generated around -9V with respect to the ground level of the system.

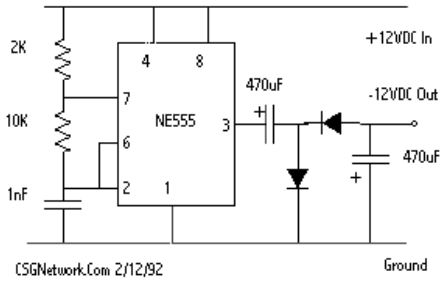

Figure 3-19 Negative voltage generator circuit

Figure 3-20 shows the base circuit. It is designed for five parallel channels. Right now, four channels are actively used; the last channel will be in use for future applications. As can be seen at the top-left area, two outputs are made available to the DAQ: output from rectifier and output from band-pass filter.

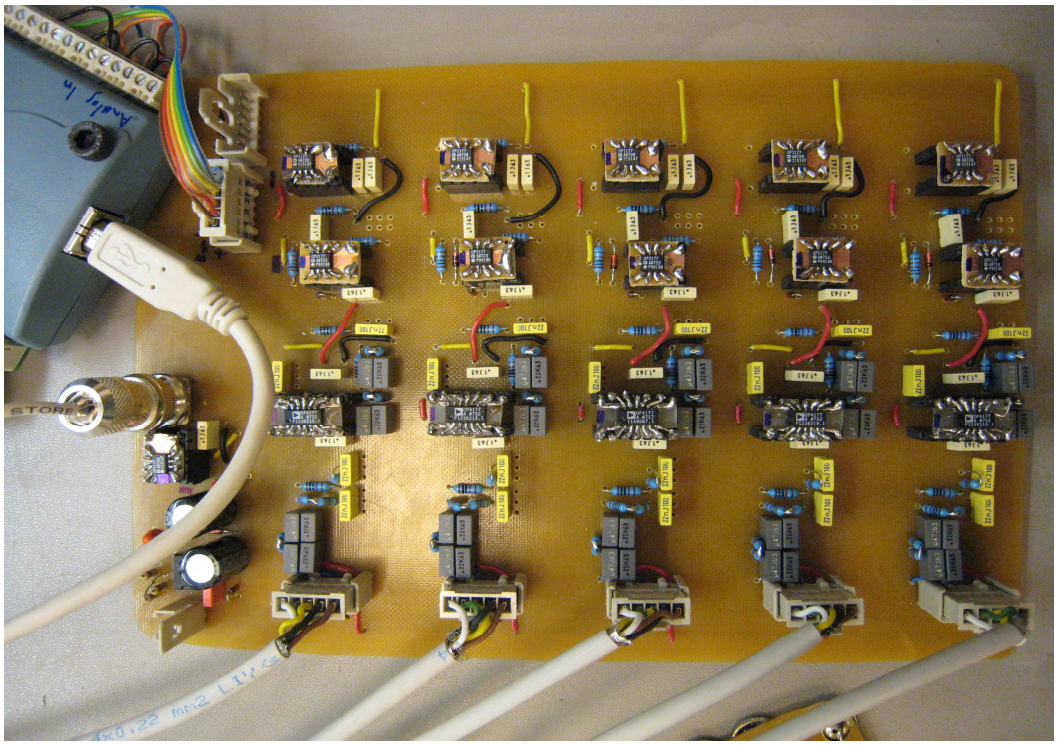

Figure 3-20 The base circuit

Figure 3-21 contains the all hardware of this research. The base circuit is also surrounded by the aluminum foil that is connected to the ground to reduce the effect of ambient electromagnetic field. The hand of the subject is forced under the static load to measure approximately similar SEMG signals. Reference electrode is away from the Ag/AgCl electrodes and placed on the upper arm. MATLAB is used as the software to implement signal processing algorithms.

Figure 3-21 EMG signal acquisition and processing system

4 FEATURE EXTRACTION METHODS FOR SEMG SIGNALS

In order to get useful information from the raw SEMG signal, mathematical transformations reveal hidden specifications of the signals. Some of the specific transformation methods based on both time and frequency domains are applied to SEMG signal to obtain distinct features to be used for further processing.

In the data acquisition part the raw SEMG signals are preconditioned by using analog circuit discussed previous section. After this process signal is exposed to various transformation techniques. In this chapter, introduction of these techniques, their intended use and some experimental results are presented.

4.1 Mathematical Transformations in Time Domain

4.1.1 Energy Method

Amplitude of the signal is varying through time. The strength of the signal can be measured by applying the integral to the area under the curve of the signal. Since the negative part of the signal also exists, the energy of the signal is computed as the area under the squared signal.

The energy for continuous time signal:

$$E = \int_{-\infty}^{\infty} |x(t)|^2 \, dt \tag{4.1}$$

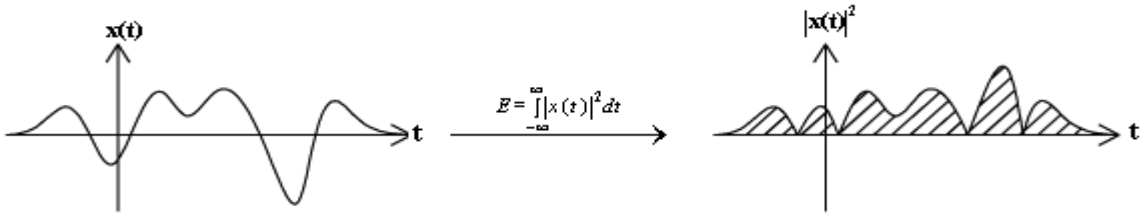

Figure 4-1 Energy of continuous time signal

This method determines the feature of the SEMG signal as its energy. For discrete time signals, the energy of signal is:

$$E_i = \sum_{n=0}^{N-1} \left| x_i(n) \right|^2 \tag{4.2}$$

The feature for each motion is $f_i = E_i$ and feature vector for four motions is $F = f_i$, i=1, 2, 3, 4.

4.1.2 Time Windows

Energy method only presents the energy of the signal in time domain. However, the random structure of the SEMG signals does not have smoothly distributed amplitude. In other words, the integral of the area under the curve of amplitude changes all the time. Energy deviation provides more information with respect to the total energy of the signal, since energy is directly proportional to the number of active MUAPs. For instance, increase in the force requires increase in the number of active MUAPs and brings together more biopotential.

The energy deviation of the SEMG signal is revealed by portioning the signal into several segments. Each segment reflects the change of energy distribution during the time. In this research, SEMG signal is divided into three parts and each divided part is multiplied by a window. The result presents the smoother version of the original signal. Since terminals of the window suppress the signal and the middle part of the window increase the signal amplitude.

The energy of each window reveals is a feature. The number of window used in this process determines the number of feature in the feature vector. Since the signal is divided three times, three different energy deviations are observed as a feature of the signal.

There are many different types of window function, e.g. Hamming, Hanning, triangular, rectangular, trapezoidal, Kaiser**,** Blackman, Gaussian, etc. In this research, Hamming and trapezoidal windows are selected to be a representative of window function technique in the feature extraction methods.

4.1.2.1 Hamming Window

As discussed above, the SEMG signal is divided into three parts. Every part intersects each other. The intersection part is known as overlap. In this research, three tenth of window length is a part of overlap area. The feature is determined as the energy of the windowed signal as represented below.

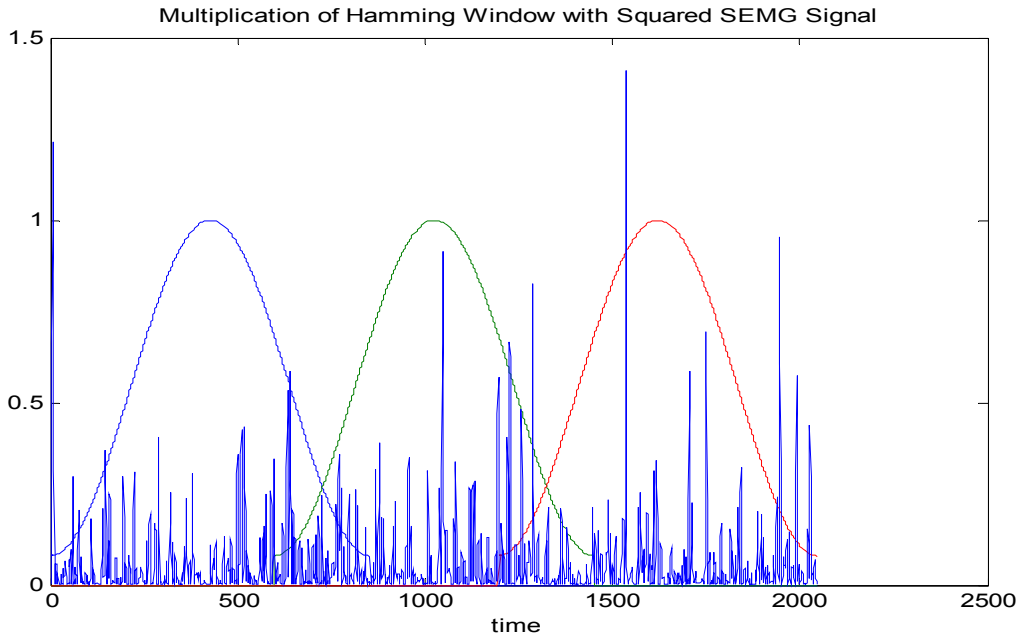

Figure 4-2 Multiplication of Hamming window with squared SEMG signal

$$E_i = \sum_{n=0}^{N-1} \left(W_i(n) \left| x(n) \right| \right)^2 \tag{4.3}$$

The feature for each motion is $f_i = E_i$ and feature vector for four motions is $F = f_i$, i=1, 2, 3.

4.1.2.2 Trapezoidal Window

The overlap between the windows is selected as one ninth of the window the length. The integral of each curve under the trapezoidal window [13] equals to each other. That is why the height middle window

$$E_i = \sum_{n=0}^{N-1} \left(W_i(n) \left| x(n) \right| \right)^2 \tag{4.4}$$

The feature for each motion is $f_i = E_i$ and feature vector for four motions is $F = f_i$, i=1, 2, 3.

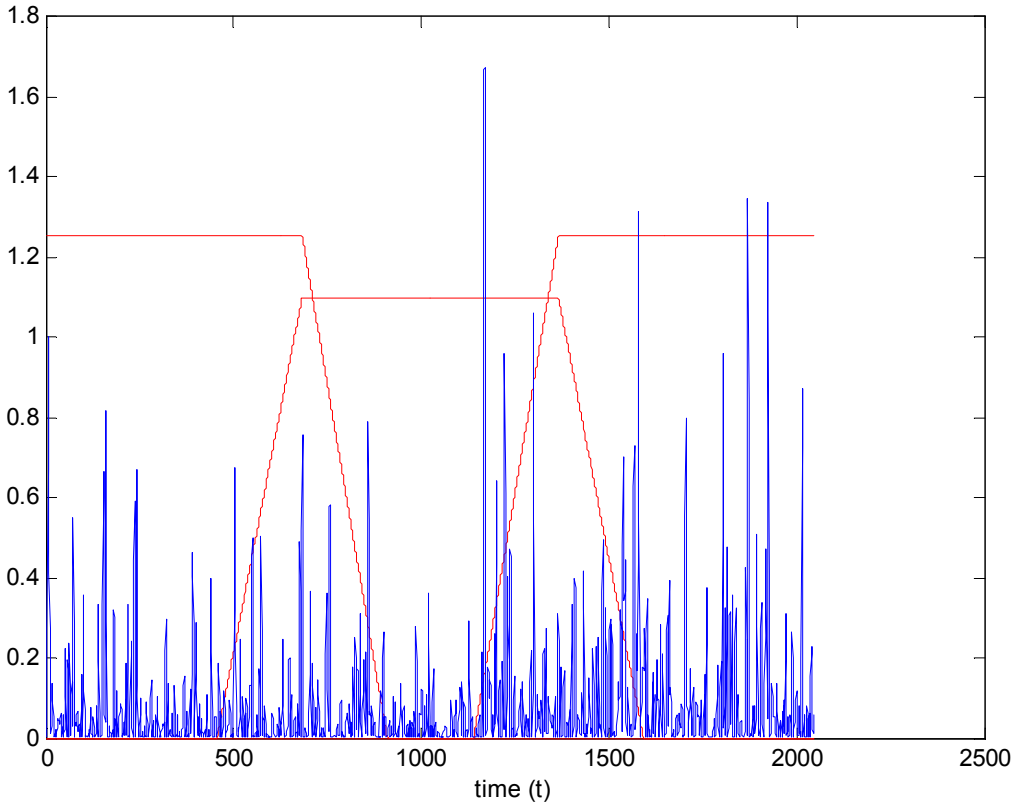

Figure 4-3 Multiplication of Trapezoidal window with squared SEMG signal

4.2 Mathematical Transformations in Frequency Domain

Until now we obtain time-amplitude representation of the signal. However, this kind of representations can not always reveal the distinguishing marks of the signal to be processed for other applications. Since other significant parameter of signal, that is, frequency components play an important role in signal characterization. All the frequency components of the signal are represented in the frequency spectrum. Fourier transform provides the constitution of the frequency spectrum.

Fourier transform of x(t):

$$X(f) = \int_{-\infty}^{\infty} x(t) e^{-j2\pi f t}, \text{ for every real number } f \tag{4.5}$$

The independent variable t denotes time; the transform variable f denotes ordinary frequency (in Hz). x is reconstructed from the X by means of inverse transform. Inverse transform of X(f):

$$x(t) = \int_{-\infty}^{\infty} X(f) e^{j2\pi f t}, \text{ for every real number } t \tag{4.6}$$

The main idea in Fourier transform is that x(t) is multiplied by an exponential term at some frequency and integrated till the end of the time. Here, exponential term can also be expressed as

$e^{j2\pi f t} = \cos(2\pi f t) + j\sin(2\pi f t)$, that is, this equation is a real part of the cosine of frequency and imaginary part of sine of frequency.

Figure 4-4 demonstrates an example of Fourier transformation on muscle flexor pollicis longus. The first graph of the Figure 4-4 is the time-amplitude representation of SEMG signal and the second graph represents the frequency spectrum of it.

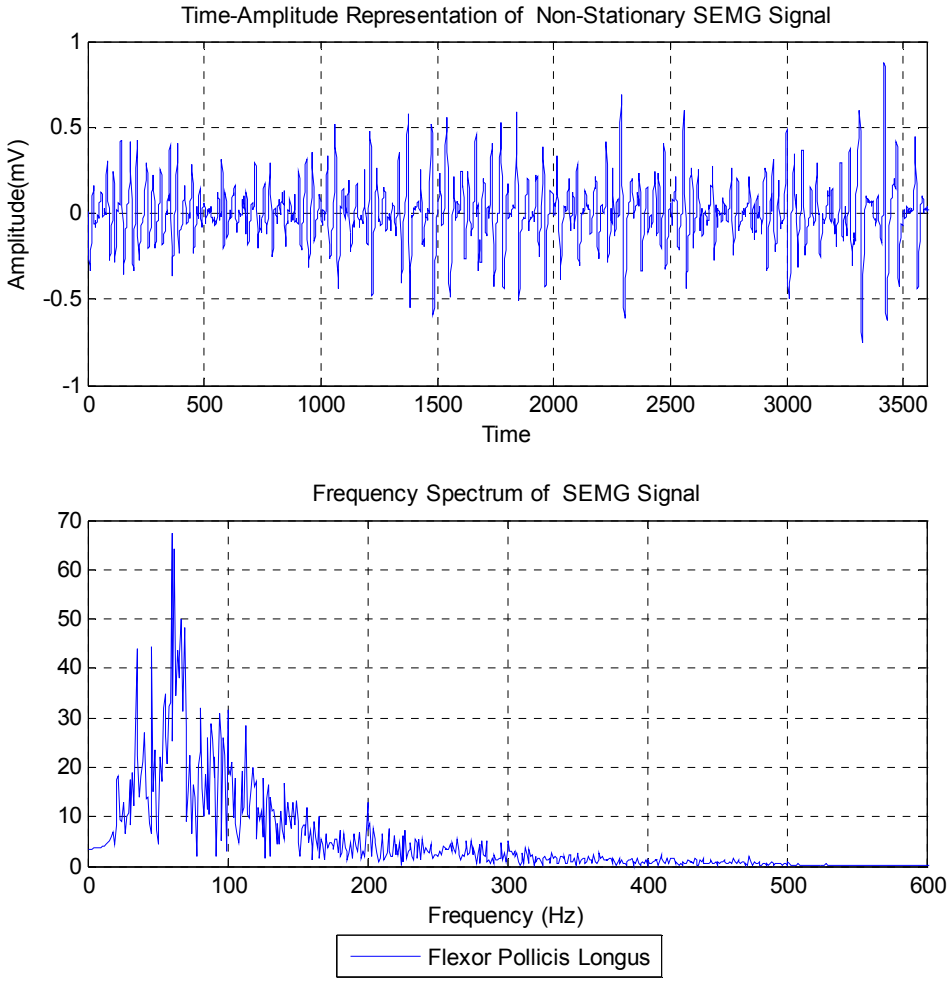

Figure 4-4 Time and frequency domain representations of the SEMG signal

Fourier transform is a reversible transform. This specification enables transfer between the raw and transformed signal. Both time and frequency information of the signal can not be reached simultaneously. Since frequency spectrum does not contains the time information of the signal or time-amplitude representation does not represents frequency information. In other words, frequency spectrum does not specify at what time the frequency components appear.

To emphasize the inadequacy of stand-alone usage of frequency information in some cases, comparison of SEMG signal with a stationary signal is plotted (Figure 4-5).

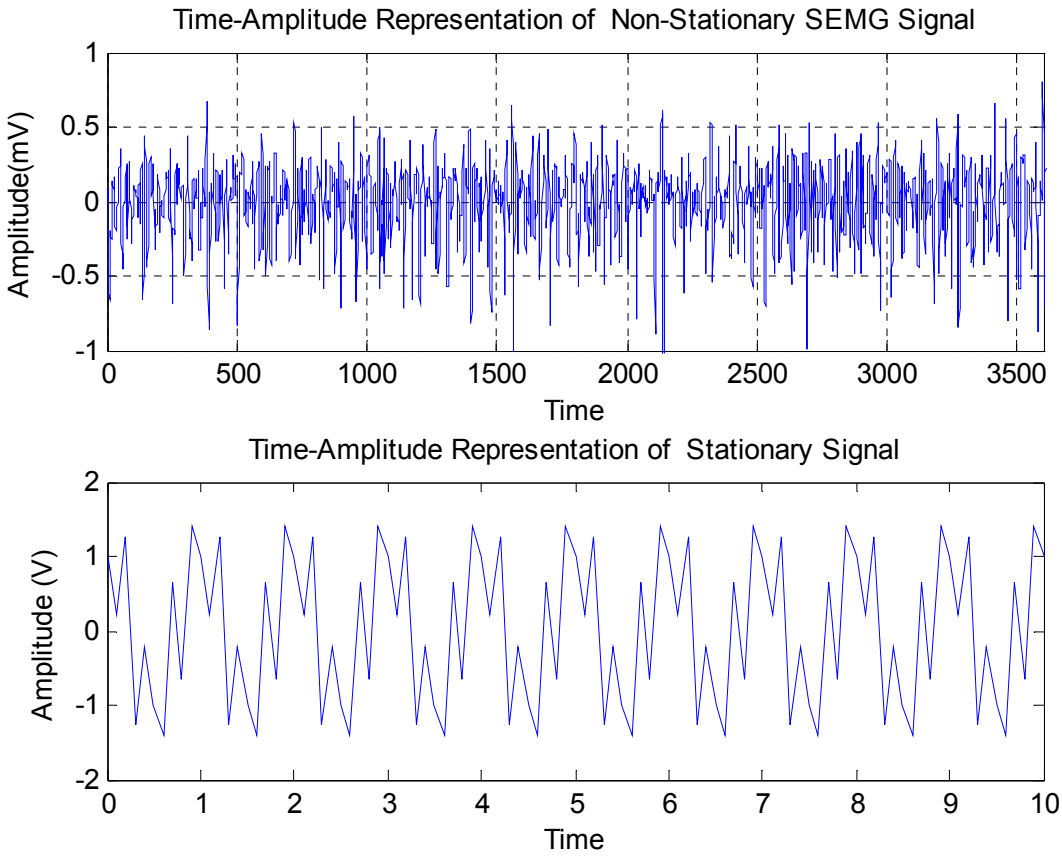

Figure 4-5 Comparison of non-stationary and stationary SEMG signals

As observed from Figure 4-4, frequency content of stationary signal does not change through the time. The frequency components of this signal, ($y = \cos(2\pi * 1 * t) + \sin(2\pi * 6 * t)$), are 1 Hz and 6 Hz. It is evident that all the frequency components present at all the time. On the contrary, frequency contents of the non-stationary SEMG signal changes through the time. In other words, each time interval has different frequency components. It is the main specification of SEMG signals whose frequency range changes in between 6-500Hz. However, Fourier transform can not answer at what time these frequency components exists. If the need is only based on frequency spectrum of the stationary or non-stationary signal, Fourier transform gives the sufficient answer.

On the other hand, Fourier transform does not bring a useful solution for determination the feature of signal. Figure 4-6 shows the SEMG signal of thumb during its extension. As observed from the figure, its frequency spectrum contains the range between approximately 20-500 Hz and has the same range with the frequency spectrum of the SEMG signal of thumb

during its flexion. 20-500Hz frequency band is valid for the entire SEMG signals, so it is not a distinctive feature for further signal processing techniques. In other words, each channel has the same frequency components; so Fourier transform can not specify the differences between SEMG signals that are collected from four different channels.

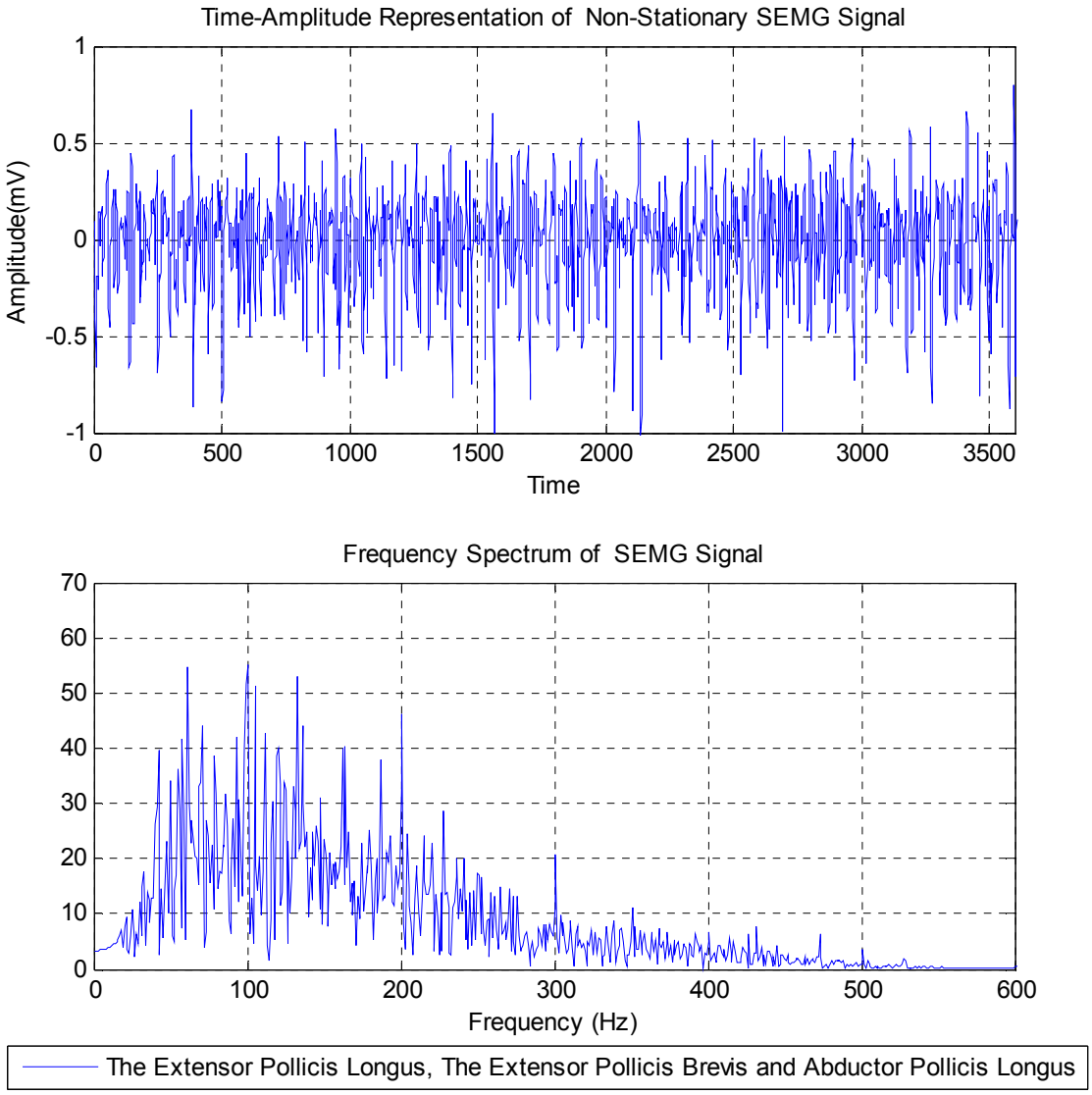

Figure 4-6 SEMG signal of thumb during extension

Although thumb flexion and extension SEMG signals differentiate from each other in time domain, they have almost similar frequency spectrum. Since these signals have the same frequency band but they appears at different times.

Fourier transform only informs us about the spectrum of the signal; however do not give any information concerning when the frequency content exists.

4.2.1 Spectral Energy Density

To compare the feature obtained from the FFT with other techniques, spectral energy density is selected as feature of the SEMG signal. The energy spectral density describes how the energy of a signal is distributed with frequency.

Spectral energy density of signal x(t) can be expressed as:

$$E(f) = \left| \int_{-\infty}^{\infty} x(t) e^{-j2\pi f t} \right|^2 = \left| X(f).X^*(f) \right|^2 \tag{4.7}$$

For discrete time signals, the energy can be expressed as the following:

$$E(f) = \left| \sum_{0}^{N-1} x[n] e^{-j f n} \right|^2 = \left| X(f).X^*(f) \right|^2 , \tag{4.8}$$

where X(f) is the discrete time Fourier transform of x(t).

The feature for each motion is $f_i = E_i$ and feature vector for four motions is $F = f_i$, i=1, 2, 3, 4.

4.3 Time-Frequency Representation

4.3.1 The Short Time Fourier Transform (STFT)

Transient signals, which are varying in time in an unexpected way (like a speech signal or an EEG signal) needs the notion of frequency analysis that is local in time.

The Fourier transforms do not specify that how the frequency content of signal changes over time. Short-Time Fourier Transform is substituted for the Fourier transform to prevent encountering the time related needs and was found by Dennis Gabor (1946). Wigner distribution is one of the time-frequency representations; however is not included in our comparison.

Only a particular section of the signal during that time is windowed and signal is defined by two dimensions, time and frequency. Frequency information inside the constant sized time window is revealed; in other words STFT is the Fourier transform of the windowed signal.

STFT compromises between time and frequency information. The drawback of this transformation is that firstly certain length of time window is selected and used for all the frequencies signal contains. However, to obtain the time vs. frequency spectrum more accurately, window size should be variable.

4.3.1.1 Continuous-Time STFT

In continuous-time STFT, the function is first multiplied by a window function which is nonzero for a short interval of time and the Fourier transform is applied while the window is sliding along the time axis [51]. Mathematical expression of the continuous-time STFT is represented as following;

$$STFT\ \{x(t)\} \equiv X(\tau,\omega) = \int_{-\infty}^{\infty} x(t)\omega(t-\tau)e^{-j\omega t}dt \quad , \tag{4.9}$$

where $\omega(t)$ which is the window function (Gaussian, Hamming, Hann, Bartlett or Kaiser are popular windows), $x(t)\omega(t-\tau)$ is the multiplication result by the window function (Figure 4-7). $X(\tau,\omega)$ is the Fourier transform of the $x(t)\omega(t-\tau)$. Complex function represents the phase and the magnitude of the signal over time and frequency.

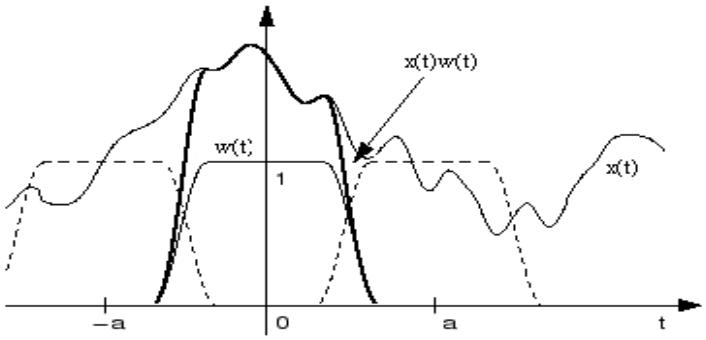

Figure 4-7 Multiplication of window and the signal in STFT [52]

w(t) localized around the origin moves throughout the real line and supplies the time-frequency behavior of the x(t) function as depicted the Figure 4-8 below.

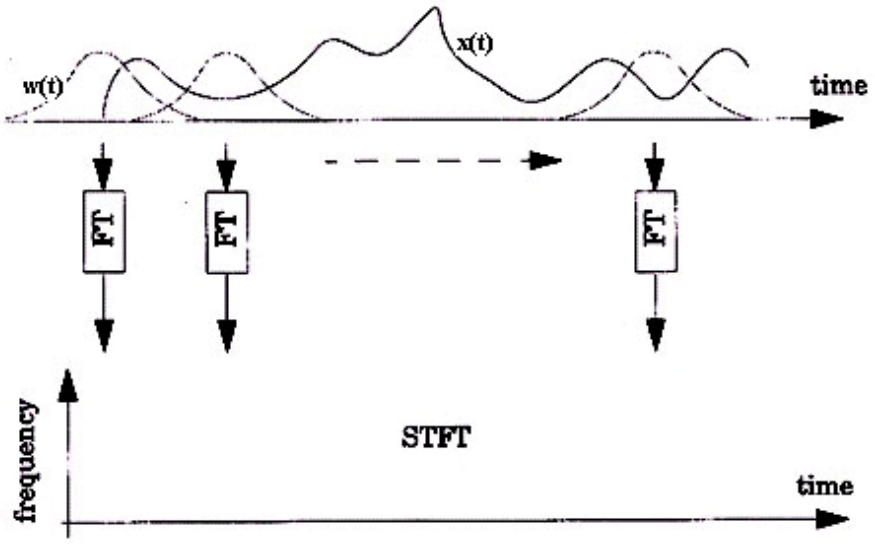

Figure 4-8 STFT depiction [53]

4.3.1.2 Discrete Time STFT

Short time discrete Fourier transform is defined as

$$STFT\{x[n]\} \equiv X(m,\omega) = \sum_{n=-\infty}^{\infty} x[n]\omega[n-m]e^{-j\omega n} = \sum_{n=0}^{R-1} x[n]\omega[n-m]e^{-j\omega n} \quad (4.10)$$

where w(n) is the window function of length R. Some parameters such as block length(R), the type of window, amount of time-skip have to be chosen according to desired time-frequency resolution [54].

The time-skip or overlap parameter selection is represented in Figure 4-9.

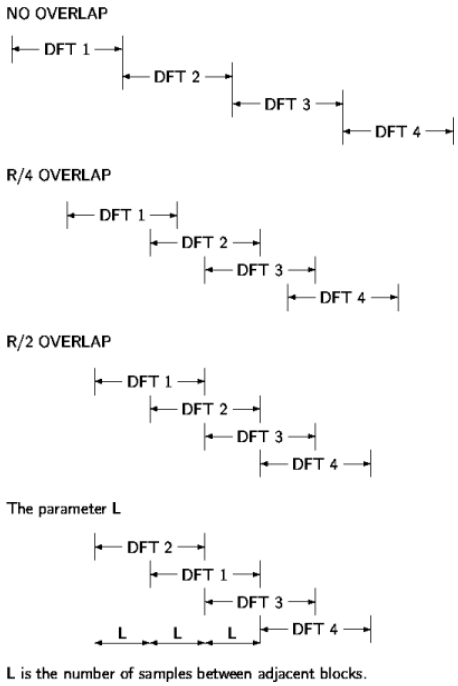

Figure 4-9 Overlap parameter selection [54]

4.3.1.3 The Resolution Problem of STFT

The disadvantage of STFT is to have limited time–frequency resolution due to the Heisenberg Uncertainty Principle. In summary, this principle denotes that time – frequency information of a signal can not be revealed explicitly. However, it is known that the time intervals in which certain band of frequencies appears. This is also stated as resolution problem.

Choice of narrow window in the STFT transform limits the low frequency representation in the frequency domain. Similarly, wide window selection leads to reduce the frequency resolution for low frequency, provides better resolution for pulse signals and also good time resolution for all. To obtain satisfactory resolution both time and frequency window of medium width could be a good choice for STFT. The trade off in the STFT is preference on good frequency resolution and poor time resolution or good time resolution and poor frequency resolution [54, 55, 56].

In this research, SEMG signal is sampled at 2048Hz and recorded through the first 0.8ms time interval. In addition, length of the window selected as 1/10 length of the conditioned SEMG signal. As discussed above, 0.1* length sized Hamming window is determined to try to balance the time-frequency resolution.

Here are various time-frequency resolution examples revealed by changing size of the window. Figure 4-10 is formed with wide window that has 0.3* length of the SEMG signal of the Extensor Digitorum. Figure 4-11 is the 2D representation containing frequency and time.

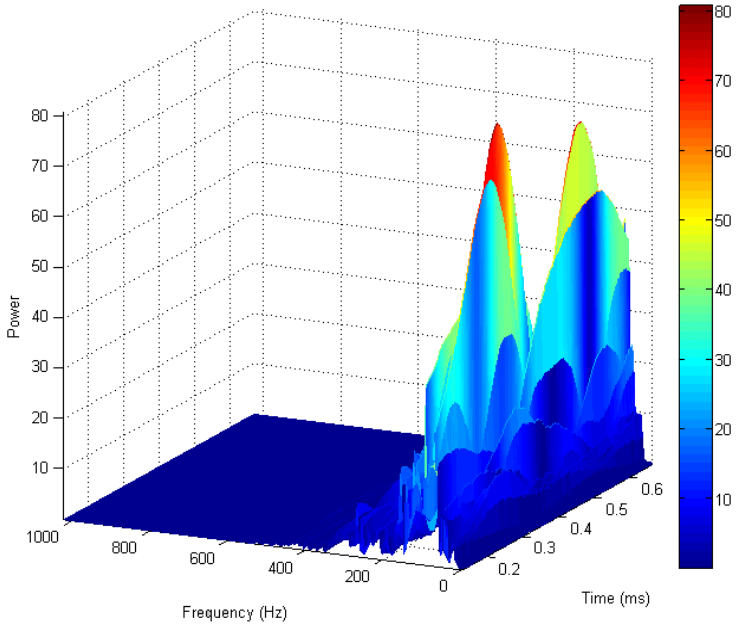

Figure 4-10 Time-Frequency resolution of extensor digitorum

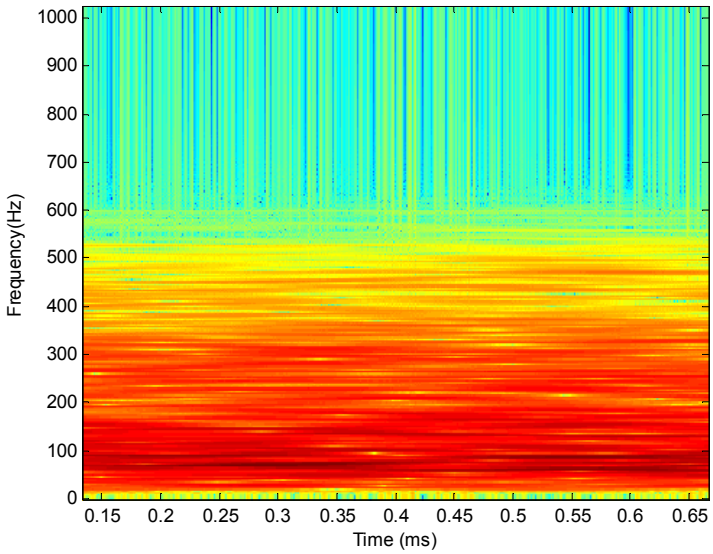

Figure 4-11 2-D Representation of Figure 4-10

Figure 4-12 is formed with narrow window (compactly supported) that has 0.025*length of the SEMG signal of the Extensor Digitorum. Figure 4-13 is the 2D representation containing frequency and time.

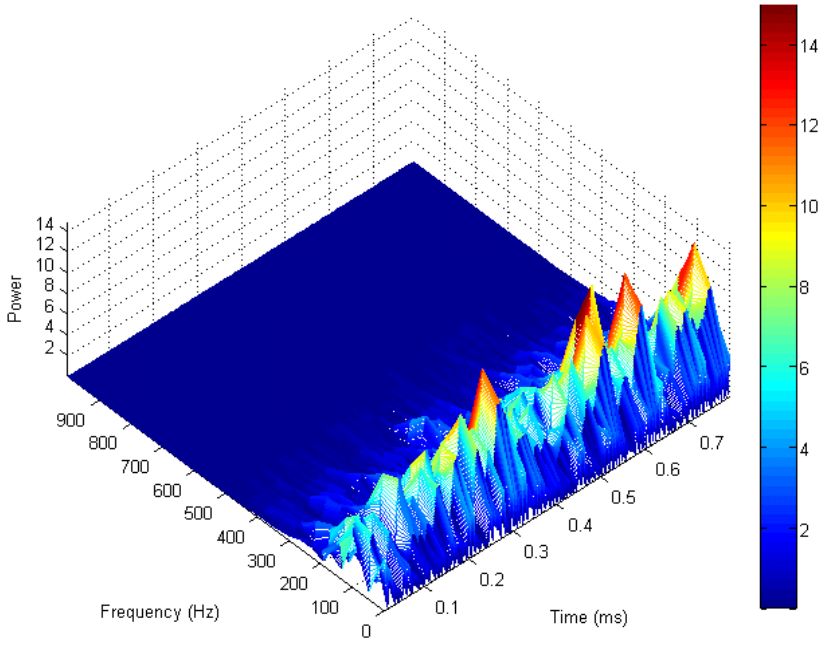

Figure 4-12 Narrow window time-frequency resolution of extensor digitorum

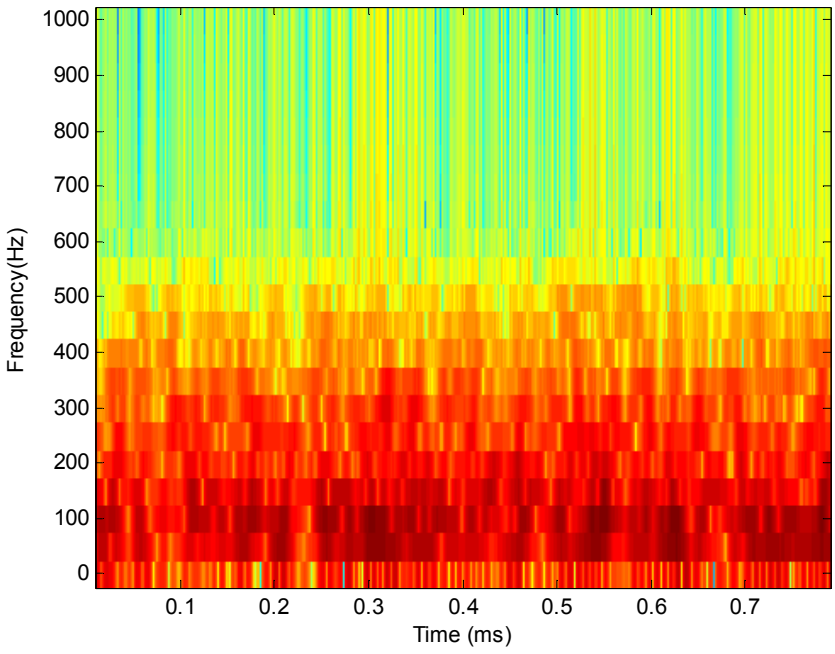

Figure 4-13 2-D Representation of Figure 4-12

The main idea under this issue is that in the Fourier Transform, it can be thought that it has infinite window and the result gives perfect frequency resolution, whereas no time information. STFT is the finite length windowed version of the Fourier Transform so only a finite length of the signal is exposed to Fourier transformation. It leads to loss of information out of the window. That is since wider window provides better frequency resolution but poor time resolution and it gives limited frequency information limited by a band of frequency. All in all, fixed size window in the STFT leads to the trade-off between time and frequency resolution. The uncertainty problem of STFT reveals the need of wavelet transform [52, 57].

4.3.1.4 The Features of STFT

In this research, central frequency, variance of frequency, energy of the signal, 0, 1st and 2nd moments of frequency distribution are selected as features of the SEMG signals [13].
Moments of the frequency distribution can be defined below:

$$\begin{aligned} M_0(t) &= \sum_k f_k^0 \left| STFT(t,k) \right| \\ M_1(t) &= \sum_k f_k^1 \left| STFT(t,k) \right| \\ M_2(t) &= \sum_k f_k^2 \left| STFT(t,k) \right| \end{aligned} \tag{4.11}$$

Central frequency is:

$$f_{Central} = \frac{M_1}{M_0} \tag{4.12}$$

Variance of frequency is:

$$f_{variance} = \frac{M_2}{M_0} - \left(\frac{M_1}{M_2} \right)^2 \tag{4.13}$$

Energy of the signal is:

$$E(t) = \sum_n \left(w[n-t]x[n] \right)^2 \quad , \tag{4.14}$$

where w is the Hamming window and x[n] is the discrete time SEMG signal.

Features and their changes with time:

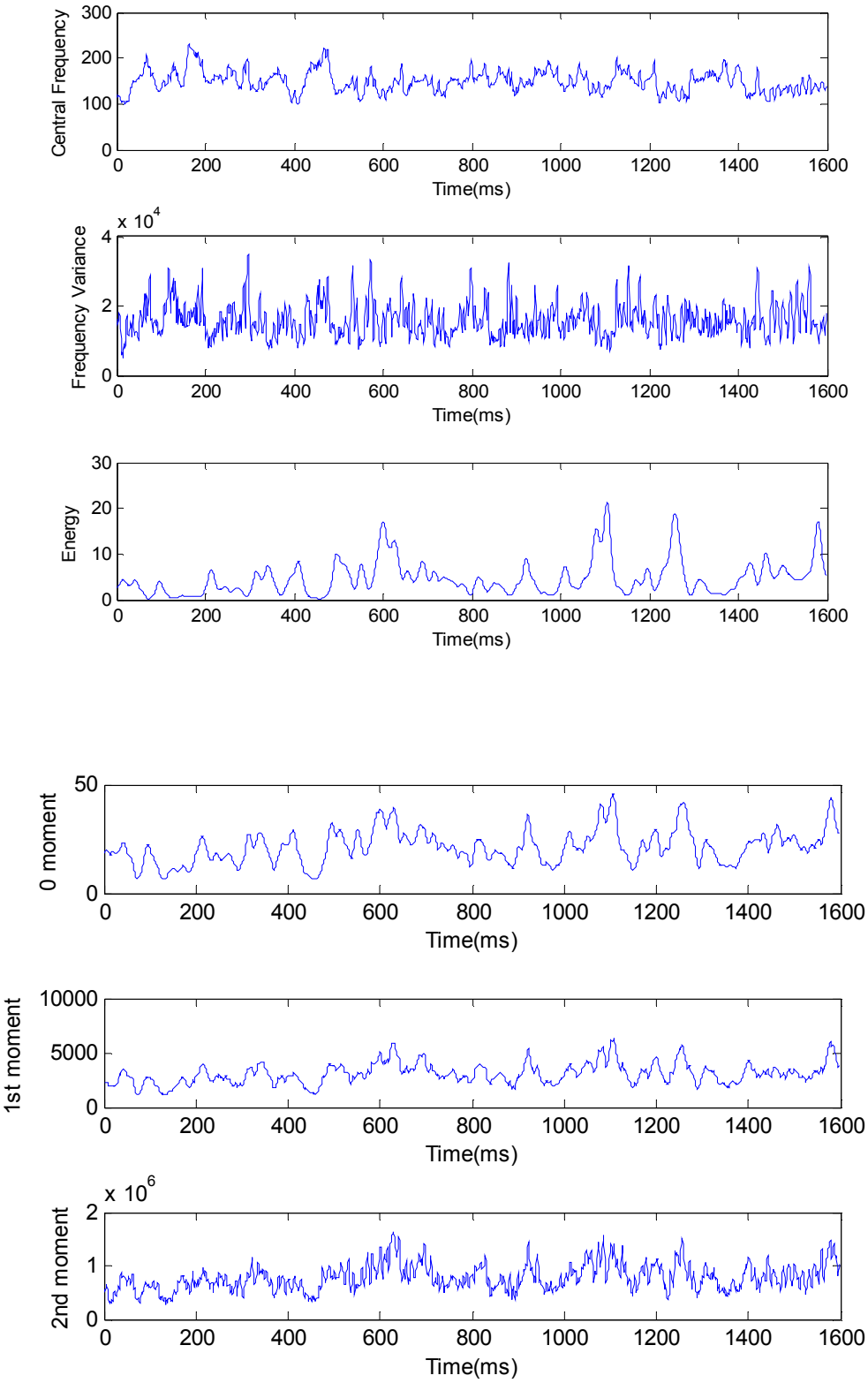

Figure 4-14 Features and their changes in time

4.4 Multiresolution Analyses (MRA)

MRA brings a solution to Heisenberg uncertainty principle to a certain extent by analyzing the signals at various frequencies with diverse resolutions [38, 56]. This technique does not employ the same size window to reduce the time-frequency resolution problem. The main property of the MRA is to provide good time resolution and poor frequency resolution at high frequencies and good frequency resolution and poor time resolution at low frequencies. MRA is preferred if the signal has high frequency components for short time intervals and low frequency components for long time intervals. Since nature of most of the signal shows these characteristics, it is reasonable to apply this method to the signals.

4.4.1 Wavelet Analysis

The Wavelet transform is a kind of MRA and provides both time and frequency information concurrently. As specified before, Wavelet transform is developed to reduce the Heisenberg uncertainty which STFT is faced with [58].

The comparison of Wavelet transform to the other transforms enlightens its functional specification. Wavelet analysis makes a similar operation as Fourier transform in terms of signal is divided into its constituent part for analysis. The difference comes into existence owing to the signal division form. The Fourier transform decomposes the signal into a series of sine waves at various frequencies, whereas Wavelet transform analyzes various sharp features on the signal better by using non-uniform shape of wavelet, that is, it decomposes the signal into its wavelets which is scaled and shifted version of the mother wavelet.

To illustrate, the observation of sine wave and a wavelet (e.g. Debauchies 5) (in Figure 4-15) in the sense of their comparison presents that sine wave shows smooth and infinite characteristics whereas wavelet has irregular shape, limited duration and its average equals to zero[59 , 62].

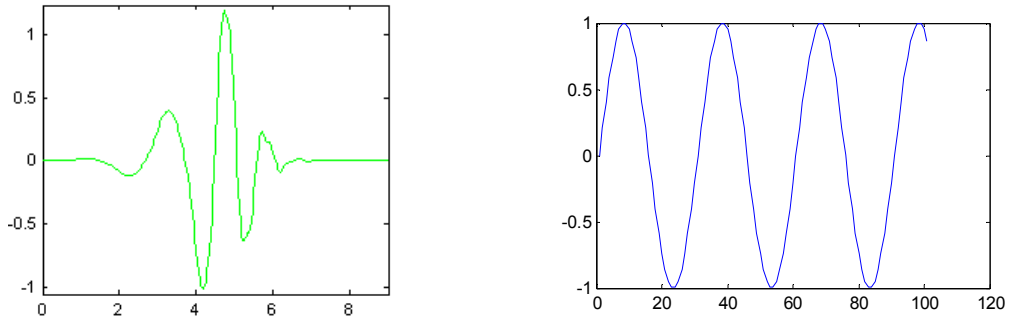

Figure 4-15 Debauches-5 Wavelet and Sine wave

Wavelet analysis uses variable sized windows to the needs and reveals the detail information of data which can not be represented via other transform techniques. One of the best specialties of the wavelet provides better analyses for non-stationary signals.

Since the biomedical signals (in this research, EMG signals) are non-stationary, wavelet transform is the one of the best choices to analyze the signal. This preference in all the transform methods acquires us to have correlation between the time and frequency analyses of the non-stationary characteristic EMG signal. As discussed before, the Fourier transform just gives information about frequency constituents of the signal but there is a deficit about the time relation of each frequency. The need of association between frequency domains with their location in time is supplied by wavelet transform. Time domain information is obtained by translation of mother wavelet and frequency domain information is yielded by dilations and compressions of the mother wavelet. The application of translation and dilation/compression processes (as in Figure 4-16) on mother wavelet reveals the relation between the wavelet and segmented section of the signal, that is, wavelet coefficients for each wavelet segment of the signal are calculated.

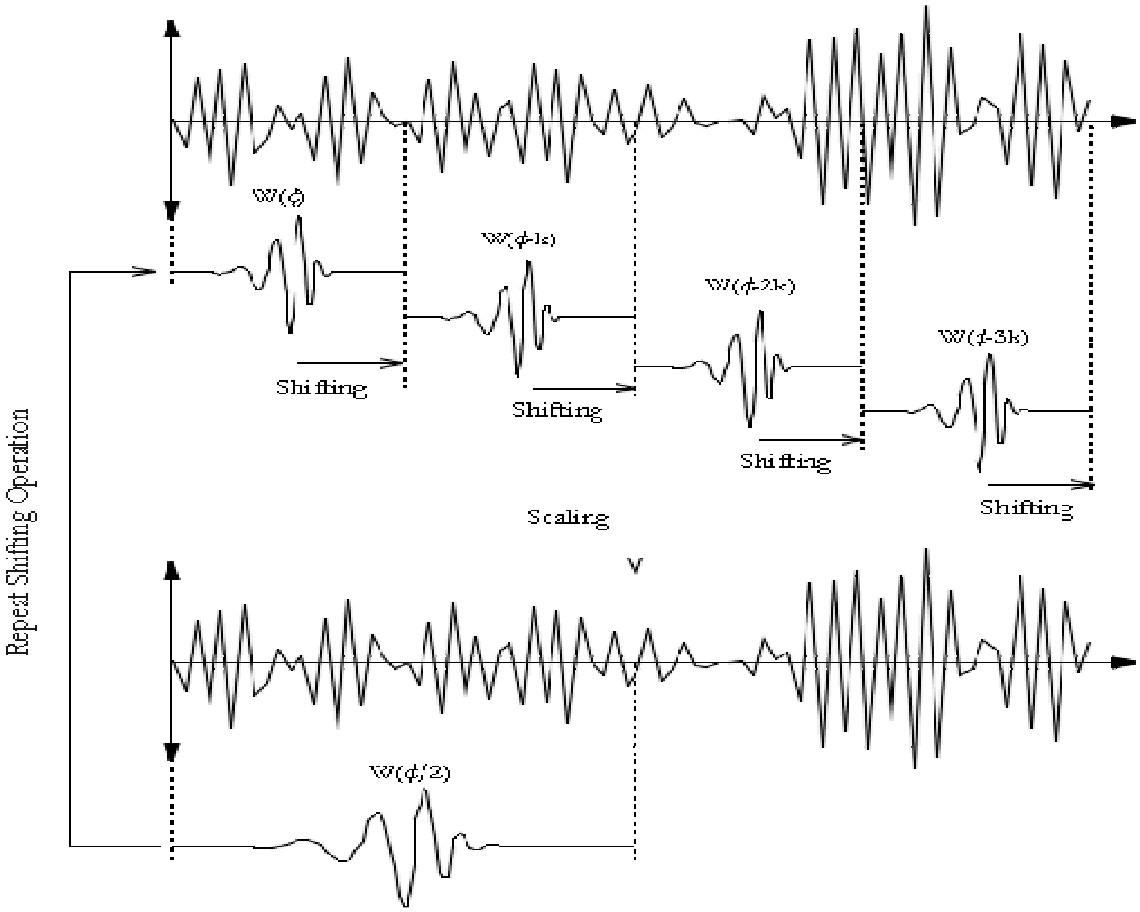

Figure 4-16 Wavelet Transformation [60]

4.4.2 Continuous Wavelet Transform (CWT)

There has been a similarity between STFT and Wavelet. The signal is multiplied by Wavelet function in Wavelet transform and is multiplied with a window in STFT. The multiplication continues during the different segments of the time interval of the signal.

There are also some differences between them. First of all, in wavelet analysis and synthesis Fourier transform does not employed. Secondly, window size is not fixed, that is, it is varying for each spectral component.

The continuous wavelet transform is the sum over all time of the signal multiplied by scaled and shifted versions of the wavelet function (ψ).

The CWT equation below function of scale and position computes the wavelet coefficients.

$$C(scale, position) = \int_{-\infty}^{\infty} f(t)\psi(scale, position, t)dt \tag{4.15}$$

CWT is a function of two variables, scale factor and shifting.

4.4.2.1 Scale Factor (a)

Scale factor provides for wavelet stretching and compressing characterized of it. As represented from the Figure 4-17, compressed wavelet is existed by the decreasing the scale factor, it means that there is an inversely relation between frequency and scaling factor.

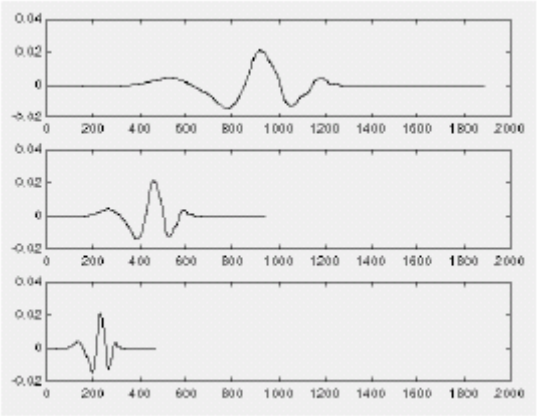

Figure 4-17 Frequency and Scaling Factor Relation in Wavelet Transform [61]

Scale factor affects the wavelet by stretching or compressing the length of wavelet. These two conditions of wavelet reveal two different results. Compressed wavelet is compared with the smaller portion of the signal, whereas the stretched wavelet extends throughout the signal and is compared with the wider range of the signal.

Figure 4-18 Compressed and stretched wavelets [61]

The frequency relation is established due to the speed of changes in detail of the measured signal feature. All in all, compressed or low scale wavelet is associated with high frequency (w) provides more information about the signal feature related to the changing details, while stretching signal or high scale wavelet is associated with low frequency (w) provides coarser information about the feature of signal.

4.4.2.2 Shifting

As implied by its name, it provides for wavelet shifting its onset.

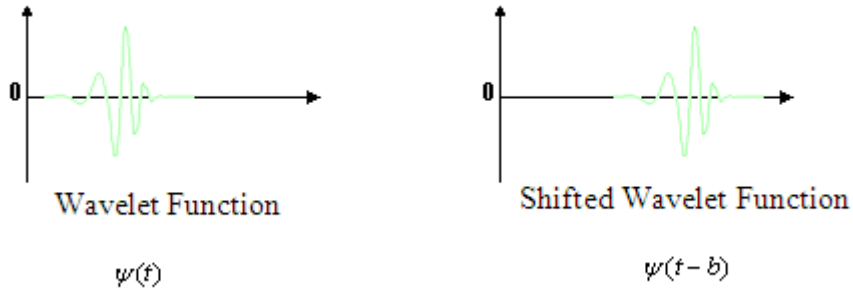

Figure 4-19 Shifting wavelet function

The continuous wavelet transform for continuous time signal depends on a and b parameters and its coefficients are represented as the following function,[62]

$$C(a,b) = \int_R s(t) \frac{1}{\sqrt{a}} \psi\left(\frac{t-b}{a}\right) dt \text{, where } a \in R^+ \{0\}, b \in R \tag{4.16}$$

A CWT is formed in this order:

i. Firstly, wavelet transform is applied to the onset of the signal.
ii. Secondly, C is calculated by using CWT function and its value represents the correlation between the wavelet and selected region of the signal. The result changes with the preferred type of the wavelet.
iii. Thirdly, wavelet has to be shifted to the right to make the first and second steps for new section of the signal. After the completion of shifting process, new step is setting scale of the wavelet to a new value and all the steps have to be repeated for each of the new scale.

iv. In the end, various coefficients are obtained for every scale and shifting parameter and their values (C) are represented by various color changes on the scale-time graph.

Figure 4-20 represents an example of a SEMG signal after the CWT. In this example, coefficients of the measured SEMG signal are demonstrated during the time length of signal with the scale number 64.

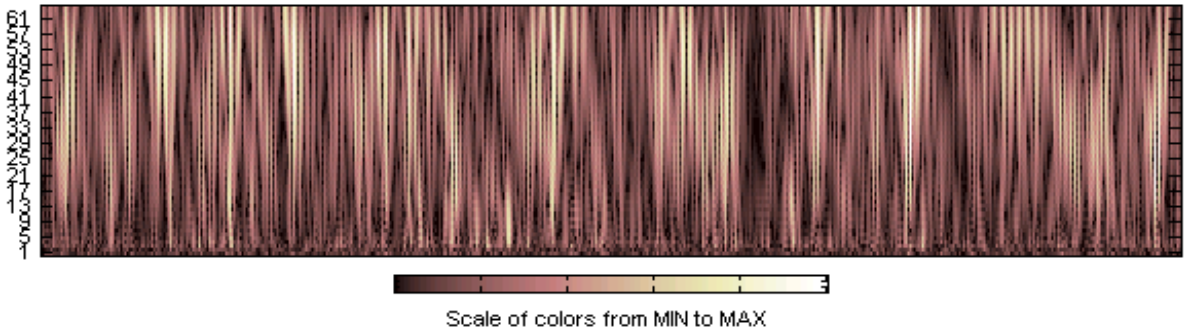

Figure 4-20 Example for a SEMG after CWT

4.4.3 The Discrete Wavelet Transform (DWT)

Thus far continuous wavelet transform is sampled and discretized by computers. In other words, it does not mean that this is the real discrete wavelet transform. The CWT presents extremely redundant information about the signal and brings together amount of computational load (Figure 4-20). The DWT eliminates the redundant information and number of computation and provides adequate information for decomposition and reconstruction of the signal.

In general, low frequency parts of the signal contain fundamental part of the signal and high frequency constituents represent the detail properties of the signal. In wavelet analysis, approximations and details are used as definition of the high scale, low frequency and low scale, high frequency components of the signal respectively. To separate the original signal into its both low and high frequency components and reveal two signals, two complementary filters, low and high pass filters are performed. After the filtering operation, generated signals are downsampled to prevent the double size of the original data number. Figure 4-21 shows the basic level of discrete wavelet transform. First level decomposition analysis is the first approximation and detail of the original signal.

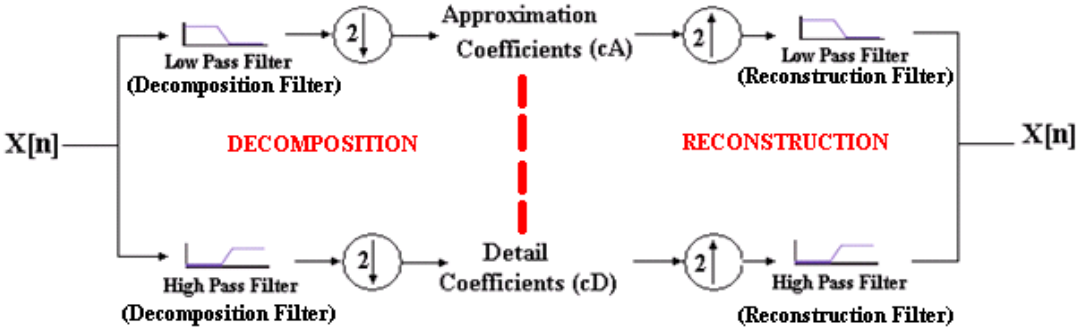

Figure 4-21 First level decomposition

Firstly the signal is passing through both low and high pass filters simultaneously.

$$y[n] = (x * g)[n] = \sum_{k=-\infty}^{\infty} x[k]g[n-k] \tag{4.17}$$

The detail coefficients are obtained from the high pass filters and the approximation coefficients are generated from the low pass filter. Two filters are related to each other and called quadrature mirror filter.

According to Nyquist theory, filtered signal is downsampled by removing half of the sample of the signal.

$$y_{low}[n] = \sum_{k=-\infty}^{\infty} x[k]g[2n-k]$$
$$y_{high}[n] = \sum_{k=-\infty}^{\infty} x[k]g[2n-k] \tag{4.18}$$

Down sampling operator can be expressed as below:

$$y_{low}[n] = (x * g) \downarrow 2$$
$$y_{high}[n] = (x * h) \downarrow 2 \tag{4.19}$$

4.4.3.1 The Scaling Function

The difference between the wavelet (ψ) and scaling function (ϕ) is that ψ defines the details of the original signal and its integral equals to zero, $\int \psi(x)dx = 0$ while ϕ defines the approximations and its integral equals to one, $\int \phi(x)dx = 1$.

$$\begin{aligned}
&a = 2^j, j \in Z \text{ , where } j \text{ is the level number} \\
&b = k2^j, k \in Z, \text{where } k \text{ is the translation parameter} \\
&\psi(x-b): \text{Translation} \\
&\frac{1}{\sqrt{a}}\psi\left(\frac{x}{a}\right): \text{Change of scale} \\
&\frac{1}{\sqrt{a}}\psi\left(\frac{x-b}{a}\right): \text{Both translation and change of scale}
\end{aligned} \tag{4.21}$$

The continuous time signal for discrete analysis is expressed below,

$$C(a,b) = \int_R s(t)\frac{1}{\sqrt{a}}\psi\left(\frac{t-b}{a}\right)dt, \text{ where } a = 2^j, b = k2^j, (j,k) \in Z^2 \tag{4.22}$$

$$\begin{aligned}
\phi_{j,k}(x) &= 2^{-j/2}\phi(2^{-j}x - k), j \in Z, k \in Z \\
\psi_{j,k}(x) &= 2^{-j/2}\psi(2^{-j}x - k), j \in Z, k \in Z
\end{aligned} \tag{4.23}$$

Decomposition level can be increased with performing the same processing on each separated signals and reveals the wavelet decomposition tree. The tree is also known as filter bank. This is a five level example for multilevel decomposition on Flexor Digitorum Superficialis and Flexor Digitorum Profundus. In this research, 500ms (1024 points, sampled at 2048Hz) record is selected from the original SEMG signal and five-level decomposition is used to reconstruct back A1, A2, A3, A4 and A5. This study is repeated for Daubechies 2, 3, 4 and 5, Coiflets 1, 2, 3 and 4, Symlets 4,5,6,7 and 8. The features are determined as energy of each level under these wavelet families.

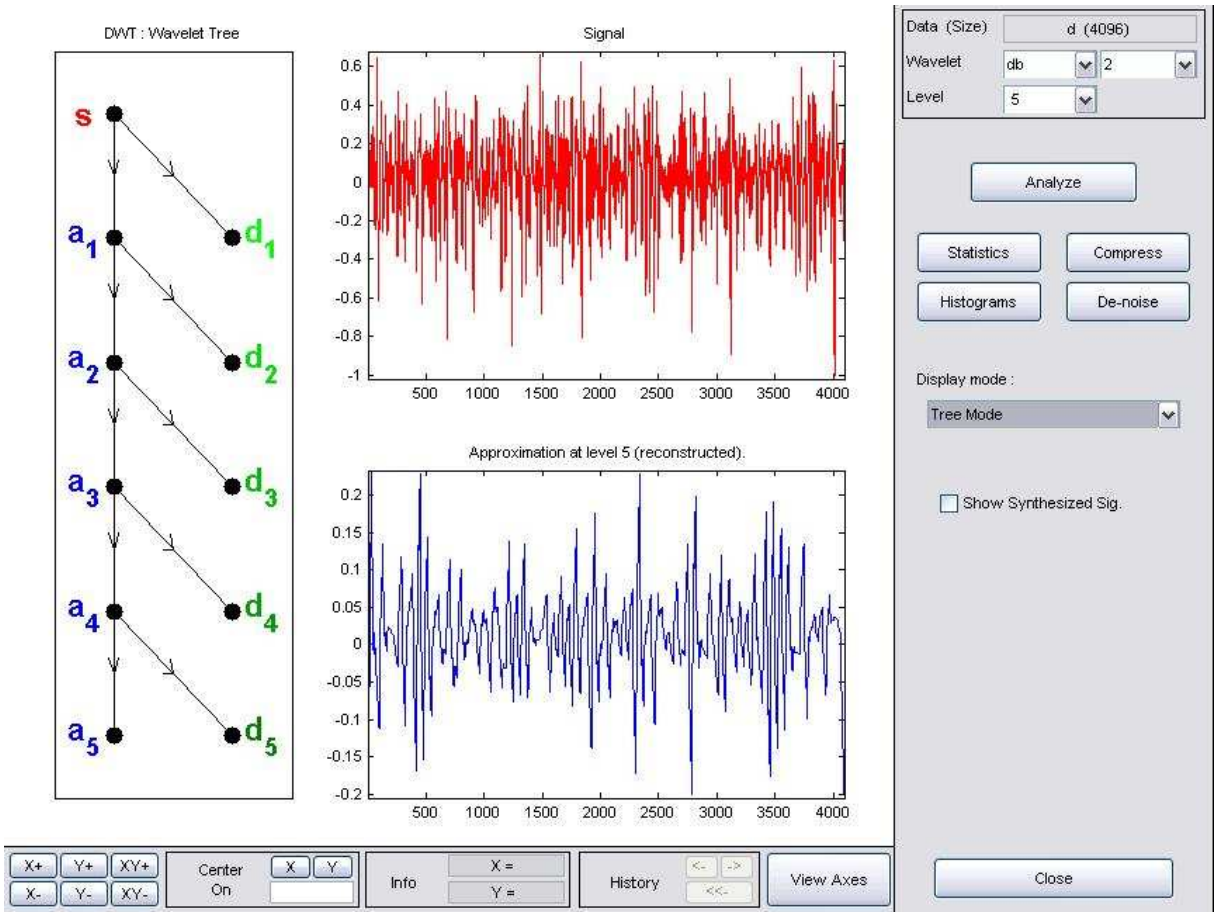

Figure 4-22 Demonstration of the decomposition tree

As observed from the decomposition tree in Figure 4-22, A1 is an approximation of A0 and D1 is a detail of A0. In addition, A0 can also be obtained various ways depending on the decomposition level. For example,

S=A0= A3+D1+D2+D3

A0=A5+D1+D2+D3+D4+D5

A2=A1+D1+D2

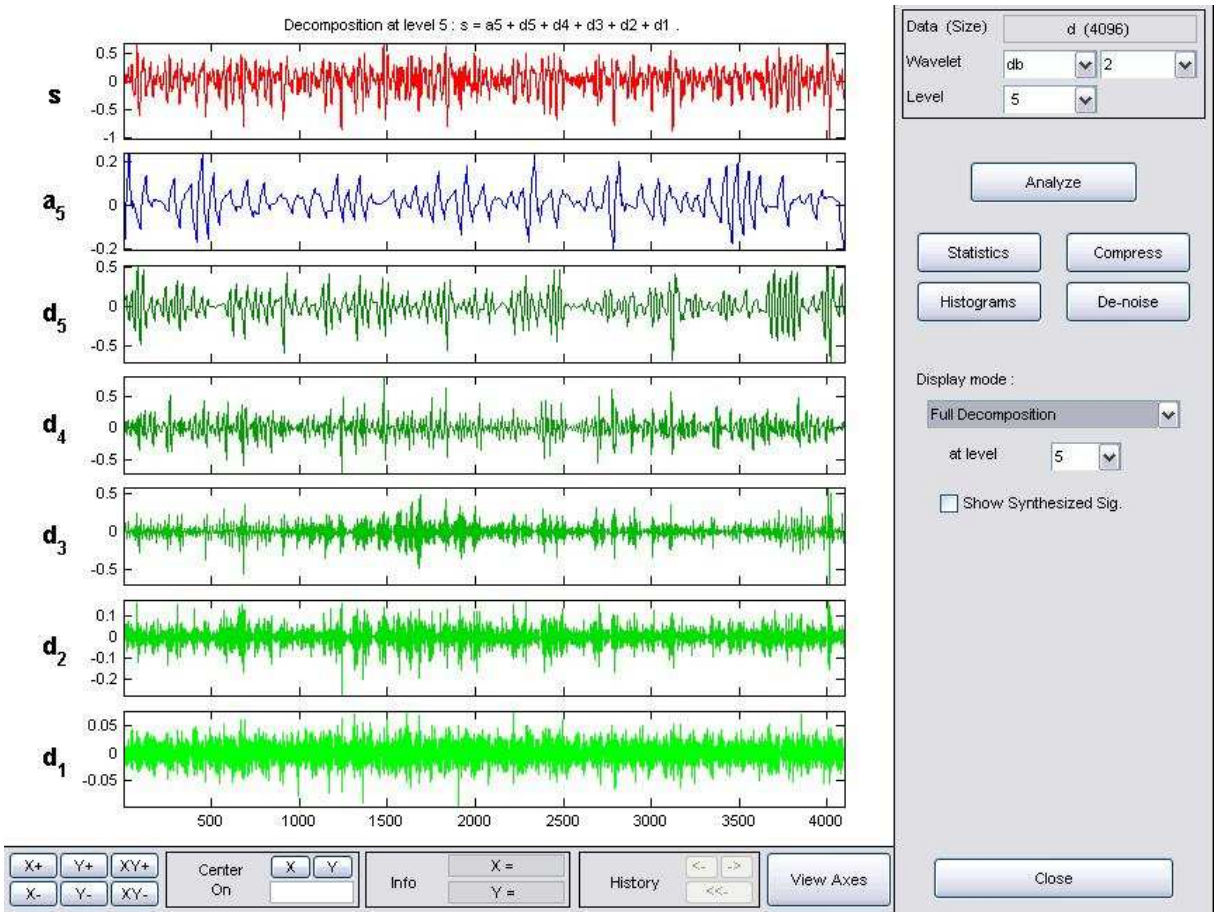

Figure 4-23 Decomposition of the SEMG signal at level 5

At each level in the Figure 4-23, the SEMG signal is decomposed into low and high frequencies. Owing to the decomposition process the input signal must be a multiple of 2^n where n is the number of levels.

In this example, SEMG signal consists of 4096 samples. For five levels of decomposition six output scales are generated (Figure 4-24).

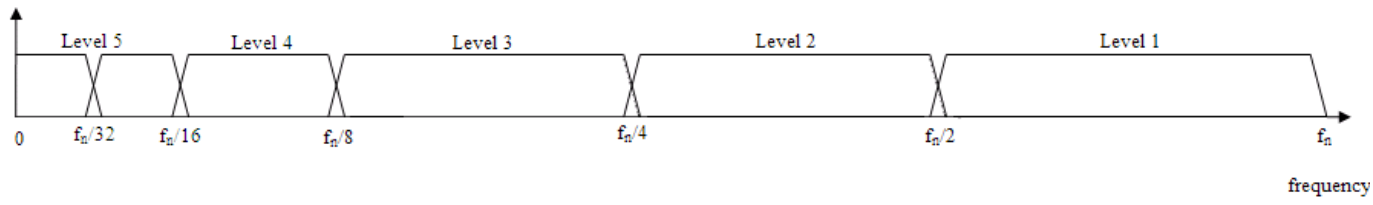

Figure 4-24 Levels of decomposition

Figure 4-25 represents the both approximation and detail for each level of the decomposition of the original signal. As observed from the figure 4-25, the approximation coefficients are obtained from the fundamental part of the signal. In other words, these parts convey more information regarding signal. Therefore, approximations of the signal are used in the experiments.

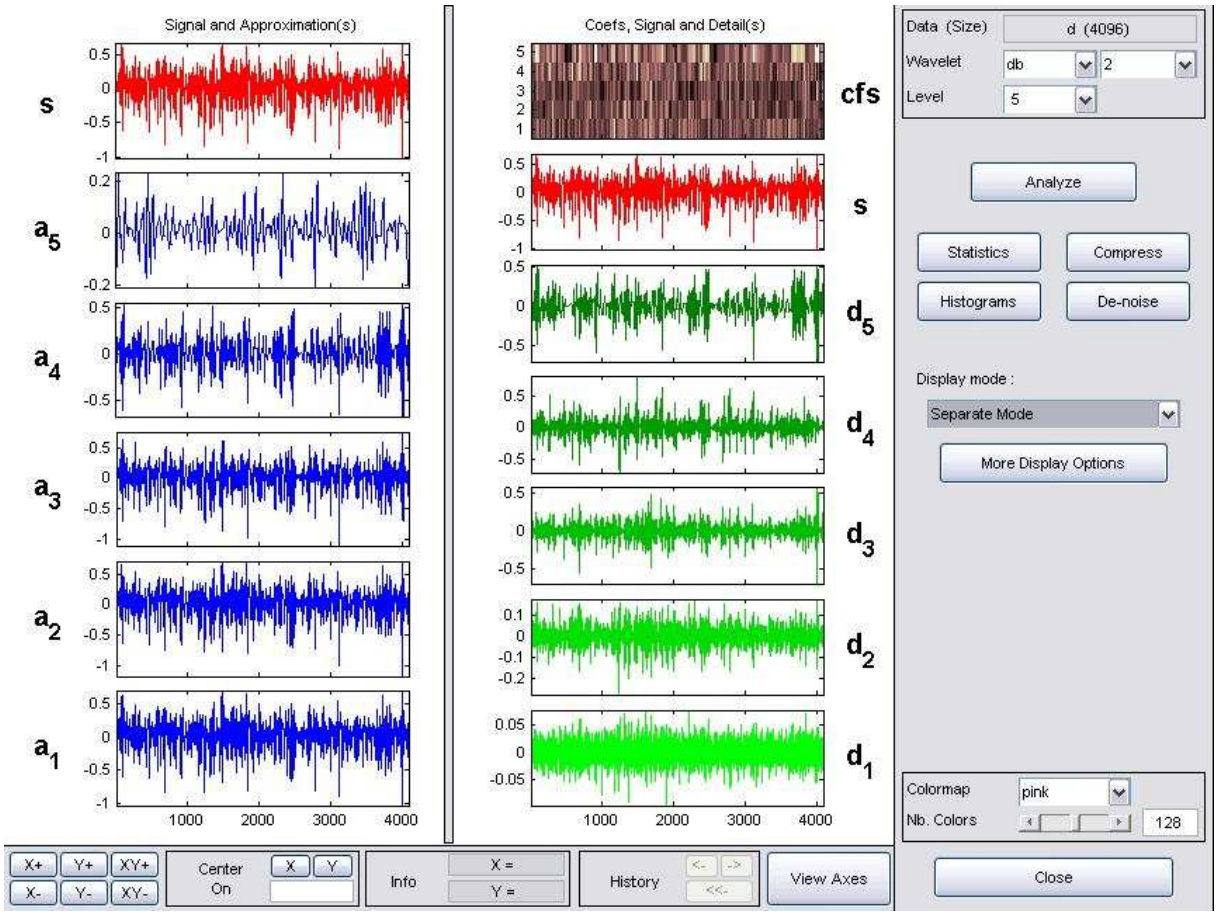

Figure 4-25 Approximations and details of the original signals

The last limit of the decomposition continues until the single sample of the detail signal is left. Number of optimum levels is decided based on the nature of the signal and experience or by using entropy based criterion. The level is also selected depending on the low-pass cut off frequency.

4.4.4 Wavelet Packet Analysis (WPA)

The wavelet packet method provides for signal various analysis choices. In discrete wavelet analysis, after the first decomposition of the original signal, other decompositions are made on the approximation side. It offers n+1 ways of decomposition for n level decomposition of signal. Wavelet packet method differs from the discrete wavelet method in terms of the decomposition diversity. Since WPA realizes the decomposition both of two branches, detail and approximation and provides $2^{2^{n-1}}$ various ways to encode the original signal. In other words, WPA generalization of DWT is a full decomposition tree of the original signal. Figure 4-26 shows the five-level Wavelet packet decomposition tree of a SEMG signal.

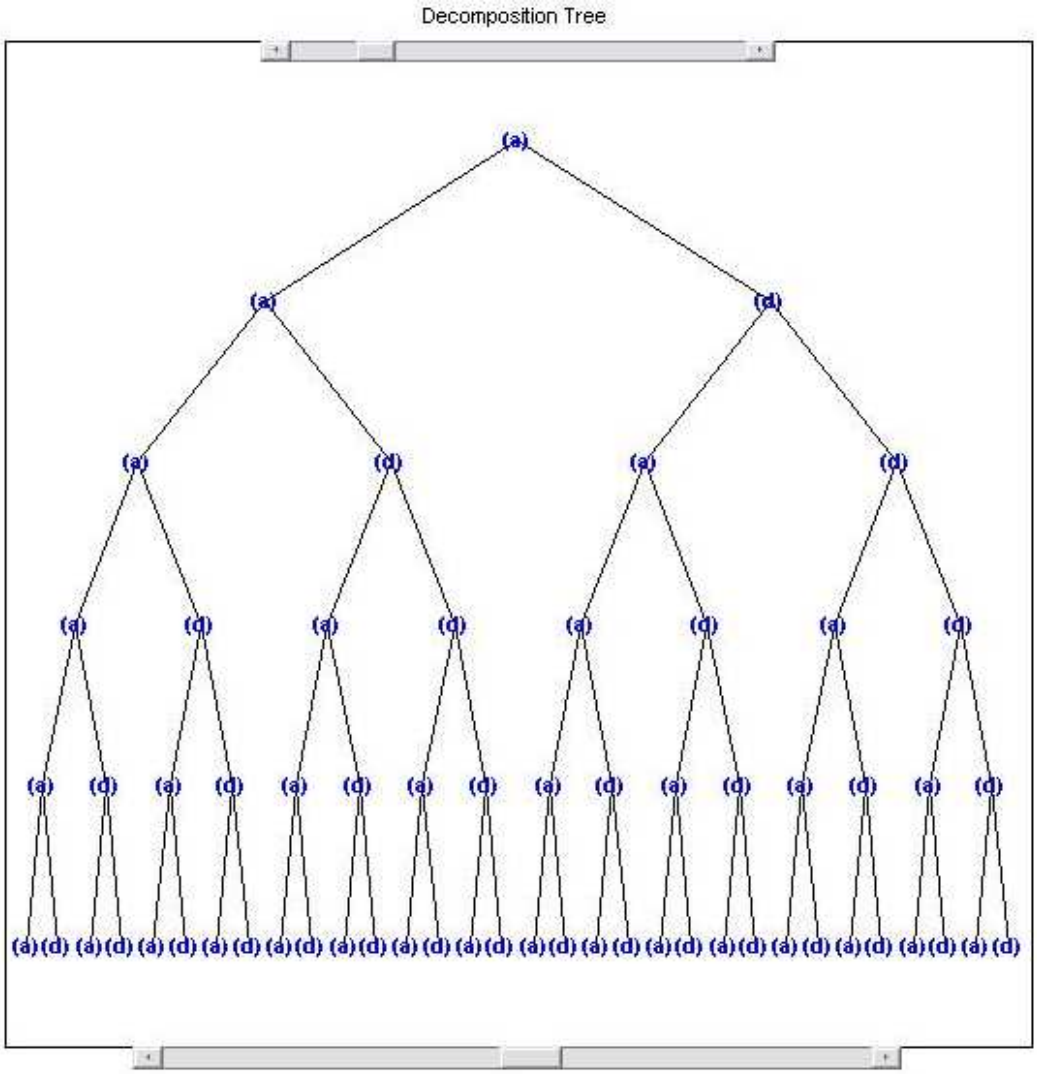

Figure 4-26 Five-level wavelet packet decomposition tree of a SEMG signal

The decomposition tree in Figure 4-27 shows the energy of each approximation and detail of the original signal. As seen, they are the fundamental part of the signal approximation based part has more energy with respect to the details.

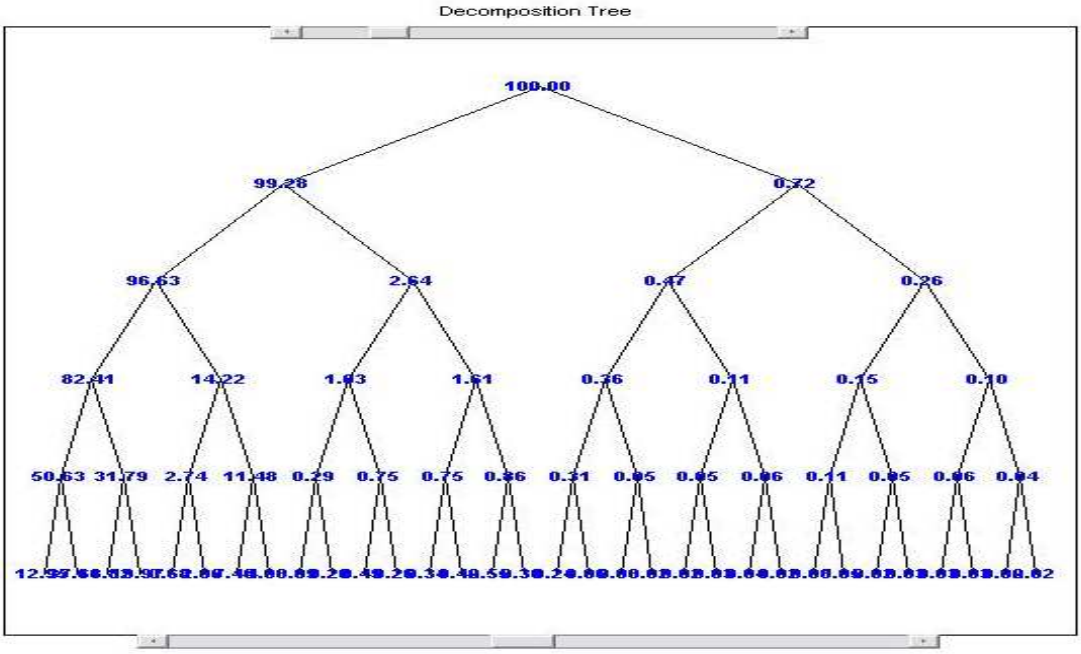

Figure 4-27: Energy Demonstration of Each Node

Entropy-based criterion provides the best convenient decomposition of a signal. Figure 4-28 represents an example of entropy-based criterion applied to the previous tree.

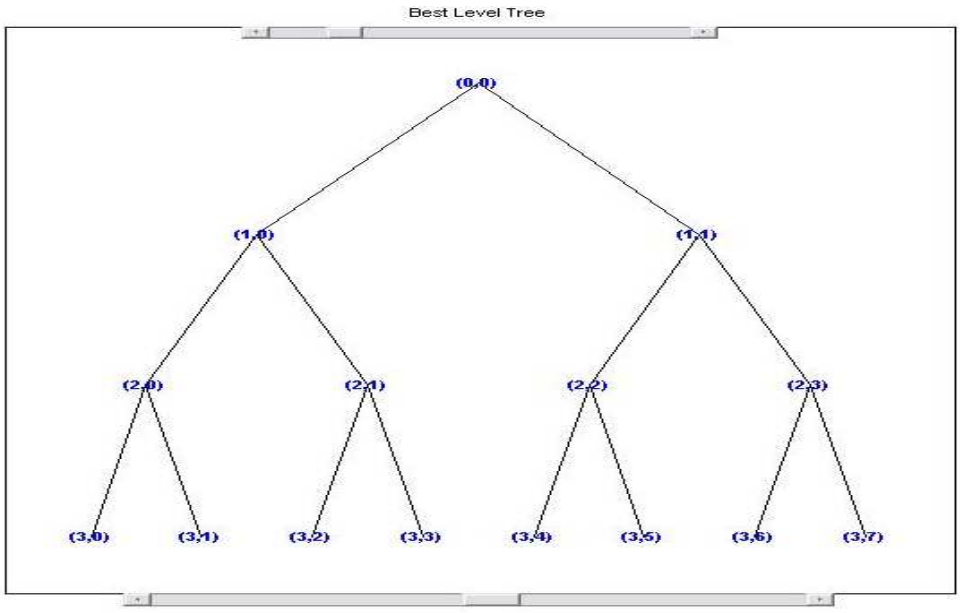

Figure 4-28 Selection of the best level tree

Depending on the information above, in this research feature extraction method is applied to the third level and by using of entropy-based criterion best level is selected for decomposition [64].

The graphs in figure 4-29 represent the signals each node has. Sum of each signal composes the original signal itself. As computed and introduced before, (3, 0), (3, 1), (3, 2), (3, 3), (3, 4) are selected as features of the SEMG signal. (3,5), (3,6), (3,7) are not preferred due to their quite small value. Under processes, the small valued signals are affected by round-off error and can not reflect the exact result. That is since the first groups contains five nodes is selected as features to be used in classification process.

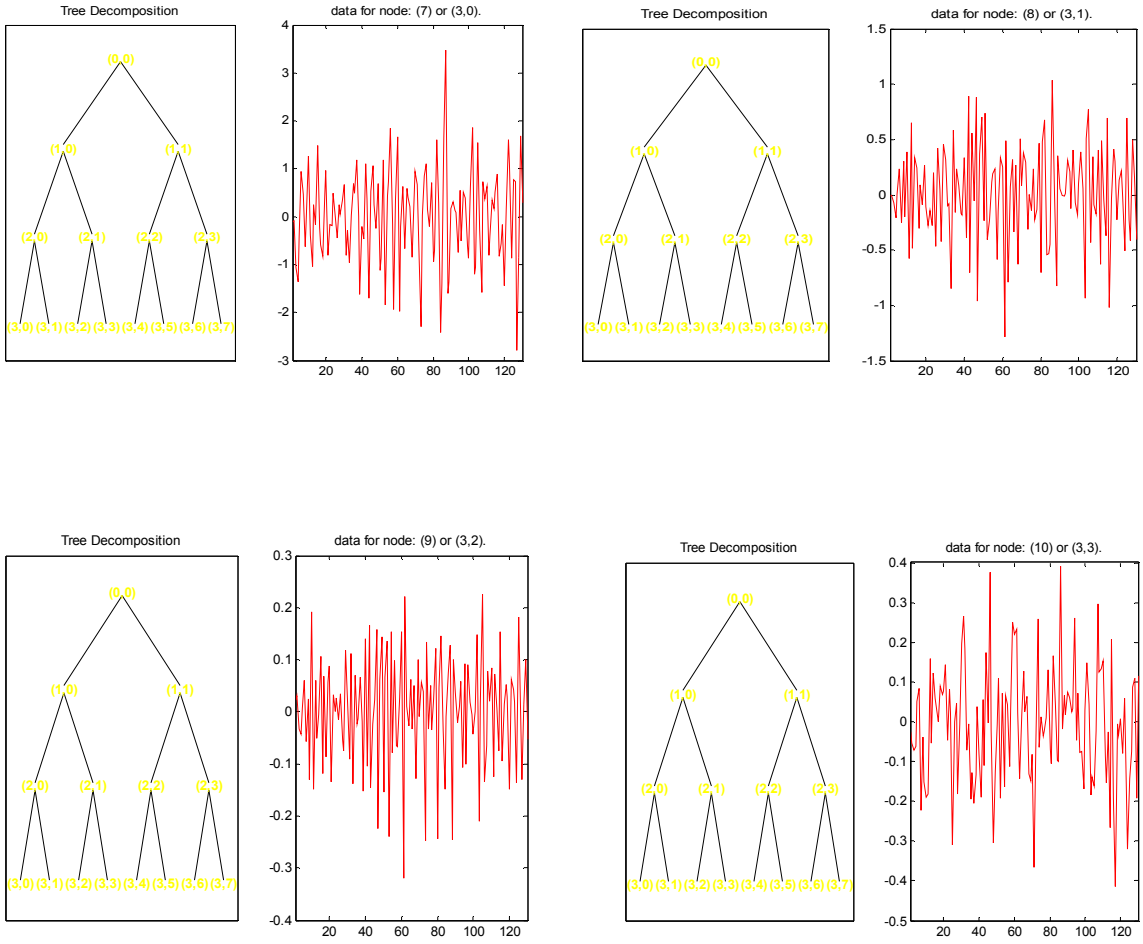

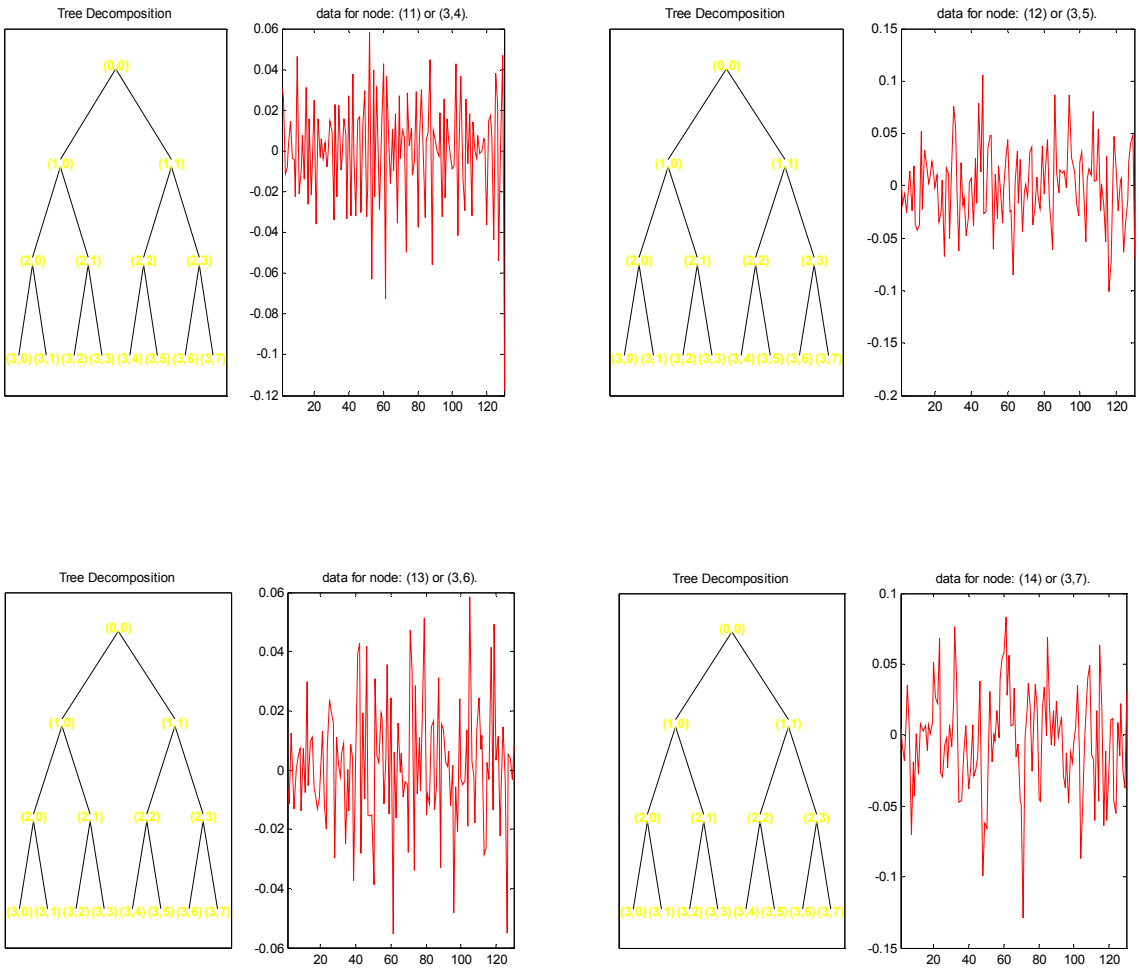

Figure 4-29 Decomposition of the original SEMG signal

5 EXPERIMENTAL STAGE OF FEATURE EXTRACTION METHODS

The aim of the thesis after the data acquisition part is completing the rest of the thesis study by making a satisfactory classification of four different data. In the experiment part of the thesis, approximately 200 sets of data were collected by means of data acquisition device and sent them to the PC to make the various feature extraction implementations. 40 data for each gesture, that is, flexion to palm, extension of digits, flexion of thumb and extension of thumb are collected for determining their features. Each data cluster for each gesture is not measured simultaneously. To illustrate, for the gesture of flexion to palm, 40 data is collected only connecting related muscle group (flexor digitorum superficialis and flexor digitorum profundus) to the circuit. To increase the fidelity and pureness of the signal and decrease the possibility of the contribution of other muscles to the signal, first of all, only one channel is connected to the system. Four times, 40 data are collected for each gesture in separate times. Features of each gesture are determined trying all discussed methods in the previous chapter despite the highly nonlinear conditions for sensitive SEMG signals. After collecting features for 160 data, feature selection process is applied to each of them by removing small amount of outliers from the feature cluster. The rest of pure features are prepared to another process. Their mean value is computed by dividing sum of the selected features to their number. Finally, each method has its feature vector for each gesture.

The last 40 data are measured for recognition of two gestures, flexion of digits to palm and extension of digits when all the channels are connected to circuit. Difficulty of classification reveals at this moment. Since, when someone wants to extent his/her digits voluntarily, neighbors of that muscle also contract involuntarily. In other words, when all the electrodes are connected to the system; but only one gesture is intended to flexion/extraction, the other muscles also contract and send their signal to the circuit simultaneously. The intense of the involuntary contraction of neighborhood muscles changes directly proportional to their distance from the objective gesture of the muscle.

In this research, to compare the feature extraction methods they are four different gestures form four different classes. Each of these classes has its certain feature vector. In other words, the features are as if identification card of each class. The features of each class are called reference features (f_{ref}). The new features of the intended muscle contraction are called input features (f_{inp}). Here is the classification structure of the signals.

In ideal case, If f_{ref}-f_{inp}=0, features are completely matched coming features find their class with %100 accuracy.

This equality can be generalized in this way:

$$f_{ref} - f_{inp} \leq e$$, where e is the error.

For use in comparison of different methods, this equation is normalized.

$$\frac{f_{ref} - f_{inp}}{f_{ref}} \leq e_n$$, where e_n is the normalization error.

In this research, e_n is also called proximity.

Proximity is determined based on all the normalized error of the data. In this research, normalized error of 40 data per each gesture is computed. As to the results, proximity is determined without conflicting one feature to more than one class or features of different gestures to one class. Finally, proximity is selected as 0.15.

If $\frac{f_{ref_c} - f_{inp_k}}{f_{inp_c}} \leq 0.15$ where $k = 1,2,3,4$ and $c = 1,2,3,4$, input n(k) belongs to class c

Otherwise, input k does not belong to any classes.

For giving an example, normalization error is computed for two different gestures, flexion to palm or extension to digits. In this example, computation result shows the normalization error of the randomly selected one data for each two gestures. Since normalization error is the core of the classification method, this is demonstrated as a comparison of feature extraction methods below. Normalization error of involuntarily extraction and flexion of the muscles does not specified; but their normalized error range is in between 0.8-1.2.

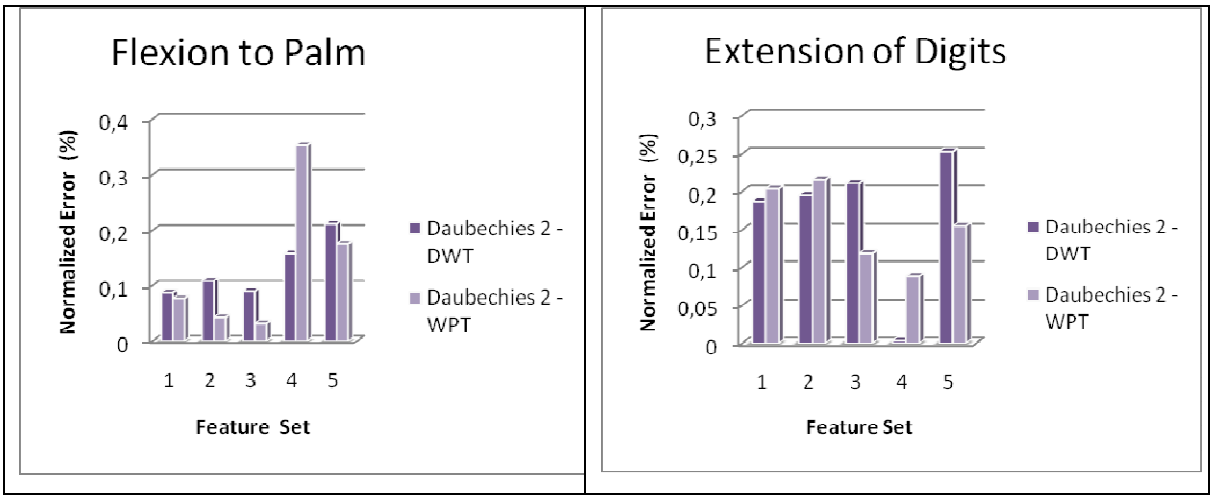

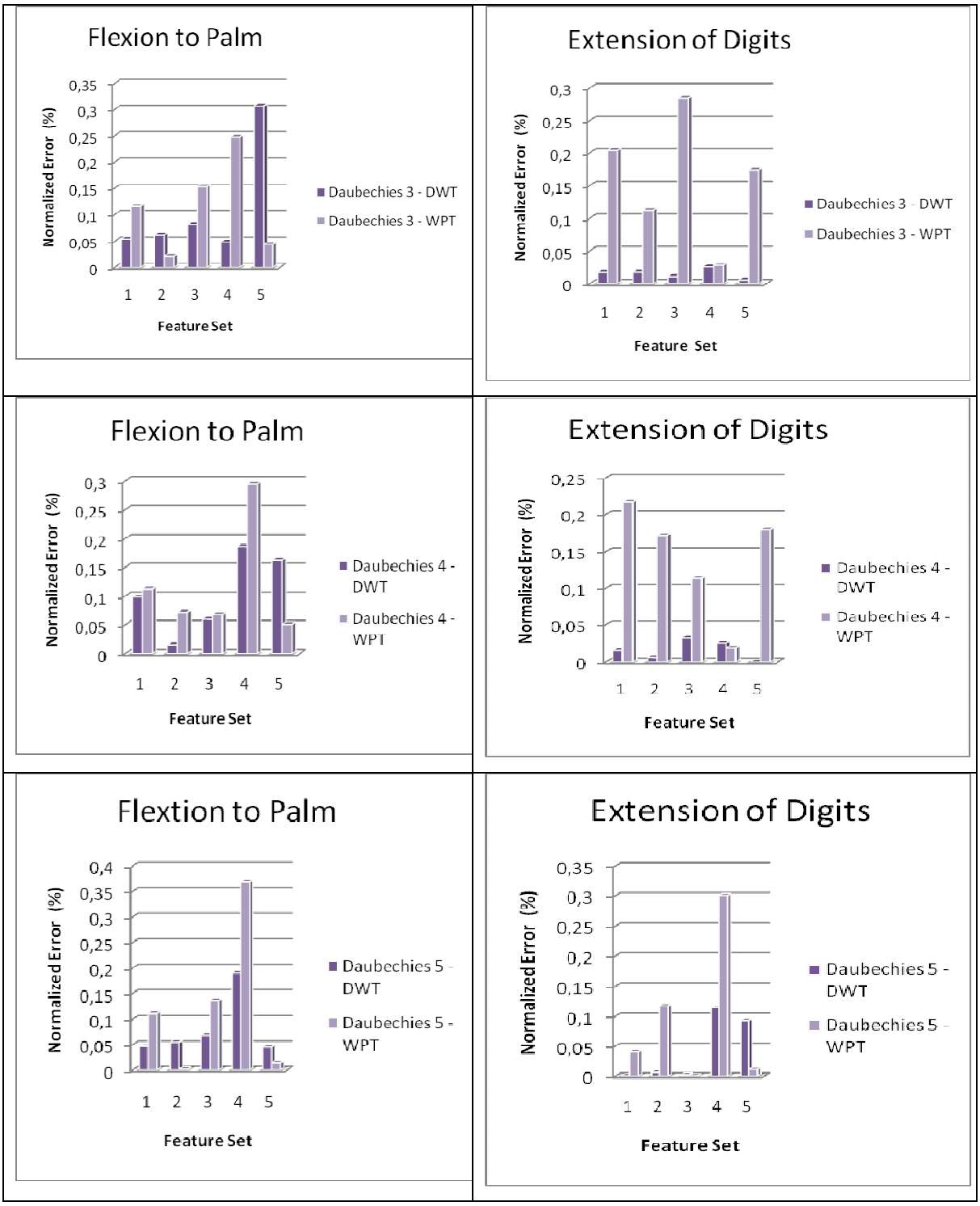

Figure 5-1 Normalization Error for the data of flexion to palm and extension of digits as to the Daubechies Family of DWT and WPT

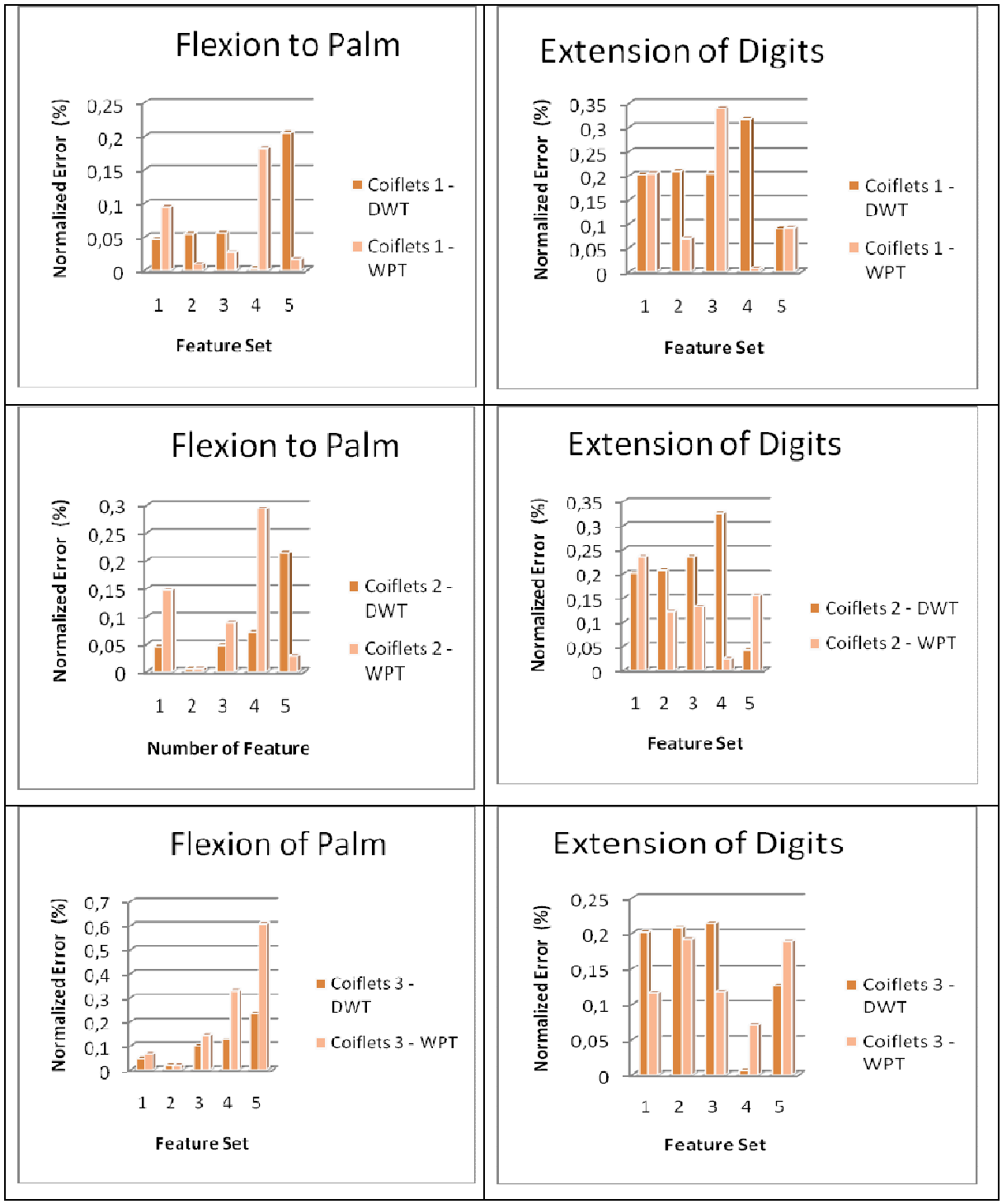
Flexion to Palm
Normalized Error (%)
0,25
0,2
0,15
0,1
0,05
0
1 2 3 4 5
Feature Set
Coiflets 1 - DWT
Coiflets 1 - WPT
Extension of Digits
Normalized Error (%)
0,35
0,3
0,25
0,2
0,15
0,1
0,05
0
1 2 3 4 5
Feature Set
Coiflets 1 - DWT
Coiflets 1 - WPT
Flexion to Palm
Normalized Error (%)
0,3
0,25
0,2
0,15
0,1
0,05
0
1 2 3 4 5
Number of Feature
Coiflets 2 - DWT
Coiflets 2 - WPT
Extension of Digits
Normalized Error (%)
0,35
0,3
0,25
0,2
0,15
0,1
0,05
0
1 2 3 4 5
Feature Set
Coiflets 2 - DWT
Coiflets 2 - WPT
Flexion of Palm
Normalized Error (%)
0,7
0,6
0,5
0,4
0,3
0,2
0,1
0
1 2 3 4 5
Feature Set
Coiflets 3 - DWT
Coiflets 3 - WPT
Extension of Digits
Normalized Error (%)
0,25
0,2
0,15
0,1
0,05
0
1 2 3 4 5
Feature Set
Coiflets 3 - DWT
Coiflets 3 - WPT

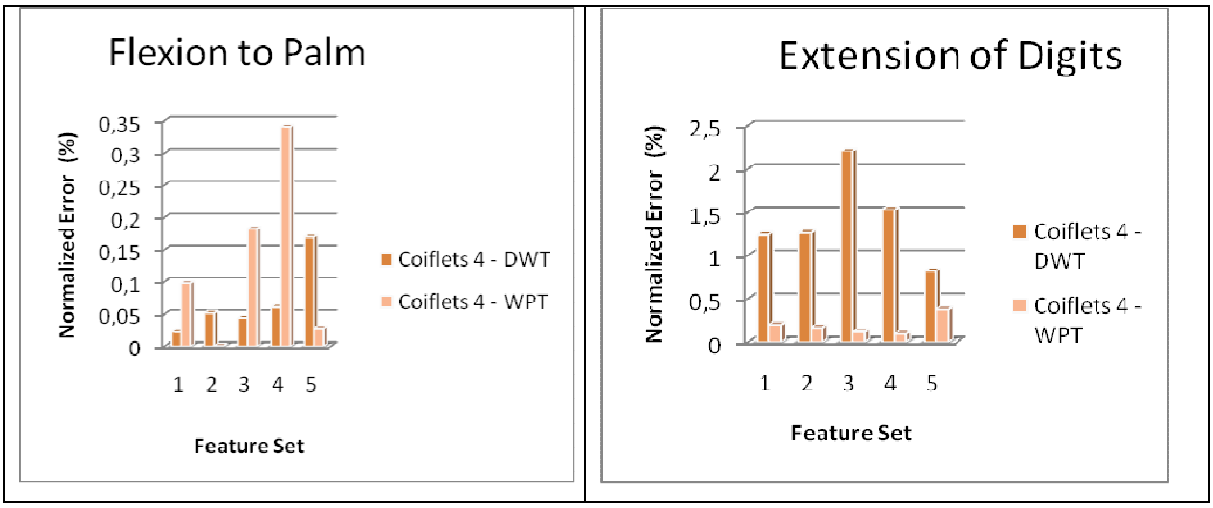

Figure 5-2 Normalization Error for the data of flexion to palm and extension of digits as to the Coiflets Family of DWT and WPT

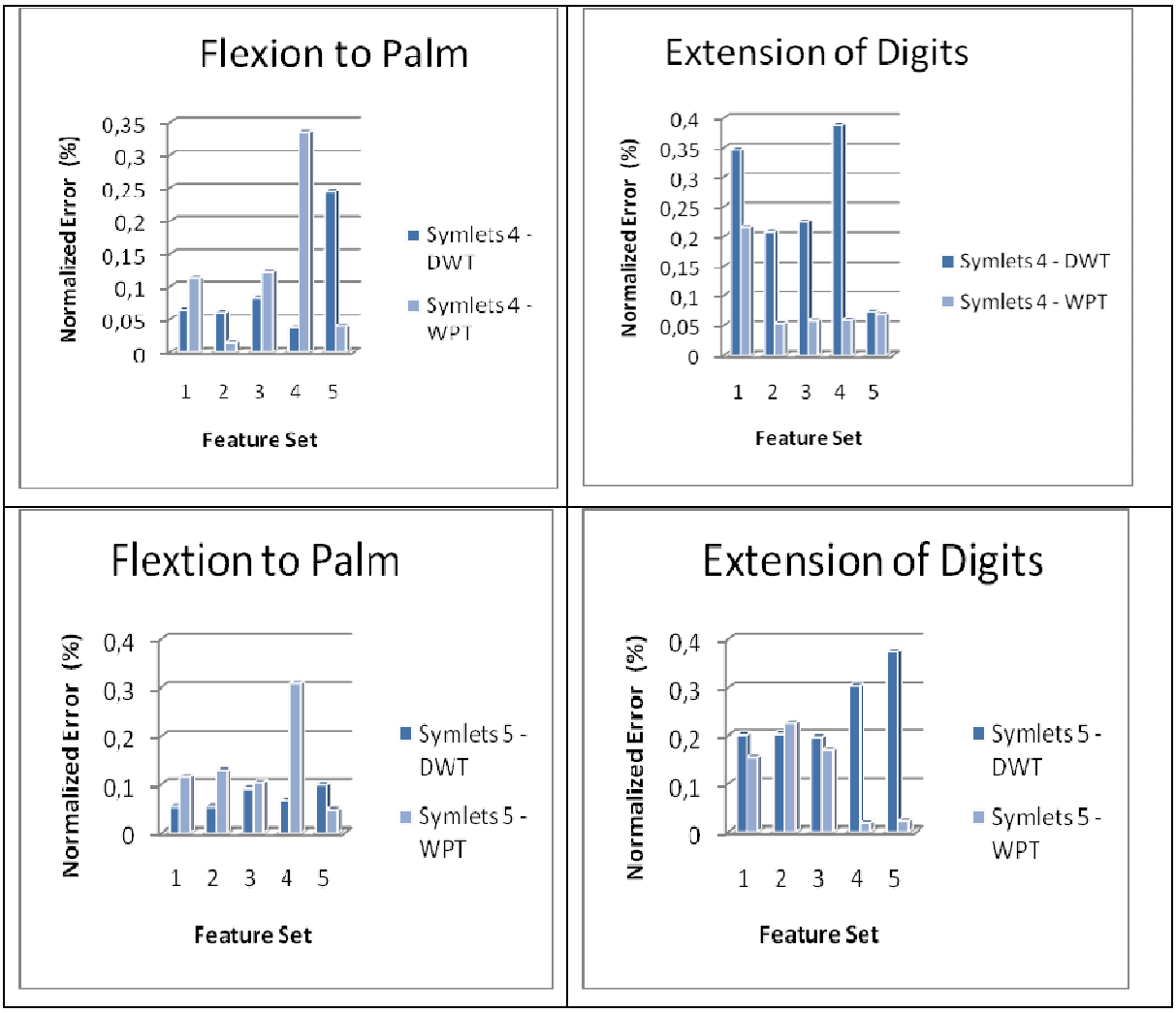

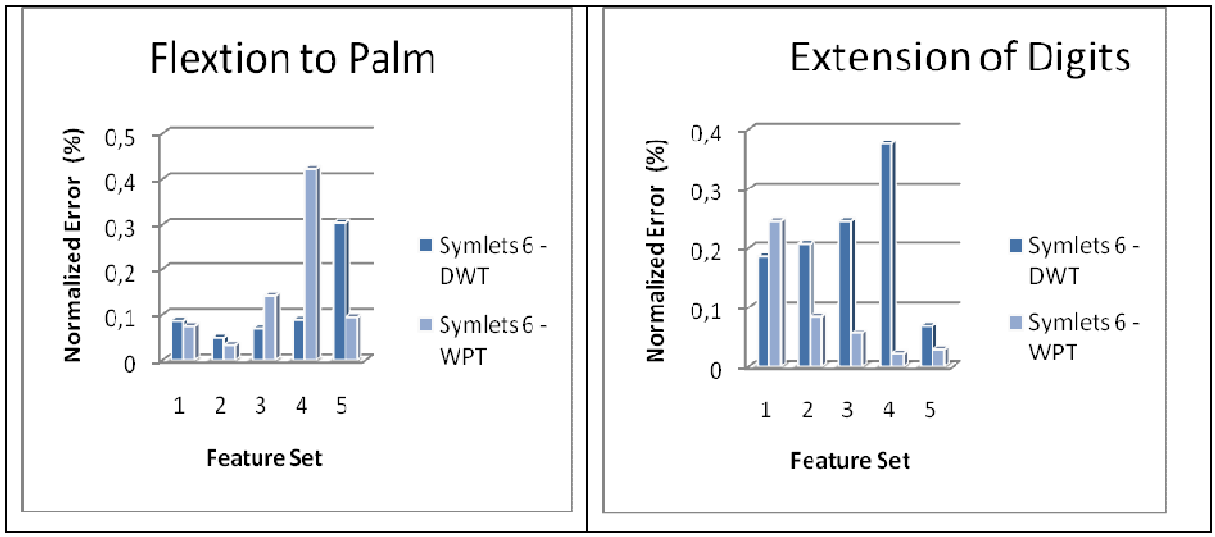

Figure 5-3 Normalization Error for the data of flexion to palm and extension of digits as to the Symlets Family of DWT and WPT

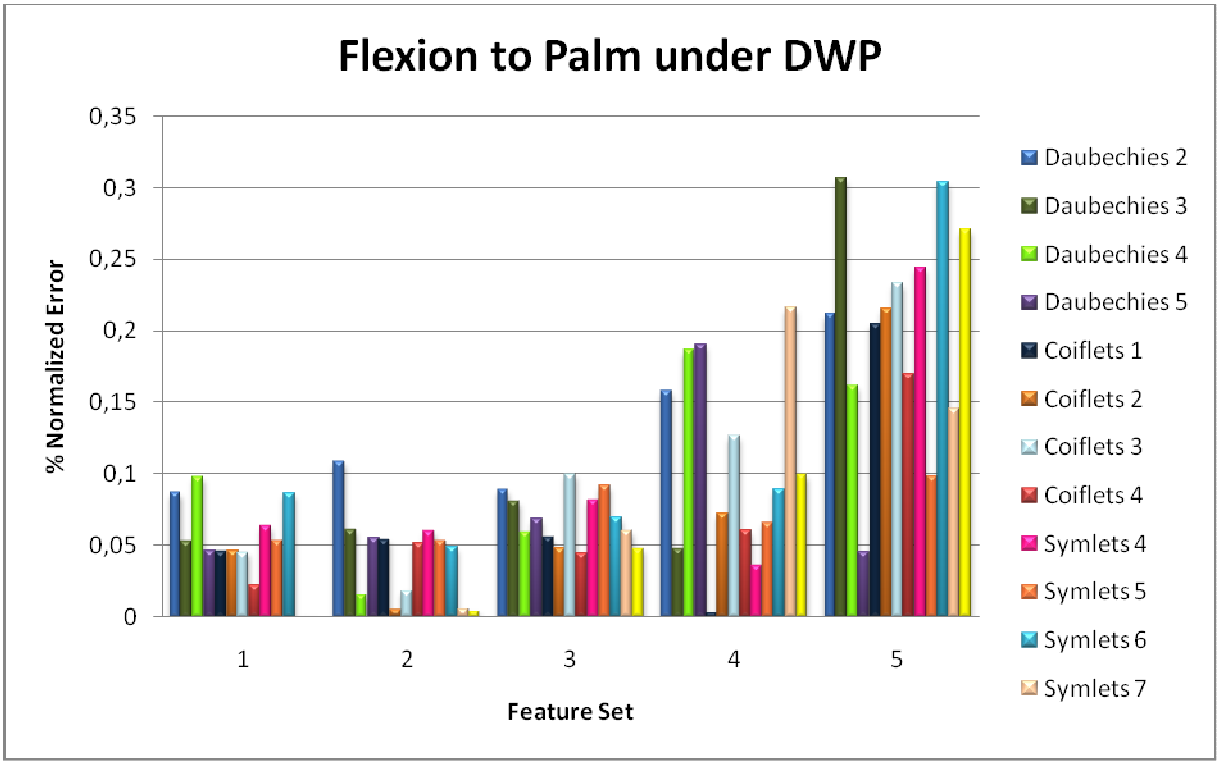

Figure 5-4 Normalization error for the data of flexion to palm as to the Daubechies, Coiflets and Symlets Families of DWT

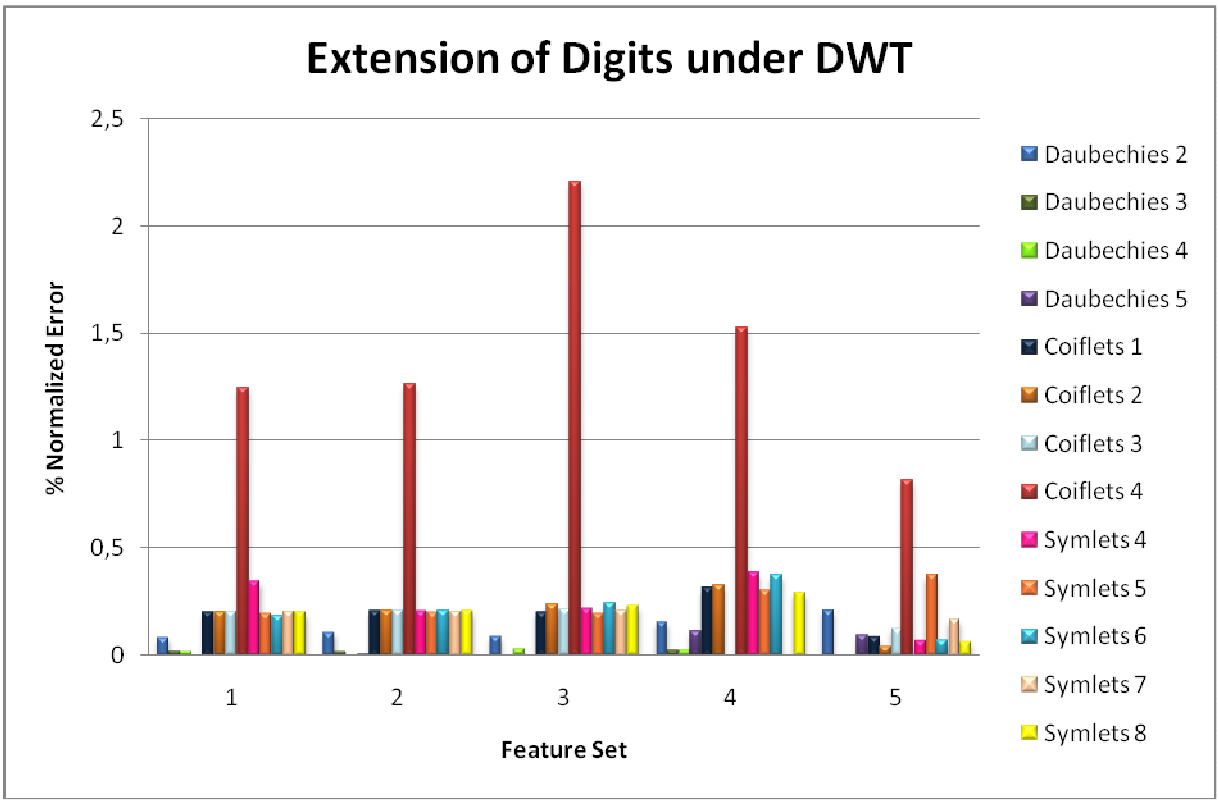

Figure 5-5 Normalization error for the data of extension of digits as to the Daubechies, Coiflets and Symlets Families of DWT

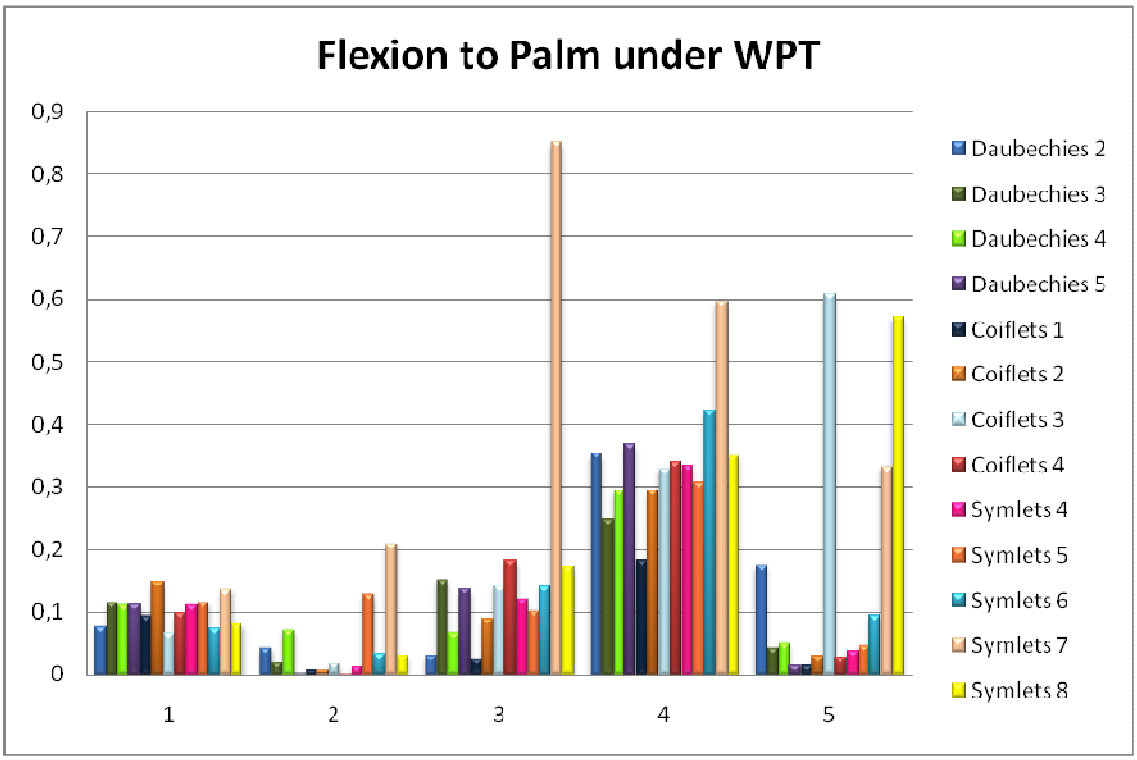

Figure 5-6 Normalization error for the data of flexion to palm as to the Daubechies, Coiflets and Symlets Families of WPT

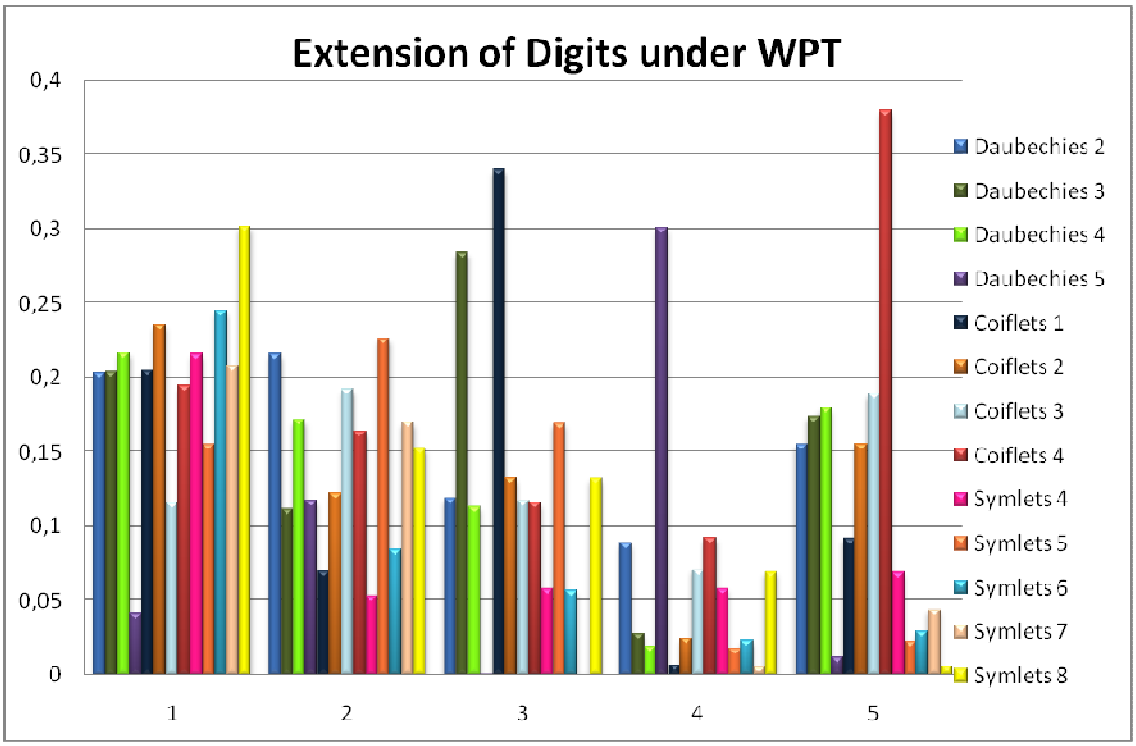

Figure 5-7 Normalization error for the data of extension of digits as to the Daubechies, Coiflets and Symlets Families of WPT

FEATURE EXTRACTION BASED ON TIME DOMAIN						
ENERGY METHOD	HAMMING WINDOW			TRAPEZOIDAL WINDOW		
FLEXION TO PALM	FLEXION TO PALM			FLEXION TO PALM		
266,31900	45,38306	59,58591	72,04104	85,42414	116,60819	144,20464
244,6832632	42,5538054	57,88132248	66,65856434	90,94911562	123,7644691	143,8636434
NORMALIZED ERROR (%):	NORMALIZED ERROR (%):			NORMALIZED ERROR (%):		
0,081239919	0,062341673	0,028607182	0,074713986	0,064677014	0,061370318	0,002364654
EXTENSION OF DIGITS	EXTENSION OF DIGITS			EXTENSION OF DIGITS		
420,3101949	66,41298	95,30775	122,95934	165,41328	242,80172	286,35682
471,6587769	70,41865916	122,9484754	123,3430343	144,9595434	250,4956791	276,175086
NORMALIZED ERROR (%):	NORMALIZED ERROR (%):			NORMALIZED ERROR (%):		
0,1221683	0,0603147	0,2900155	0,0031205	0,1236523	0,0316883	0,0355561

Figure 5-8 Normalization error for the data of flexion to palm as to the Energy, Hamming and Trapezoidal Window methods

FEATURE EXTRACTION ON TIME & FREQUENCY DOMAIN					
STFT (with Hamming Window)					
F1 (M0)	F2 (M1)	F3 (M2)	F4 (E)	F5 (fexp)	F6 (fvar)
FLEXION TO PALM					
88,9514305	11384,0214	2590743,045	7,200505727	130,3871493	12535,72834
128,2685459	17421,37834	3912283,969	9,737582608	137,332679	12261,55674
NORMALIZED ERROR (%):					
0,442006555	0,530336049	0,510101118	0,35234704	0,053268514	0,021871214
EXTENSION OF DIGITS					
125,2535061	19303,59666	4538716,503	11,70533116	154,6943847	12542,99321
190,574978	28446,79048	6512800,567	18,76944208	149,6345156	11935,88573
NORMALIZED ERROR (%):					
0,5215141	0,4736523	0,4349432	0,6034952	0,0327088	0,0484021

Figure 5-9 Normalization error for the data of flexion to palm as to the STFT methods

5.1 Classification Performance Comparison of the Feature Extraction Methods

In time domain feature extraction methods, windowing methods show the better performance then the energy methods. Hamming window is the most successful with respect to the energy method and Trapezoidal window. However, their performance is not preferred when using this classification method as seen in Figure 5-10. As a frequency domain experiment, spectral energy was selected as a feature; however it does not give any satisfactory classification result.

In STFT transform, M0, M1, M2 and E did not give satisfactory results. Energy is better than moments but; worse than central and variance frequency. Central and variance frequency gives the most satisfactory result in STFT transform and can be preferred as a feature (Figure 5-11).

In discrete wavelet transform, Daubechies 2, 3, 4, 5, Coiflets 1, 2, 3, 4, Symlets 4, 5, 6, 7, 8 are tested on the SEMG signal until level 5. Energy of the each level is the feature vector of the signal. According to classification performance of DWT method, symlet5 at level 2 and Daubechies5 at level 3 & level 5 are selected the best bands of the SEMG signal (Figure 5-12).

In wavelet packet transform, Daubechies 2, 3, 4, 5, Coiflets 1, 2, 3, 4, Symlets 4, 5, 6, 7, 8 are tested on the SEMG signal at level 3, for LLL, LLH, LHL, LHH and HLL. The satisfactory results are obtained by Coiflets 3-LHH, Symlets 7-LHH & HLL (Figure 5-13).

Since Wavelet transform provides multiresolution representation and shapes of the selected wavelets are similar to MUAP, Wavelet transform provides the best energy localization and gives the best satisfactory results with respect to the others. In addition, Wavelet Packet transform includes more detail and distinguishing information in its features its results outperform the discrete wavelet transform in average.

T-test was also applied to features to guarantee the results. In this test, p value is about 0.05 for all the evaluation results. Classification technique based on normalized errors of the features is tested in this way.

All the observations show that the classification performance of the time–frequency based feature extraction methods gives the more satisfactory results. Moreover, all the experienced methods can be ordered with respect to the success of their classification performances as following:

Energy Method, Trapezoidal Window, Hamming Window, Short Time Fourier Transform, Discrete Wavelet Transform, Discrete Wavelet Packet Transform.

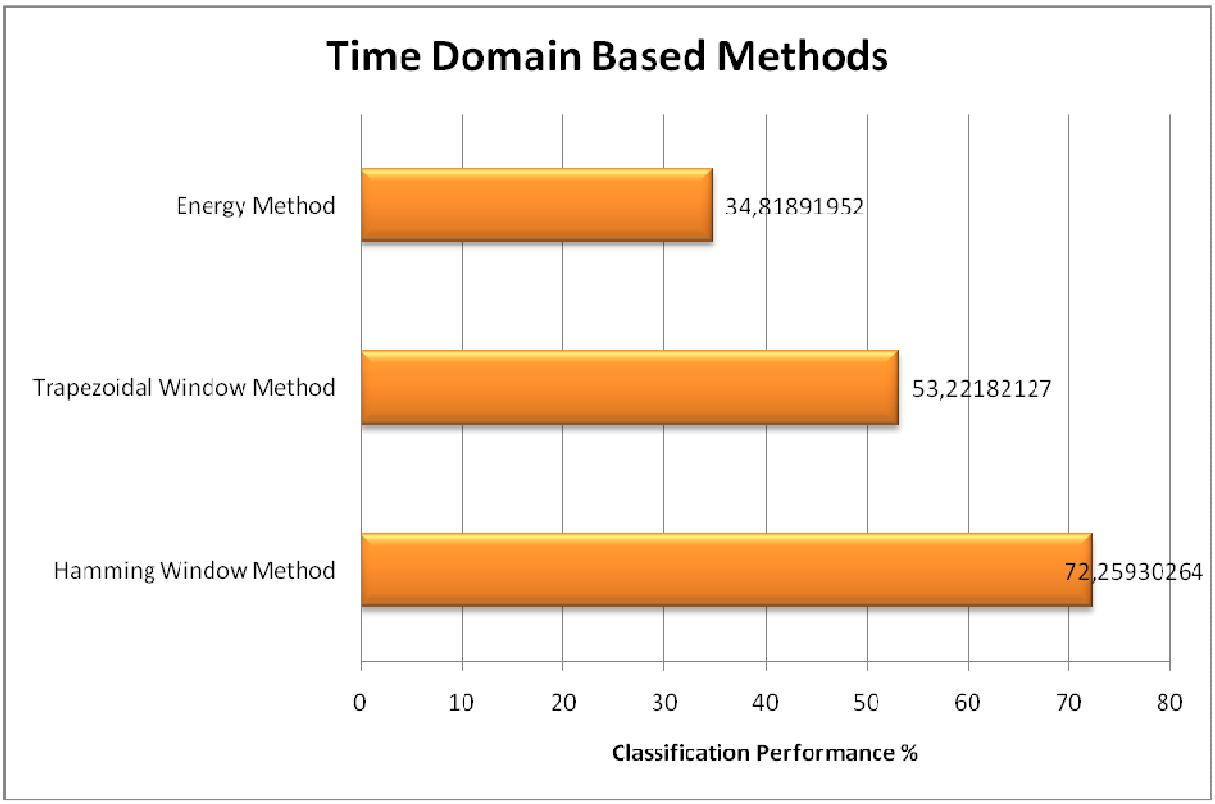

Figure 5-10 Classification performance of Energy and Window Methods

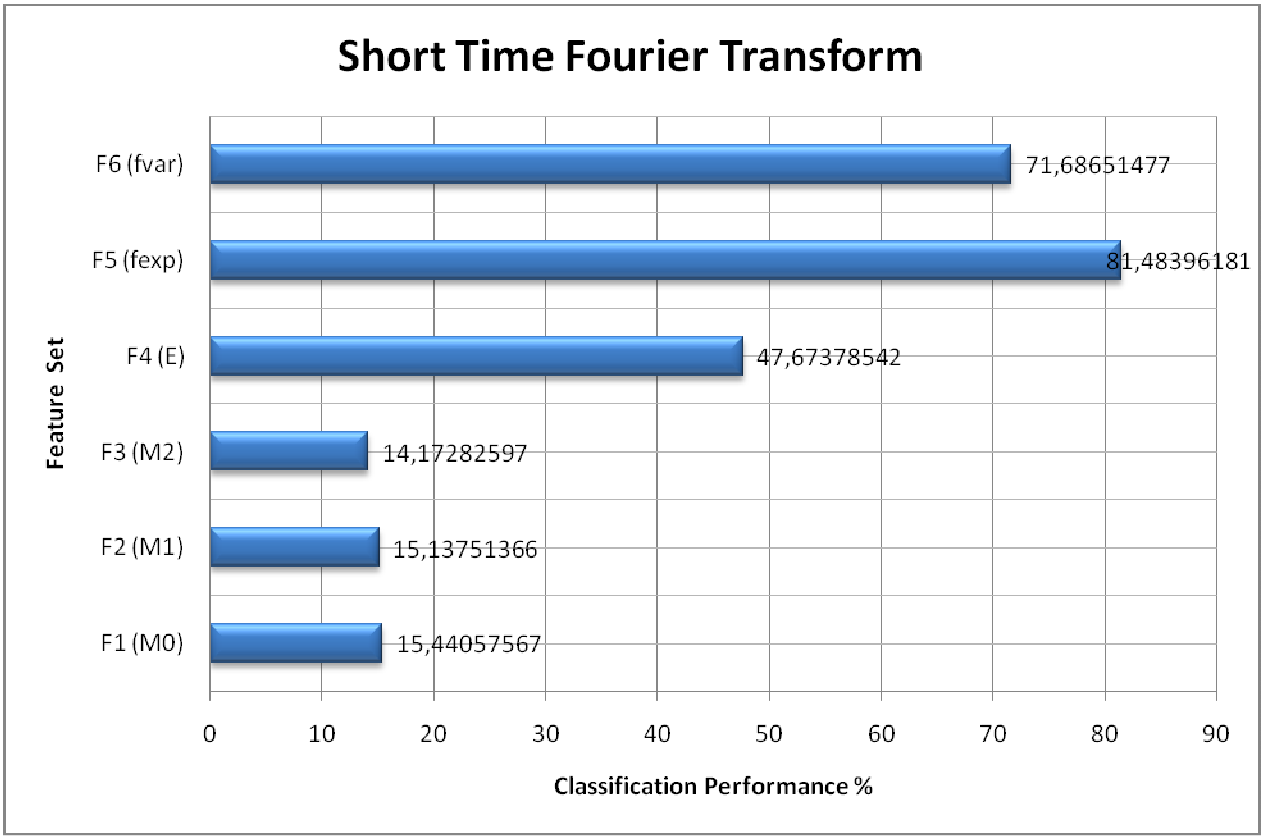

Figure 5-11 Classification performance of STFT

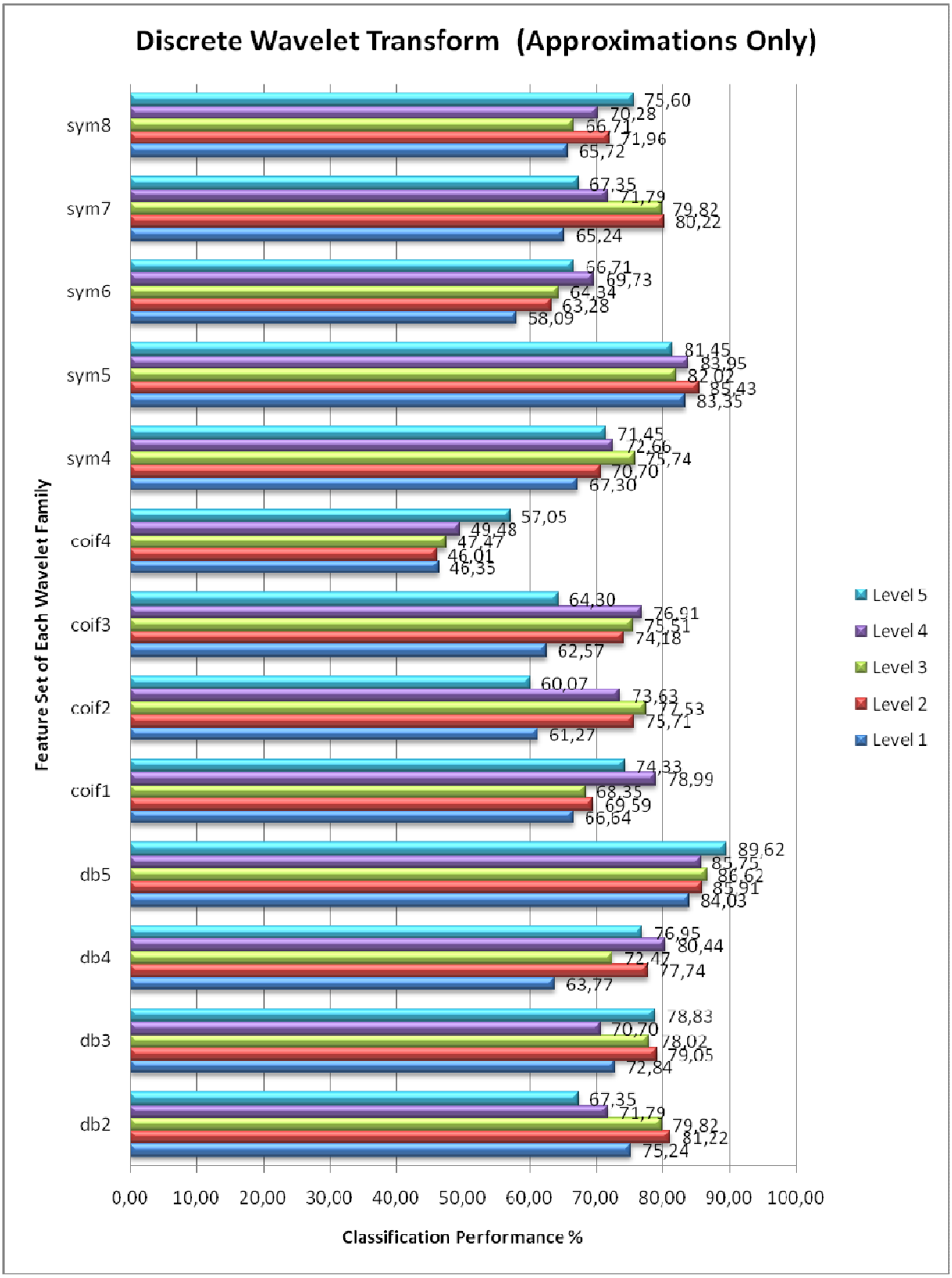

Figure 5-12 Classification performance of DWT

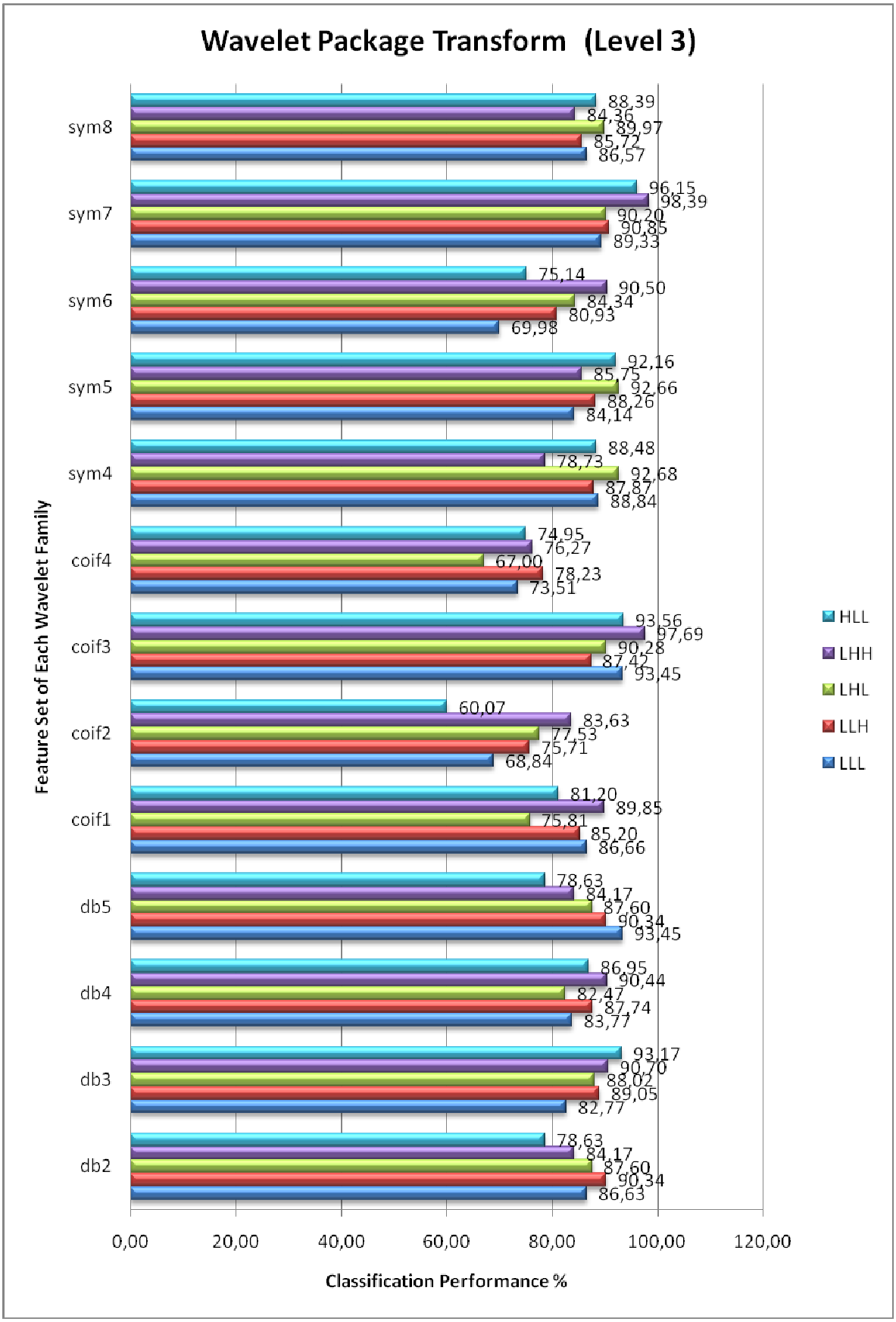

Figure 5-13 Classification performance of WPT

6 CONCLUSION

This thesis presents both hardware design for SEMG signal measurement and comparison of the feature extraction methods by applying on measured and recorded SEMG signals.

In the first part of the thesis, the measurement circuit is designed and built to measure the weak and noisy SEMG signal. In order to reduce many diverse noises, motion artifacts and DC offset from the signal, band-pass filters, high CMRR instrumentation amplifier (In-Amp), low noise operational amplifiers, %1 tolerances resistors, wide ground spaces on the PCB, aluminum foil surrounded circuits, two separate circuits, shielded cables, strips, silicon, proper design against common mode signal are considered and implemented. Specification of the proper design is based on the elimination of common mode signal and reducing the noises. Common mode signal is removed in three ways. Some negative proportion of the common mode signal is applied back to the body through the reference electrode to suppress the common mode noise in the acquired SEMG signal. Differential amplifier in the In-Amp subtracts two input voltage and sent the SEMG signals without common mode voltage in ideal case. In-Amp has high CMRR is employed to approximate it to the ideal case. Electrodes and amplifier are placed onto the same PCB which is contact with skin. The base circuit includes band pass filter, rectifier, and reference electrode. Amplifier must be as close as possible to the signal entrance not to amplify both signal and common mode together. That is since two separate circuits are produced. In the base circuit, band pass filter eliminates the noises in the range between 20-500 Hz, so DC offset can also be removed here. Five parallel filtering and rectification circuits are built on the same board of the base circuit each for one gesture. Outputs of the base circuit are transferred to the PC by a DAQ which makes the A/D and D/A conversion.

The second part of the thesis begins after obtaining digital SEMG signal. To use the measured SEMG signals for the multi-functional prosthesis, prehensile SEMG signals have to be classified. For this purpose, signals are measured and recorded for each gesture and they are defined by applying several feature extraction methods. Many diverse feature extraction methods exist. In this research some of them are selected to their time-frequency criterion. Only time domain functions, only frequency domain functions and both of them are compared. Finally, time-frequency analysis outperforms only time and only frequency based methods. Time and frequency related methods, Short Time Fourier Transform, Discrete

Wavelet Transform and Wavelet Packet Transform can also be separated within their self as to their classification performance. The feature extraction methods using Wavelet Packet Transform yield better performance and make the classification with the better accuracy. Three wavelet families, Daubechies, Symlets and Coiflets are experienced in both wavelet transforms. Their best level and best nodes are specified after the experiments. In future studies, henceforth, these levels and nodes will be used.

Future work contains real time classification, comparison of various classification methods, compact circuit design, and haptic interfaced mechanical design of hand.

7 REFERENCES

[1] Graupe, D. and W. K. Cline., "Functional Separation of EMG Signals via ARMA Identification Methods for Prosthesis Control Purposes," IEEE Tr. on Systems, Man, and Cybernetics SMC-5 (2), 252–259, (March 1975),

[2] Basmajian, M,D., De Luca, C,J., "Muscles Alive", Williams & Wilkins, Baltimore,1985.

[3] Zardoshti, M., Wheeler, B., Badie, K., Hashemi, M, R., "EMG Feature Evaluation for Movement Control of Upper Extremity Prostheses", IEEE Trans. Rehabil. Eng. 3 324-33.

[4] Englehart, K., Hudgins, B., Parker, P., Stevenson, M., "Time-Frequency Representation for Classification of the Transient Myoelectric Signal", In ICEMBS'98. Proceedings of the 20th Annual International Conference on Engineering in Medicine and Biology Society. ICEMBS Press, (1998).

[5] Englehart, K., "Signal Representation for Classification of the Transient Myoelectric Signal". Doctoral Thesis. University of New Brunswick, Fredericton, New Brunswick, Canada, (1998a)

[6] Englehart, K., Hudgin, B., Parker, P.A. and Stevenson M., "Improving Myoelectric Signal Classification using Wavelet Packets and Principle Component Analysis", In ICEMBS'99. Proceeding of the 21st Annual International Conference on the Engineering in Medicine and Biology Society, ICEMBS Press. (1999)

[7] Englehart, K., Hudgin, B., Parker, P.A., "A Wavelet-Based Continuous Classification Scheme for Multifunction Myoelectric Control", In IEEE Transactions on Biomedical Engineering, vol. 48, No. 3, pp. 302-311, (2001).

[8] Crawford, B., Miller, K., Shenoy, P., Rao, R., "Real-Time Classification of Electromyographic Signals for Robotic Control", (2005).

[9] Zhang, X., Yang, Y., Xu, X., Zhang, M., "Wavelet Based Neuro-Fuzzy Classification for EMG Control", (2002).

[10] Nishikawa, D., Yu, W., Yokoi, H., Kakazu, Y., "On-Line Supervising Mechanism For Learning Data In Surface Electromyogram Motion Classifiers".

[11] Boostani, R., Moradi, M.H., "Evaluation of the Forearm EMG signal Features for the control of a Prosthetic Hand".

[12] Kilby, J., Hosseini, H.G., "Wavelet Analysis of Surface Electromyography Signals".

[13] Du ,S., Vuskovic, M., "Temporal vs. Spectral Approach to Feature Extraction from Prehensile EMG Signals", Proc. of the IEEE Internat. Conference on Information Reuse and Integration (IEEE IRI-2004), Las Vegas, Nevada, Nov. 8-10, 2004, pp. 344-250.

[14] Carreño, R., Vuskovic, M., "Wavelet Transform Moments for Feature Extraction from Temporal Signals", 2nd Internat. Conference in Control, Automation and Robotics (ICINCO 2005), 14-17 September, Barcelona, Spain, 2005.

[15] Haihua, Liu et al, "Wavelet Transform and Real-Time Learning Method for Myoelectric Signal in Motion Discrimination", (2005).

[16] Zheng, L., He, X., "Classification Techniques in Pattern Recognition", WSCG, conference proceedings, ISBN 80-903100-8-7, (2005).

[17] Arieta, A, H., Katoh, R, Yokoi, H., Wenwei, Y., "Development of multi-DOF electromyography prosthetic system using the adaptive joint mechanism", Applied Bionics and Biomechanics, Volume 3, pages 101 – 112, (2006).

[18] Zhao, Z., Chen, X., Zhang, X., Yang, J., Tu, Y., Lantz, V., Wang, K., "Study on Online Gesture SEMG Recognition", Advanced Intelligent Computing Theories and Applications. With Aspects of Theoretical and Methodological Issues ,pages 1257-1265, (2007).

[19] Shenoy, P., Miller, K. J., Crawford, B., Rao, P.N., "Online Electromyographic Control of a Robotic Prosthesis".

[20] Marieb.;**"**Human Anatomy & Physiology 5th edition, Benjamin Cummings", San Francisco,2001

[21] "Touch Bionics" [Online] Available: http://www.touchbionics.com

[22] “Neuromuscular Physiology”[Online] Available: http://bioweb.usc.edu/courses/2003-fall/documents/bisc306-lab_06.pdf

[23] “Basic Motor Pathway” [Online] Available: http://thalamus.wustl.edu/course/basmot.html

[24] Bear, Cannor, Paradiso, “Neuroscience Exploring the Brain”.

[25] “The Brain From Top to Bottom” [Online] Available: http://thebrain.mcgill.ca/flash/index_d.html

[26] “Motor Systems: Control of Movement & Behavior” [Online] Available: http://www.colorado.edu/intphys/Class/IPHY3730/09motorsystems.html

[27] Robertus., “Lecture Notes” [Online] Available: http://courses.cm.utexas.edu/jrobertus/ch339k/overheads-1.htm

[28] Mann, M, D., “The Nervous System in Action”

[29] Horch, K., Dhillon, G., “Neuroprosthetics Theory and Practice”

[30] Muzumdar, A., **“**Powered Upper Limb Prostheses: Control, Implementation and Clinical Application”, (2004).

[31] Moore, K. L., “Clinically Oriented Anatomy”

[32] Häyrynen, T., Tulkki, J., “Low Power Biomorphic Neural Circuits on Floating Gate MOS and SET Transistors”, [Online] Available:http://www.lce.hut.fi/publications/annual2003/node14.html

[33] Malmivuo, J., Plonsey, R., “Bioelectromagnetism Principles and Applications of Bioelectric and Biomagnetic Fields”

[34] “Wikipedia The Free Encyclopedia” [Online] Available: http://en.wikipedia.org/wiki/Action_potential

[35] “Encyclopedia Britannica- the Online Encyclopedia” Available: http://www.britannica.com/eb/article-9003611/action-potential

[36] Konrad, P.,“A Practical Introduction to Kinesiological Electromyography”, 2005

[37] Raez, M.B.I., Hussain, M.S., Mohd-Yasin, F., “Techniques of EMG Signal Analysis: Detection, Processing, Classification and Applications”.

[38] Bronzino, D., “The Biomedical Engineering Handbook Volume I”

[39] Webster, J.G., “Medical Instrumentation Application and Design”

[40] Eriksson, L., Sebelius, F., Balkenius, C., “Neural Control of a Virtual Prosthesis”

[41] Andreas, J. L., “Psychophysiology Human Behavior & Physiological Response”

[42] De Luca, C.J., “The use of surface electromyography in biomechanics”, Journal of Applied Biomechanics, 13 (2): 135-163.”, (1997).

[43] Childress, D, S., “Upper-Limb Prosthetics: Control of Limb Prostheses”, Atlas of Limb Prosthetics: Surgical, Prosthetic and Rehabilitation Principles.

[44] de Oliveira, A., Soares, A. B., “EMG Pattern Recognition for Prosthesis Control”

[45] McClellan, J. H., Schafer, R. W., Yoder, M. A., “DSP First A Multimedia Approach”.

[46] Herrera, A., Bernal, A., Isaza, D., Adjoadi, M., “Design Of An Electrical Prosthetic Gripper Using EMG and Linear Motion Approach”.

[47] Hassul, M. , Zimmerman, D., “Electronic Devices and Circuits”

[48] Newby, B., “Electronic Signal Conditioning”

[49] Kutz, M., “Design of Artificial Arms and Hands For Prosthetic Application”, 32.1-32.61

[50] Jonassen, N.,”Human Body Capacitance Static or Dynamic”, EOS/ESD Symposium 98-1 13.

[51] Hannaford, B., Lehman, S., “Short Time Fourier Analysis of the Electromyogram: Fast Movements and Constants Contraction”.

[52] “A Short Introduction to Gabor Analysis” [Online] Available: http://www.math.ucdavis.edu/~strohmer/research/gabor/gaborintro/node3.html

[53] Qian, S., Chen, D., “Joint Time Frequency Analysis-Methods and Applications”,(2007).

[54] Selesnick, I., “Short Time Fourier Transform”.

[55] Schniter, P., “Short Time Fourier Transform”.

[56] Akay, M.; “Time Frequency And Wavelets in Biomedical Signal Processing”

[57] “Wikipedia The Free Encyclopedia” [Online] Available: http://en.wikipedia.org/wiki/Short-time_Fourier_transform

[58] Kumar, D.K., Pah, N. D., Bradley, A., “Wavelet Analysis of Surface Electromyography to Determine Muscle Fatigue”.

[59] Burrus, C, S., Gopinath, R, A., “Introduction to Wavelets and Wavelet Transforms: A Primer”

[60] Moshou, D., Hostens, I., Papaioannou, G., Ramon, H., “Wavelets and Self Organizing Maps in Electromyogram (EMG) Analysis”.

[61] Wavelet Toolbox for use with MATLAB

[62] Vetterli, M., Kovačević, J., “Wavelets and Subband Coding”

[63] Signal Processing Toolbox for use with MATLAB

[64] Saito, N., Coifman, R. R., “Local Discriminant Basis and their applications”, J. Math. Imag. Vis., Vol. 5, no 4, pp. 337-358. (1995)

8 APPENDICES

8.1 Schematic of the Circuit on Electrodes

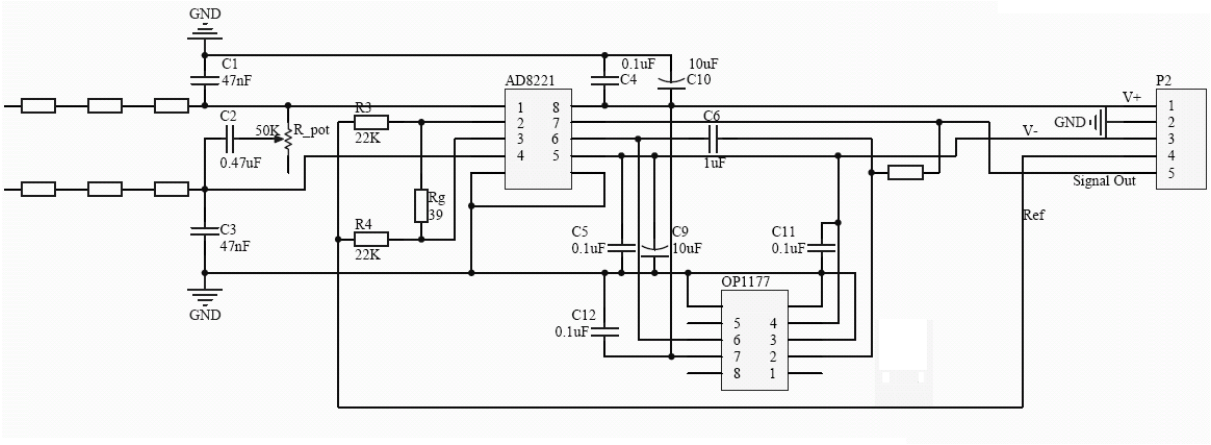

8.2 Design of the Circuit on Electrodes

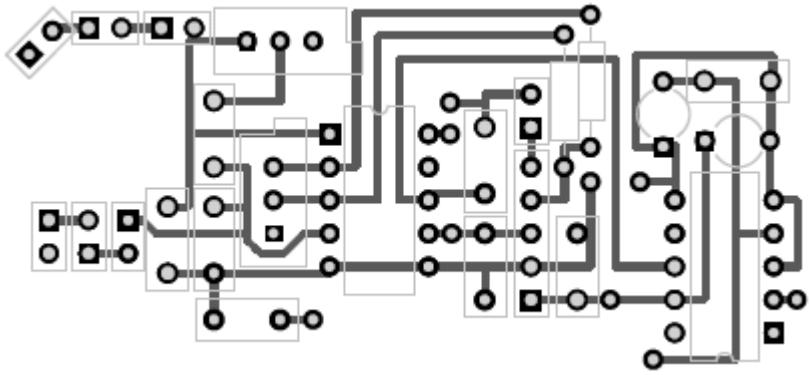

8.3 Schematic of the Base Circuit

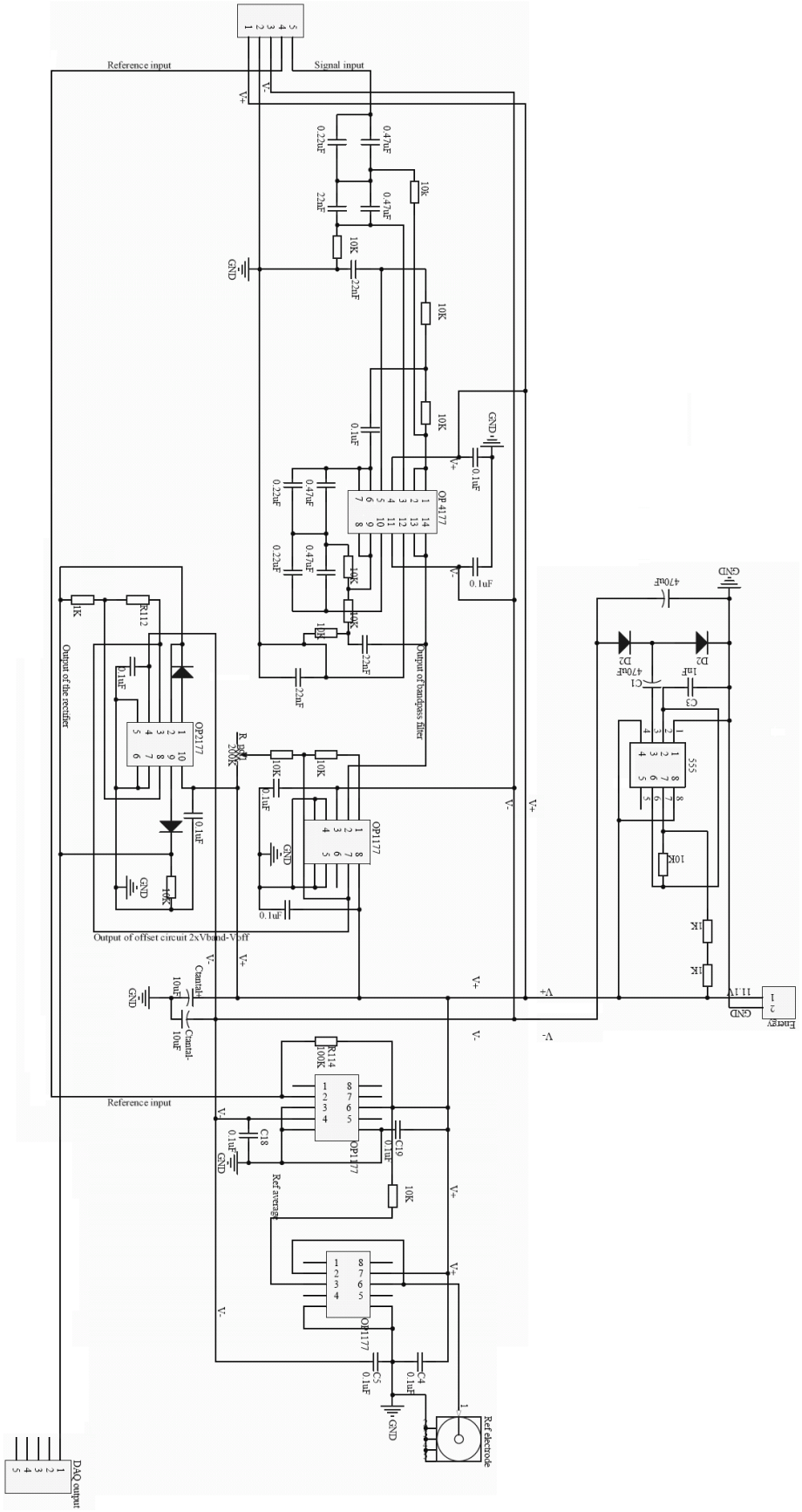

8.4 Design of the Base Circuit

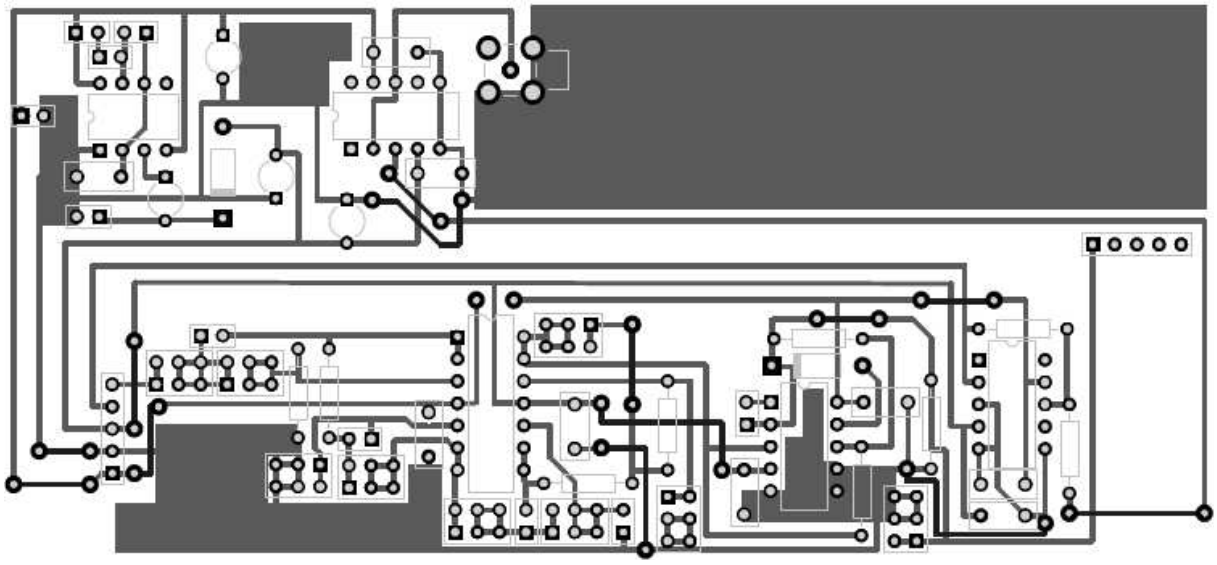

8.5 MATLAB Codes

Data Acquisition:

```
samplerate=2048;
sampleno=2048*10+3;
ai = analoginput('mcc',0);
addchannel(ai,0:3);
ai.LogToDiskMode = 'overwrite';
set(ai,'SampleRate',samplerate);
set(ai,'SamplesPerTrigger',sampleno);  % Acquisiton for 10 sec
set(ai, 'TriggerType', 'Immediate');
set(ai,'LogFileName','emg.daq');
set(ai,'LoggingMode','Disk&Memory');
addchannel(ai, 1, 'Chan1');
ch1 = ai.Chan1;
addchannel(ai, 2, 'Chan2');
ch2 = ai.Chan2;
addchannel(ai, 3, 'Chan3');
ch3 = ai.Chan3;
addchannel(ai, 4, 'Chan4');
ch4 = ai.Chan4;
start(ai);
wait(ai,12);
[d,t] = getdata(ai);
%All the chanells together in one plot
% [data,time] = daqread('emg.daq','Samples',[1 sampleno]);
% % subplot(2,2,1),plot(t*samplerate,d(:,1));
% % xlabel('Samples'), ylabel('Signal (Volts)')
% subplot(2,2,2),plot(t*samplerate,d(:,2));
% xlabel('Samples'), ylabel('Signal (Volts)')
% subplot(2,2,3),plot(t*samplerate,d(:,3));
% xlabel('Samples'), ylabel('Signal (Volts)')
% subplot(2,2,4),plot(t*samplerate,d(:,4));
% xlabel('Samples'), ylabel('Signal (Volts)')
plot(t*samplerate,d(:,2));
xlabel('Samples'), ylabel('Signal (Volts)')
save 40 d
```

Truncation of Signal

```
File=input('What is the name of the file?\n','s')
load(File, 'd');
figure(1),plot(d(:,2));
Beginning = input('What is the number of the beginning sample?\n');
WindowDuration = 2;%Input('How many seconds is the duration?\n');
N=2048; % N is the number of samples of the signal per second
newd=[];
newd=d(Beginning:Beginning+N*WindowDuration-1,2);
d=newd;
save (File, 'd');
figure(2),plot(d);
```

Energy Method- Spectral Density:

```
%Clear Registery
clc
clear all
close all
clf
%Parameters
N=2048; % N is the number of samples of the signal per second
Beginning=1;  %The beginning sample of reasonable signal
WindowDuration=1;  %Number of seconds in a signal window

X_SIM=[];

for j=20:31
    %Recorded Data
    name=int2str(j);
    load(name,'d');
    %SEMG signal
    semg=d;

    %Filter out outside of the desired bandwidth (20-500Hz)
    %4th Order Butterworth bandpass filter is employed
    n=4; %Order of filter
    Wn=[20 500]/1024;
    [B,A]=butter(n,Wn);
        filtered=filtfilt(B,A,semg);
        filtered=filtered(Beginning:Beginning+N*WindowDuration-1,:);
```

```
    %FFT of selected region of SEMG signal
    y=fft(abs(filtered(Beginning:Beginning+N*WindowDuration-1)),N);
    m=abs(y(1:1025));
    f=2048*(0:1024)/2048;

     %Here Energy Method is applied on the signal window to extract
     %the feature vector
    for h=1:4
        X_SIM1=0;
        for i=1:size(filtered,1)
            X_SIM1=X_SIM1+(filtered(i,h))^2;
            t(i)=i;
        end
        X_SIM(j,h)=X_SIM1;
    end
end
%For Spectral Density
for h=1:4
    X_SIM1=0;
    for i=1:size(filtered,1)
        X_SIM1=X_SIM1+(y(i,h))^2;
        t(i)=i;
    end
    X_SIM(j,h)=X_SIM1;
end
end
%Write them to excel file
xlswrite('EMGdata.xls', X_EM, 'EMG', 'A1');
```

Hamming Window Method

```
%Parameters
N=2048; % N is the number of samples of the signal per second
Beginning=1;  %The beginning sample of reasonable signal
WindowDuration=1;  %Number of seconds in a signal window
X_HMM=[];

%Parameters
N=2048; % N is the number of samples of the signal per second
```

```
Beginning=1;  %The beginning sample of reasonable signale
WindowDuration=1;  %Number of seconds in a signal window
%Recorded Data
load 31;
%SEMG signal
semg=d(:,4);

%Filter out outside of the desired bandwidth (20-500Hz)
%4th Order Butterworth bandpass filter is employed
n=4; %Order of filter
Wn=[20 500]/1024;
[B,A]=butter(n,Wn);
filtered=filtfilt(B,A,semg);
filtered=filtered(Beginning:Beginning+N*WindowDuration-1);

    %Hamming Window
    numofwindow=3; %Number of Window
    overlap=0.3; %It means that %30 overlap
    WS=N/((numofwindow)-(numofwindow-1)*overlap); %Window Size
    WS=ceil(WS);
    overlap=fix(overlap*WS);
    i=(WS-overlap);
    HW=hamming(WS); %Hamming Window
    W1(1:WS,1)=HW; %Apply Hamming window at the end of window size
    W1(WS+1:N,1)=0; % Other parts become zero.
    W2(1:i,1)=0; %Since it is the first part of the signal,then it is zero
    W2(i+1:i+WS,1)=HW; % Second window applied to the signal
    W2(i+WS+1:N,1)=0; %Out of the second window range,then it becomes zero
    W3(1:N-WS,1)=0; % Out of third window range equals to zero
    W3(N-WS+1:N,1)=HW; %This is third window range&since hamming is here

W=[W1 W2 W3];    %Triple Hamming
    %Here the triple hamming window is applied on the signal window to
extract
    %the feature vector
    FX=[0 0 0]; % Feature Vector of SEMG
    for i=1:size(filtered)
        FX(1,1)=FX(1,1)+W(i-Beginning+1,1)*(filtered(i,1))^2;
        FX(1,2)=FX(1,2)+W(i-Beginning+1,2)*(filtered(i,1))^2;
        FX(1,3)=FX(1,3)+W(i-Beginning+1,3)*(filtered(i,1))^2;
```

```
    end

    X_HMM(1,1)=FX(1,1);
    X_HMM(1,2)=FX(1,2);
    X_HMM(1,3)=FX(1,3);

%Write them to Excel File
xlswrite('EMGdata.xls', X_HMM, 'EMG', 'S1');
```

STFT

```
%Parameters
N=2048; % N is the number of samples of the signal per second
Beginning=1;  %The beginning sample of reasonable signal
WindowDuration=0.8;  %Number of seconds in a signal window
X_STFT=[];

for j=1:40
    %Recorded Data
    name=int2str(j);
    load(name,'d');
    %SEMG signal
    semg=d;
%Filter out outside of the desired bandwidth (20-500Hz)
    %4th Order Butterworth bandpass filter is employed
    n=4; %Order of filter
    Wn=[20 500]/1024;
    [B,A]=butter(n,Wn);
    filtered=filtfilt(B,A,semg);
    y=filtered(Beginning:Beginning+N*WindowDuration-1);
    %STFT Processing of SEMG
    R=round(length(y)/10); %block length
    window=hamming(R);
    nfft=R;
    L=1;
    fs=N;
    numoverlap=R-L;
    [S,f,t,p]=spectrogram(y,window,numoverlap,nfft,fs);
    pxx=abs(S);
%Extracted Features
    f_exp =[];
```

```
f_var =[];
M0 = [];
M1 = [];
M2 = [];
E = [];
for i=1:size(pxx,2)
    % 0 moment Calculation
    m0(i) = sum(pxx(:,i)); % cumulative power
     % 1st moment Calculation
    tt = 0 ;
    for k =1:size(pxx,1)
        tt = tt + pxx(k,i)*f(k);
    end;
    m1(i) = tt; %/m0(i);
     %2nd moment Calculation
    tt = 0;
    for k =1:size(pxx,1)
        tt = tt + f(k)*f(k)*pxx(k,i);
    end;
    m2(i) = tt;
     f_exp = [f_exp m1(i)/m0(i)];
    f_var = [f_var m2(i)/m0(i)- power((m1(i)/m0(i)) ,2)];
    f_std = sqrt(f_var);
    energy = sum(power(hamming(nfft).*y(i:i+nfft-1),2 ));
     M0 = [M0 m0(i)];
    M1 = [M1 m1(i)];
    M2 = [M2 m2(i)];
    E = [E energy];
end;


m_M0=mean(M0);
m_M1=mean(M1);
m_M2=mean(M2);
m_E=mean(E);
m_f_exp=mean(f_exp);
m_f_var=mean(f_var);


X_STFT(j,1)=m_M0;
X_STFT(j,2)=m_M1;
X_STFT(j,3)=m_M2;
X_STFT(j,4)=m_E;
```

```
    X_STFT(j,5)=m_f_exp;
    X_STFT(j,6)=m_f_var;
end
```

DWT

```
%Parameters
N=2048; % N is the number of samples of the signal per second
Beginning=1;  %The beginning sample of reasonable signal
WindowDuration=0.5;  %Number of seconds in a signal window
X_DWP=[];

for j=20:31
    %Recorded Data
    name=int2str(j);
    load(name,'d');
    %SEMG signal
    semg=d(:,4);

    %Filter out outside of the desired bandwidth (20-500Hz)
    %4th Order Butterworth bandpass filter is employed
    n=4; %Order of filter
    Wn=[20 500]/1024;
    [B,A]=butter(n,Wn);
    filtered=filtfilt(B,A,semg);
    filtered=filtered(Beginning:Beginning+N*WindowDuration-1);

  [C,L]=wavedec(filtered,5,'sym8');

      A1=wrcoef('a',C,L,'sym8',1);
      A2=wrcoef('a',C,L,'sym8',2);
      A3=wrcoef('a',C,L,'sym8',3);
      A4=wrcoef('a',C,L,'sym8',4);
      A5=wrcoef('a',C,L,'sym8',5);

    %Here DWP Method is applied on the signal window to extract
    %the feature vector
    X_DWP1=0;
    for i= 1:size(A1) %i=Beginning:Beginning+N*WindowDuration-1
        X_DWP1=X_DWP1+(A1(i,1))^2;
        t(i)=i;
```

```
    end
    X_DWP(j,1)=X_DWP1;

    X_DWP2=0;
    for i= 1:size(A2) %i=Beginning:Beginning+N*WindowDuration-1
        X_DWP2=X_DWP2+(A2(i,1))^2;
        t(i)=i;
    end
    X_DWP(j,2)=X_DWP2;

    X_DWP3=0;
    for i= 1:size(A3) %i=Beginning:Beginning+N*WindowDuration-1
        X_DWP3=X_DWP3+(A3(i,1))^2;
        t(i)=i;
    end
    X_DWP(j,3)=X_DWP3;

    X_DWP4=0;
    for i= 1:size(A4) %i=Beginning:Beginning+N*WindowDuration-1
        X_DWP4=X_DWP4+(A4(i,1))^2;
        t(i)=i;
    end
    X_DWP(j,4)=X_DWP4;

    X_DWP5=0;
    for i= 1:size(A5) %i=Beginning:Beginning+N*WindowDuration-1
        X_DWP5=X_DWP5+(A5(i,1))^2;
        t(i)=i;
    end
    X_DWP(j,5)=X_DWP5;
end

xlswrite('EMGdata.xls', X_DWP, 'sym', 'A1');
```

WPT

```
%Parameters
N=2048; % N is the number of samples of the signal per second
Beginning=1;  %The beginning sample of reasonable signal
WindowDuration=0.5;  %Number of seconds in a signal window
X_WPT=[];
for j=20:31
    %Recorded Data
    name=int2str(j);
    load(name,'d');
    %SEMG signal
    semg=d(:,4);
    %Filter out outside of the desired bandwidth (20-500Hz)
    %4th Order Butterworth bandpass filter is employed
    n=4; %Order of filter
    Wn=[20 500]/1024;
    [B,A]=butter(n,Wn);
    filtered=filtfilt(B,A,semg);
    filtered=filtered(Beginning:Beginning+N*WindowDuration-1);
% Decompose "filtered" at depth 3 with db2 wavelet packets
% using Shannon entropy.
    T = WPDEC(filtered,3,'db2','shannon');
%     figure(1); % plot(T)
    %Reconstruct the contents at level 3
    %LLL,LLH,LHL,LHH,HLL respectively
    rcfs1 = wprcoef(T,[3 0]);
    rcfs2 = wprcoef(T,[3 1]);
    rcfs3 = wprcoef(T,[3 2]);
    rcfs4 = wprcoef(T,[3 3]);
    rcfs5 = wprcoef(T,[3 4]);
%Here WPT Method is applied on the signal window to extract
%the feature vector
    X_WPT1=0;
    for i= 1:size(rcfs1) %i=Beginning:Beginning+N*WindowDuration-1
        X_WPT1=X_WPT1+(rcfs1(i,1))^2;
        t(i)=i;
    end
    X_WPT(j,1)=X_WPT1;

    X_WPT2=0;
    for i= 1:size(rcfs2) %i=Beginning:Beginning+N*WindowDuration-1
```

```
        X_WPT2=X_WPT2+(rcfs2(i,1))^2;
        t(i)=i;
    end
    X_WPT(j,2)=X_WPT2;

    X_WPT3=0;
    for i= 1:size(rcfs3) %i=Beginning:Beginning+N*WindowDuration-1
        X_WPT3=X_WPT3+(rcfs3(i,1))^2;
        t(i)=i;
    end
    X_WPT(j,3)=X_WPT3;

    X_WPT4=0;
    for i= 1:size(rcfs4) %i=Beginning:Beginning+N*WindowDuration-1
        X_WPT4=X_WPT4+(rcfs4(i,1))^2;
        t(i)=i;
    end
    X_WPT(j,4)=X_WPT4;

    X_WPT5=0;
    for i= 1:size(rcfs5) %i=Beginning:Beginning+N*WindowDuration-1
        X_WPT5=X_WPT5+(rcfs5(i,1))^2;
        t(i)=i;
    end
    X_WPT(j,5)=X_WPT5;
end

xlswrite('db03data.xls', X_WPT, 'db03', 'B1');
```